



*Midwest States Pooled Fund Research Program  
Fiscal Year 2016 (Year 26)  
Research Project Number TPF-5(193) Supplement #90  
NDOT Sponsoring Agency Code RFPF-16-CONC-4*

# **DEVELOPMENT OF A PCB STEEL COVER PLATE FOR LARGE OPEN JOINTS – PHASE I**

Submitted by

Sagheer A. Ranjha, Ph.D. MIE Aust.  
Former Postdoctoral Research Associate

Mojdeh Asadollahi Pajouh, Ph.D., P.E.  
Research Assistant Professor

Robert W. Bielenberg, M.S.M.E.  
Research Engineer

Scott Rosenbaugh, M.S.C.E.  
Research Engineer

Ronald K. Faller, Ph.D., P.E.  
Research Professor & MwRSF Director

## **MIDWEST ROADSIDE SAFETY FACILITY**

Nebraska Transportation Center  
University of Nebraska-Lincoln

### **Main Office**

Prem S. Paul Research Center at Whittier School  
Room 130, 2200 Vine Street  
Lincoln, Nebraska 68583-0853  
(402) 472-0965

### **Outdoor Test Site**

4630 N.W. 36<sup>th</sup> Street  
Lincoln, Nebraska 68524

Submitted to

## **MIDWEST POOLED FUND PROGRAM**

Nebraska Department of Transportation  
1500 Nebraska Highway 2  
Lincoln, Nebraska 68502

MwRSF Research Report No. TRP-03-387a-21

March 23, 2021

## TECHNICAL REPORT DOCUMENTATION PAGE

<b>1. Report No.</b> TRP-03-387a-21	<b>2. Government Accession No.</b>	<b>3. Recipient's Catalog No.</b>	
<b>4. Title and Subtitle</b> Development of a PCB Steel Cover Plate for Large Open Joints – Phase I		<b>5. Report Date</b> March 23, 2021	
		<b>6. Performing Organization Code</b>	
<b>7. Author(s)</b> Ranjha, S.A., Asadollahi Pajouh, M., Bielenberg, R.W., Rosenbaugh, S., and Faller, R.K.		<b>8. Performing Organization Report No.</b> TRP-03-387a-21	
<b>9. Performing Organization Name and Address</b> Midwest Roadside Safety Facility (MwRSF) Nebraska Transportation Center University of Nebraska-Lincoln  Main Office: Prem S. Paul Research Center at Whittier School Room 130, 2200 Vine Street Lincoln, Nebraska 68583-0853		<b>10. Work Unit No.</b>	
		<b>11. Contract</b> TPF-5(193) Supplement #90	
<b>12. Sponsoring Agency Name and Address</b> Midwest States Pooled Fund Program Nebraska Department of Roads 1500 Nebraska Highway 2 Lincoln, Nebraska 68502		<b>13. Type of Report and Period Covered</b> Final Report: 2016 – 2021	
		<b>14. Sponsoring Agency Code</b> RFPF-16-CONC-4	
<b>15. Supplementary Notes</b> Prepared in cooperation with U.S. Department of Transportation, Federal Highway Administration.			
<b>16. Abstract</b> <p>Portable concrete barriers (PCBs) are commonly used to protect work-zone personnel and to shield motorists from hazards in construction areas. It is not uncommon to encounter longitudinal gaps within PCB installations due to the practice of constructing and connecting the barriers from different ends during setup or contractor operations. Longitudinal gaps can also be created due to tensioning issues following an impact event. These gaps can range from 6 in. to a full barrier segment length of 12.5 ft. Longitudinal gaps between adjacent installations of PCB systems pose a serious safety concern for the errant motorist.</p> <p>The objective of this research study was to brainstorm, develop, and evaluate design concepts for shielding the longitudinal gaps that occur between adjacent installations of PCB systems. Among candidate design concepts, two concepts including (1) thrie beam and toe plate design, and (2) two-piece cover plate were selected for simulation and further investigation and refinement. LS-DYNA analysis was used to evaluate the performance of the designs under MASH TL-3 impacts. Based on simulation results and input from the Midwest Pooled Fund Program member states the design concept of the thrie-beam rail with toe plate was recommended for further evaluation. Additional simulations were conducted to refine this design concept and determine critical impact points for full-scale crash testing. The final design consisted of two nested 12.5-ft long, 12-gauge thrie-beam with a 3/8-in. thick toe plate and three welded, 1/4-in. stiffeners between the two thrie-beam rails. Recommendations were provided for evaluating the proposed PCB gap spanning design through two MASH TL-3 full-scale crash tests.</p>			
<b>17. Key Words</b> Highway Safety, Crash Test, Roadside Appurtenances, Compliance Test, MASH, Portable Concrete Barrier, Work Zones		<b>18. Distribution Statement</b> No restrictions. This document is available through the National Technical Information Service. 5285 Port Royal Road Springfield, VA 22161	
<b>19. Security Classification (of this report)</b> Unclassified	<b>20. Security Classification (of this page)</b> Unclassified	<b>21. No. of Pages</b>  120	<b>22. Price</b>

## **DISCLAIMER STATEMENT**

This material is based upon work supported by the Federal Highway Administration, U.S. Department of Transportation and the Midwest Pooled Fund Program under TPF-5(193) Supplement #90. The contents of this report reflect the views and opinions of the authors who are responsible for the facts and the accuracy of the data presented herein. The contents do not necessarily reflect the official views or policies of the University of Nebraska-Lincoln, state highway departments participating in the Midwest Pooled Fund Program nor the Federal Highway Administration, U.S. Department of Transportation. This report does not constitute a standard, specification, or regulation. Trade or manufacturers' names, which may appear in this report, are cited only because they are considered essential to the objectives of the report. The United States (U.S.) government and the State of Nebraska do not endorse products or manufacturers.

## **UNCERTAINTY OF MEASUREMENT STATEMENT**

The Midwest Roadside Safety Facility (MwRSF) has determined the uncertainty of measurements for several parameters involved in standard full-scale crash testing and non-standard testing of roadside safety features. Information regarding the uncertainty of measurements for critical parameters is available upon request by the sponsor and the Federal Highway Administration.

## ACKNOWLEDGEMENTS

The authors wish to acknowledge several sources that made a contribution to this project: (1) the Midwest Pooled Fund Program funded by the California Department of Transportation, Florida Department of Transportation, Georgia Department of Transportation, Hawaii Department of Transportation, Illinois Department of Transportation, Indiana Department of Transportation, Iowa Department of Transportation, Kansas Department of Transportation, Kentucky Department of Transportation, Minnesota Department of Transportation, Missouri Department of Transportation, Nebraska Department of Transportation, New Jersey Department of Transportation, North Carolina Department of Transportation, Ohio Department of Transportation, South Carolina Department of Transportation, South Dakota Department of Transportation, Utah Department of Transportation, Virginia Department of Transportation, Wisconsin Department of Transportation, and Wyoming Department of Transportation for sponsoring this project; and (2) MwRSF personnel.

Acknowledgement is also given to the following individuals who contributed to the completion of this research project.

### **Midwest Roadside Safety Facility**

J.D. Reid, Ph.D., Professor  
C.S. Stolle, Ph.D., Research Assistant Professor  
J.S. Steelman, Ph.D., P.E., Associate Professor  
K.A. Lechtenberg, M.S.M.E., Research Engineer  
J.D. Rasmussen, Ph.D., P.E., Former Research Assistant Professor  
J.C. Holloway, M.S.C.E., Research Engineer & Assistant Director –Physical Testing Division  
A.T. Russell, B.S.B.A., Testing and Maintenance Technician II  
E.W. Krier, B.S., Construction and Testing Technician II  
S.M. Tighe, Construction and Testing Technician I  
D.S. Charroin, Construction and Testing Technician I  
R.M. Novak, Construction and Testing Technician I  
T.C. Donahoo, Construction and Testing Technician I  
J.T. Jones, Construction and Testing Technician I  
J.E. Kohtz, B.S.M.E., Former CAD Technician  
E.L. Urbank, B.A., Research Communication Specialist  
Z.Z. Jabr, Engineering Technician  
Undergraduate and Graduate Research Assistants

**California Department of Transportation**

Bob Meline, Chief, Roadside Safety Research Branch  
David Whitesel, P.E., Transportation Engineer  
John Jewell, P.E., Senior Transportation Engineer,  
Specialist

**Florida Department of Transportation**

Derwood C. Sheppard, Jr., P.E., Design Standards  
Publication Manager, Roadway Design Engineer

**Georgia Department of Transportation**

Brent Story, P.E., State Design Policy Engineer  
Frank Flanders IV, P.E., Assistant State Design Policy  
Engineer

**Hawaii Department of Transportation**

James Fu, P.E., State Bridge Engineer  
Dean Takiguchi, P.E., Engineer, Bridge Design Section  
Kimberly Okamura, Engineer, Bridge Design Section

**Illinois Department of Transportation**

Filiberto Sotelo, Safety Evaluation Engineer  
Martha Brown, P.E., Safety Evaluation Unit Chief

**Indiana Department of Transportation**

Katherine Smutzer, P.E., Standards Engineer  
Elizabeth Phillips, P.E., Standards and Policy Manager

**Iowa Department of Transportation**

Chris Poole, P.E., Roadside Safety Engineer  
Brian Smith, P.E., Methods Engineer  
Daniel Harness, P.E., Transportation Engineer Specialist  
Stuart Nielsen, P.E., Transportation Engineer  
Administrator, Design  
Elijah Gansen, P.E., Geometrics Engineer

**Kansas Department of Transportation**

Ron Seitz, P.E., Director of Design  
Scott King, P.E., Road Design Bureau Chief  
Thomas Rhoads, P.E., Road Design Leader, Bureau of  
Road Design  
Brian Kierath Jr., Engineering Associate III, Bureau of  
Road Design

**Kentucky Department of Transportation**

Jason J. Siwula, P.E., Assistant State Highway Engineer  
Kevin Martin, P.E., Transportation Engineer Specialist  
Gary Newton, Engineering Tech III, Design Standards

**Minnesota Department of Transportation**

Michael Elle, P.E., Design Standards Engineer  
Michelle Moser, P.E., Assistant Design Standards Engineer

**Missouri Department of Transportation**

Sarah Kleinschmit, P.E., Policy and Innovations Engineer

**Nebraska Department of Transportation**

Phil TenHulzen, P.E., Design Standards Engineer  
Jim Knott, P.E., Construction Engineer  
Mike Owen, P.E., State Roadway Design Engineer  
Mick Syslo, P.E., Materials and Research Engineer &  
Division Head  
Mark Fischer, P.E., PMP, Research Program Manager  
Lieska Halsey, Research Project Manager  
Angela Andersen, Research Coordinator  
David T. Hansen, Internal Research Coordinator  
Jodi Gibson, Former Research Coordinator

**New Jersey Department of Transportation**

Hung Tang, Senior Engineer, Transportation  
Joseph Warren, Assistant Engineer, Transportation

**North Carolina Department of Transportation**

Neil Mastin, P.E., Manager, Transportation Program  
Management – Research and Development  
D. D. “Bucky” Galloway, P.E., CPM, Field Operations  
Engineer  
Brian Mayhew, P.E., State Traffic Safety Engineer  
Joel Howerton, P.E., Plans and Standards Engineer

**Ohio Department of Transportation**

Don Fisher, P.E., Roadway Standards Engineer

**South Carolina Department of Transportation**

J. Adam Hixon, P.E., Design Standards Associate  
Mark H. Anthony, P.E., Letting Preparation Engineer  
Henry Cross, P.E., Design Standards Engineer  
Jason Hall, P.E., Engineer

**South Dakota Department of Transportation**

David Huft, P.E., Research Engineer  
Bernie Clocksin, P.E., Standards Engineer

**Utah Department of Transportation**

Shawn Debenham, Traffic and Safety Specialist  
Glenn Blackwelder, Operations Engineer

**Virginia Department of Transportation**

Charles Patterson, P.E., Standards/Special Design Section  
Manager  
Andrew Zickler, P.E., Complex Bridge Design and ABC  
Support Program Manager

**Wisconsin Department of Transportation**

Erik Emerson, P.E., Standards Development Engineer  
Rodney Taylor, P.E., Roadway Design Standards Unit  
Supervisor

**Wyoming Department of Transportation**

William Wilson, P.E., Architectural and Highway  
Standards Engineer

**Federal Highway Administration**

David Mraz, Division Bridge Engineer, Nebraska Division  
Office

## TABLE OF CONTENTS

DISCLAIMER STATEMENT .....	ii
UNCERTAINTY OF MEASUREMENT STATEMENT .....	ii
ACKNOWLEDGEMENTS .....	iii
LIST OF FIGURES .....	vii
LIST OF TABLES .....	x
1 INTRODUCTION .....	1
1.1 Background .....	1
1.2 Objective .....	1
1.3 Scope .....	1
2 LITERATURE REVIEW .....	3
2.1 F-Shape Portable Concrete Barrier .....	3
2.2 Access Gates .....	3
2.2.1 SafeGuard Gate System .....	4
2.2.2 ArmorGuard Steel Barrier Gate .....	5
2.2.3 MASH TL-3 Emergency Opening System .....	7
2.2.4 BarrierGuard 800 Median Gate .....	10
2.2.5 BarrierGate System .....	11
2.2.6 Vulcan Barrier System and Gate .....	13
2.3 Cover Plates .....	15
2.3.1 California Steel Channel Closure .....	15
2.3.2 New York Modular Joint System .....	16
2.3.3 Kansas Expansion Joint .....	18
2.4 Additional Patented Systems .....	18
2.4.1 Removable Barrier .....	18
2.4.2 Modules for Bridging Openings in Road Guard Barriers .....	19
2.4.3 Gate Means, Preferably for Use with Barrier Elements .....	20
2.5 Miscellaneous Gap-Spanning Systems .....	20
2.5.1 Metal Transition for Branching Concrete Barriers .....	20
3 DEVELOPMENT OF DESIGN CONCEPTS .....	22
3.1 Design Criteria .....	22
3.2 Design Concepts .....	22
3.2.1 Concept No. 1 – Internal Modular System 1 .....	23
3.2.2 Concept No. 2 – Internal Modular System 2 .....	25
3.2.3 Concept No. 3 – External Modular Cover Plates .....	27
3.2.4 Concept No. 4 – Thrie Beam and Toe Plate .....	29
3.2.5 Concept No. 5 – Cover Plate .....	31
3.2.6 Concept No. 6 – Cover Plate and Beam .....	33
3.2.7 Concept No. 7 – Two-Piece Cover Plate .....	35
3.3 Design Concept Selection .....	37

4 SIMULATION OF CONCEPT NO. 7 – TWO-PIECE COVER PLATE .....	38
4.1 Evaluation Criteria .....	38
4.2 Initial Design Details .....	38
4.3 Simulation Model.....	42
4.4 Model Analysis – Cover Plate Cap Thickness.....	45
4.5 Refinement of Two-Piece Cover Plate Design .....	49
4.5.1 Addition of End Plate Stiffener Tube .....	49
4.5.2 Cap Thickness and Incremental Cap Stiffeners .....	50
4.5.3 End Plate Thickness and Loop Configuration .....	53
4.6 Single ¼-in. Thick Cover Plate Over 6.25-ft Long Gap.....	55
4.7 Multiple Impact Points Analysis – Test Designation No. 3-11 .....	57
4.8 Summary and Conclusions .....	59
5 SIMULATION OF CONCEPT NO. 4 – THRIE BEAM AND TOE PLATE .....	60
5.1 Initial Design Details .....	60
5.2 Simulation Model.....	65
5.3 Simulations of Thrie Beam and Toe Plate Model with Rail Variations .....	67
5.3.1 Single Thrie-beam rail .....	67
5.3.2 Nested Thrie-beam rail .....	69
5.4 Multiple Impact Points Analysis – Test Designation No. 3-11 .....	72
5.5 Nested 12-Gauge Rail and 37.5-in. Gap .....	73
5.6 Summary and Conclusions .....	75
6 SELECTION OF PREFERRED DESIGN CONCEPT .....	76
7 SELECTED CONCEPT DESIGN SIMULATION AND CRITICAL IMPACT POINT ANALYSIS.....	77
7.1 Investigation of Roll Angle Concern – 12.5-ft Long Gap .....	79
7.1.1 Toe Plate Design Modifications – 12.5-ft Long Gap.....	82
7.2 Investigation of Maximum Load in the Gap-Spanning Hardware.....	87
7.3 Simulation of Revised Design – 3-ft Gap .....	90
7.4 Recommend Full-Scale Crash Testing and Critical Impact Point Selection .....	94
7.4.1 Recommended Full-Scale Crash Tests .....	94
7.4.2 Critical Impact Points .....	95
8 PCB GAP-SPANNING HARDWARE – FINAL DESIGN .....	97
8.1 Design Details.....	97
9 SUMMARY, CONCLUSIONS, AND RECOMMENDATIONS .....	114
10 REFERENCES .....	116

## LIST OF FIGURES

Figure 1. Free-Standing, F-Shape, Portable Concrete Barrier .....	3
Figure 2. SafeGuard Gate System.....	4
Figure 4. ArmorGuard Gate Hinge System [7].....	6
Figure 5. Original MASH TL-3 Emergency Opening System [13].....	8
Figure 6. Modified Emergency Opening System [13].....	9
Figure 7. TxDOT Median Barrier Gate [14].....	10
Figure 8. BarrierGuard 800 Gate System [18].....	11
Figure 9. BarrierGuard 800 Joint System [18].....	11
Figure 10. BarrierGate System [22].....	12
Figure 11. Vulcan Barrier Gate Assembly [23].....	14
Figure 12. Vulcan Barrier (a) Portable Steel Longitudinal Barrier [25]; (b) Vulcan Barrier Transition; and (c) Vulcan Gate System [26] .....	14
Figure 13. California Steel Channel Closure System. [29].....	16
Figure 14. New York Modular Joint System [30] .....	17
Figure 15. Example of Steel Cover Plate at Expansion/Contraction Joints.....	18
Figure 16. Removable Barrier [33].....	19
Figure 17. Module for Bridging Openings in Road Guard Barriers [34] .....	19
Figure 18. Gate Means, Preferably for Use with Barrier Elements [35] .....	20
Figure 19. Layout of the Branching Transition and Barrier Mounted Sign Installation [36].....	21
Figure 20. Concept No. 1 – Internal Modular System 1 .....	23
Figure 21. Design Details, Concept No. 1 – Internal Modular System 1 .....	24
Figure 22. Concept No. 2 – Internal Modular System 2.....	25
Figure 23. Design Details, Concept No. 2 – Internal Modular System 2 .....	26
Figure 24. Concept No. 3 – External Modular Cover Plate.....	27
Figure 25. Design Details, Concept No. 3 – External Modular Cover Plate .....	28
Figure 26. Concept No. 4 – Thrie Beam and Toe Plate.....	29
Figure 27. Design Details, Concept No. 4 – Thrie Beam and Toe Plate .....	30
Figure 28. Concept No. 5 – Cover Plate .....	31
Figure 29. Design Details, Concept No. 5 – Cover Plate .....	32
Figure 30. Concept No. 6 – Cover Plate and Beam.....	33
Figure 31. Design Details, Concept No. 6 – Cover Plate and Beam .....	34
Figure 32. Concept No. 7 – Two-Piece Cover Plate.....	35
Figure 33. Design Details, Concept No. 7 – Two-Piece Cover Plate .....	36
Figure 34. Design Details, Concept No. 7 .....	40
Figure 35. Design Details, Concept No. 7 .....	41
Figure 36. F-Shape PCB Barrier Model .....	43
Figure 37. Two-Piece Cover Plate Model.....	44
Figure 38. Sequential Images, Impact Point at 4.3 ft Upstream from Cover Plate Joint with Cap Thickness of ¼ in. ....	46
Figure 39. Lateral Displacement and Plastic Hinge Formation for Impact Point 4.3 ft Upstream from Cap Joint.....	48
Figure 40. Model of (a) Baseline Cover Plate and (b) Modified Design with Stiffener Box Tube .....	49
Figure 41. Simulated Damage in (a) Baseline Cover Plate and (b) Modified Design with Stiffener Box Tube.....	49

Figure 42. Model of (a) Cover Plate with Three Stiffeners and Box Tube, (b) 12.5-ft Long Gap-Spanning Configuration .....50

Figure 43. Simulation with Three Stiffeners, Impact Point 4.3 ft Upstream from Cover Plate Joint.....51

Figure 44. Von Mises Stress, ½-in. Thick End Plate .....53

Figure 45. Pin and Loop Connection Configuration.....54

Figure 46. Two Variations of 6.25-ft Gap Model with Single Cap .....55

Figure 47. Simulated Impact Points.....57

Figure 48. Final Design of Two-Piece Cover Plate for PCB Gaps, 12.5-ft Gap .....59

Figure 49. Concept No. 4: Thrie Beam and Toe Plate.....61

Figure 50. Concept No. 4: Thrie Beam and Toe Plate, Stiffener Details .....62

Figure 51. Concept No. 4: Thrie Beam and Toe Plate, Thrie Beam and Terminal Connector Details .....63

Figure 52. Concept No. 4: Thrie Beam and Toe Plate, Toe Plate and Hardware Details.....64

Figure 53. Thrie Beam Model.....65

Figure 54. Thrie Beam Stiffener Model.....66

Figure 55. Thrie Beam and Toe Plate Model.....67

Figure 56. Simulations of Thrie Beam and Toe Plate Model (a) Single 12-Gauge Rail, and (b) Single 10-Gauge Rail .....68

Figure 57. Simulations of Thrie Beam and Toe Plate Model (a) Nested 12-Gauge Rail and (b) Nested 10-Gauge Rail .....70

Figure 58. Sequential Images, Impact Point 4.3 ft Upstream from Middle of Nested 12-Gauge Thrie-beam rail .....71

Figure 59. Simulated Impact Points.....72

Figure 60. 37.5-in. Gap Simulation with Nested 12-Gauge Rail.....73

Figure 61. Impact Points for Simulated Cases with 37.5-in. Gap.....73

Figure 62. Simulated Impact Points, 12.5-ft Long Gap.....77

Figure 63. Sequential Images, Downstream View: PCB with Gap-Spanning Hardware, Thrie Beam and Toe Plate (Left), and Free-Standing, F-Shape, PCB Model (Right).....80

Figure 64. Sequential Images, Overhead View: PCB with Gap-Spanning Hardware, Thrie Beam and Toe Plate (Left), and Free-Standing F-Shape PCB Simulation (Right) .....81

Figure 65. Toe Plate Deformation and Wheel Snag .....82

Figure 66. Comparison of Roll Angles with Increase in Toe Plate Thickness, 12.5-ft Gap.....83

Figure 67. Post-Impact Deformations for (a) 1-in. x 6-in. Toe Plate and 5/8-in. x 8½-in. Toe Plate.....85

Figure 68. 3-ft Long Gap-Spanning Configuration with One Stiffener Added.....90

Figure 69. Wheel Entrapment and Vehicle Roll for Impact Downstream from Barrier with 3-ft Long Barrier Gap .....90

Figure 70. Wheel Climb for Impact Points Downstream from a 3-ft Long Barrier Gap.....91

Figure 71. Comparison of Wheel Climb for 3-ft and 12.5-ft Long Gap.....92

Figure 72. Comparison of Vehicle Roll Angle for 3-ft and 12.5-ft Long Gap.....92

Figure 73. Free-Standing PCB Transition to Permanent Concrete Median Barrier, Test No. TCBT-1 .....93

Figure 74. Test Installation Layout, Test No. GSH-1 .....99

Figure 75. Gap Details, Test No. GSH-1 .....100

Figure 76. Detail C and Detail D Views, Test No. GSH-1 .....101

Figure 77. Anchor Bolt Connection Details – Traffic Side, Test No. GSH-1 .....102

Figure 78. Anchor Bolts Connection Details – Non-Traffic Side, Test No. GSH-1 .....103  
Figure 79. Section K-K and Section L-L Views, Test No. GSH-1 .....104  
Figure 80. PCB Details, Test No. GSH-1 .....105  
Figure 81. PCB Details, Section M-M and Section N-N, Test No. GSH-1 .....106  
Figure 82. PCB Rebar Details, Test No. GSH-1.....107  
Figure 83. Connector Pin Details, Test No. GSH-1 .....108  
Figure 84. Stiffener Assembly, Test No. GSH-1 .....109  
Figure 85. Stiffener Component Details, Test No. GSH-1 .....110  
Figure 86. Rail, Terminal Connector, and Toe Plate Details, Test No. GSH-1 .....111  
Figure 87. Hardware, Test No. GSH-1 .....112  
Figure 88. Bill of Materials, Test No. GSH-1.....113

## LIST OF TABLES

Table 1. Two-Piece Cover Plate Parts and LS-DYNA Parameters .....	44
Table 2. Summary of Simulation Results: Varied Cap Thicknesses, Impact Point 4.3 ft Upstream from Cap Joint .....	47
Table 3. Summary of Simulation Results: Varied Cap Thicknesses, Impact Point 8.8 ft Upstream from Cap Joint .....	47
Table 4. Summary of Simulation Results: Varied Cap Thicknesses with Stiffeners, Impact Point 4.3 ft Upstream from Cap.....	52
Table 5. Loop Contact Forces for Different Cap Thicknesses.....	54
Table 6. Summary of Simulation Results: Single ¼-in. Thick Cover Plate .....	56
Table 7. Summary of Simulation Results: Evaluation of Multiple Impact Point Investigation.....	58
Table 8. Summary of PCB GAP Thrie Beam Model Parts and LS-DYNA Parameters .....	66
Table 9. Summary of Simulation Results: Thrie Beam and Toe Plate Design with Three ¼- in. Thick Stiffeners.....	69
Table 10. Summary of Simulation Results: Nested 12-Gauge with ¼-in. Thick Stiffeners and Toe Plate.....	72
Table 11. Summary of Simulation Results: Nested 12-Gauge Rail.....	74
Table 12. Comparison of Candidate Design Concepts for PCB Gap-Spanning Hardware .....	76
Table 13. Summary of Simulation Results: Critical Impact Point Investigation, Nested 12- Gauge Rail .....	78
Table 14. Summary of Simulation Results: 12.5-ft Long Gap, Toe Plate Variations .....	84
Table 15. Summary of Simulation Results: 5/8-in. Thick, 8½-in. High Toe Plate.....	86
Table 16. Downstream Cross-Sectional Forces for Various Impact Points on 12.5-ft Gap .....	88
Table 17. Upstream Cross-Sectional Forces for Various Impact Points on 12.5-ft Gap .....	89
Table 18. MASH 2016 TL-3 Crash Test Conditions for Longitudinal Barriers.....	94

# 1 INTRODUCTION

## 1.1 Background

Portable concrete barriers (PCBs) are commonly used to protect workers in work zones and shield motorists from hazards in construction areas. It is not uncommon to encounter longitudinal gaps within PCB installations due to the practice of constructing and connecting the barriers from different ends during setup or contractor operations. Longitudinal gaps can also be created during re-tensioning procedures following an impact event. These gaps can range from 6 in. to a full barrier segment length of 12.5 ft and pose a serious safety concern for the errant motorist. Limited guidance is available for shielding this hazardous situation. The current guidance recommends overlapping two adjacent barrier runs longitudinally with a minimum of eight PCB segments and providing a minimum lateral offset of 2 ft between adjacent barrier runs. However, this is undesirable due to work-zone space constraints. The length of barrier overlap is relatively large and requires significant lateral offset between the overlapped segments, which reduces available space in constricted work zones. Thus, a need existed to develop a crashworthy and efficient method for treating longitudinal gaps in adjacent runs of free-standing PCBs.

Previous research efforts conducted to investigate gaps between adjacent PCB installations have focused on gate designs for providing emergency or maintenance access through temporary barriers. Examples of these devices include the ArmorGuard Gate, the BarrierGuard Gate, and the Vulcan barrier system. All these gate systems are proprietary with fixed lengths that can be attached to permanent or temporary concrete barrier systems. While these systems have been crash tested and demonstrated to function adequately, they are fixed-length solutions that would not be effective at spanning variable length gaps. In addition, these gates can be relatively costly to install.

The Midwest Pooled Fund Program sponsored this Phase I effort to develop potential design concepts to safeguard the variable gaps that occur between adjacent PCB installations and perform adequately under the *Manual for Assessing Safety Hardware, Second Edition* (MASH 2016) [1] Test Level 3 (TL-3) impact conditions. These design concepts needed to be adjustable for a variable gap length, easy to install and remove to make the joint spanning system as useful as possible during staging, and allow access as needed.

## 1.2 Objective

The objective of this research effort was to develop a MASH TL-3 crashworthy prototype system for protecting and shielding the longitudinal gaps between adjacent installations of PCB systems. The research focused on a system for use with the MASH TL-3 crashworthy F-shape PCB used by many of the Midwest Pooled Fund Program member states. The new system needed to be relatively easy to install and remove, capable of spanning gap lengths from 6 in. to 12.5 ft, and safely redirect impacting vehicles.

## 1.3 Scope

The research objectives were accomplished through a series of several tasks. The Phase I research effort began with a literature search to review existing designs and guidance regarding the treatment of longitudinal gaps between adjacent installations of PCB systems. Following the literature review, new ideas were brainstormed to identify potential designs for spanning the PCB

gaps. These concepts included adjustable steel caps, stiffened thrie beam, and/or other hardware to span the gap between adjacent segment ends. The design concepts were submitted to the Midwest Pooled Fund Program member states for review and comment. Preferred design concepts were selected for further analysis and evaluation. LS-DYNA computer simulation was used to evaluate and refine the preferred design concepts as well as to evaluate structural loading and determine the critical impact points for the full-scale crash testing of the system. Upon completion of the Phase I research efforts, recommendations for PCB gap-spanning hardware full-scale crash testing were made.

## 2 LITERATURE REVIEW

A literature search was conducted to review past research regarding the 12.5-ft long F-shape portable concrete barrier developed through the Midwest Pooled Fund Program, access gate designs, cover plate systems utilized between permanent concrete barriers, and other gap-spanning systems. Currently, none of these systems are ideal for efficiently bridging a variable-length gap between runs of PCB installations. However, these systems provided insight with respect to the PCB gap spanning hardware desired in this research.

### 2.1 F-Shape Portable Concrete Barrier

The Midwest Roadside Safety Facility (MwRSF) developed a free-standing F-shape PCB developed through the Midwest Pooled Fund Program. This PCB system consists of a 32-in. tall x 22.5-in. wide x 12.5-ft long F-shape concrete barrier segment with a pin-and-loop type connection, as shown in Figure 1. The barrier has been tested to TL-3 under both the National Cooperative Highway Research Program (NCHRP) Report 350 [2] and MASH safety criteria [3]. MASH TL-3 evaluation of the free-standing PCB system was conducted in accordance with test designation no. 3-11 using the 2270P vehicle in test no. 2214TB-2. Test no. 2214TB-2 utilized a 2002 Dodge Ram 1500 Quad Cab pickup truck with a mass of 5,000 lb. During the test, the 2270P vehicle impacted the PCB system with a speed of 62.0 mph and at an angle of 25.4 degrees. The PCB system safely redirected the impacting vehicle with a maximum lateral dynamic barrier deflection of 79.6 in. Thus, the temporary concrete barrier system was determined to be acceptable according to TL-3 requirements presented in MASH.



Figure 1. Free-Standing, F-Shape, Portable Concrete Barrier

### 2.2 Access Gates

Access gates are systems that are attached to concrete barriers that allow emergency vehicles to pass through and can redirect traffic. Of the access gate designs in use today, the most pertinent to this research study were those that swing away and those that telescope to span the

gap between the barriers. Currently, majority of access gate designs are limited to use in permanent concrete barriers or with proprietary steel barriers. Thus, the current knowledge of the crashworthiness of these devices when utilized with PCB systems was limited.

### 2.2.1 SafeGuard Gate System

The SafeGuard Gate System (SGS) is a heavily reinforced steel barrier system that is designed to span a permanent opening in a concrete median barrier ranging from 26 ft to 52.5 ft long, as shown in Figure 2 [4-5]. The SGS is 27.5 in. wide at its base, 20 in. wide at the top, and approximately 32.6 in. tall. The 13-ft sections quickly assemble up to 52-ft lengths. Hinge assemblies at the ends of each unit along with compressed air-activated, retractable wheels on each unit allow the SGS to be disconnected from the rigid barrier after removal of the aluminum cover plate and the 1.1-in. diameter ASTM C1018 steel connecting pin. The SGS can then be swung open from one end or completely removed to allow vehicle passage. It is suitable as a permanent and temporary work zone barrier where emergency vehicles, maintenance crews, and emergency evacuation access may be needed. It is quickly and easily opened without expensive electrical supplies or sophisticated control systems.

The SafeGuard Gate System has been fully tested and approved in accordance with NCHRP Report 350 TL-3 criteria [4-5]. The first test, test no. SGB06, was conducted according to NCHRP Report 350 test designation no. 3-10 with an 1,834-lb vehicle impacting the SGS at a speed of 61.4 mph and a 20-degree impact angle. The second test, test no. SGB07, was performed at NCHRP Report 350 test designation no. 3-11 with a 4,409-lb pickup truck with a speed of 62.5 mph and angle of 25 degrees. Two tests on the transition to the permanent concrete barrier were also conducted in accordance with NCHRP Report 350 test designation no. 3-21: one to test the hinge assembly in a 39-ft span and one to test the SGS-to-concrete barrier transition in a 26-ft span. One additional test was also conducted with an 1,807-lb vehicle at the TL-2 speed of 43.5 mph to confirm acceptable low-speed performance. The maximum dynamic deflection noted in the length of need pickup truck impact into a 39-ft long SGS was 22.5 in.



Figure 2. SafeGuard Gate System

### 2.2.2 ArmorGuard Steel Barrier Gate

The ArmorGuard Steel Barrier (AGB) Gate manufactured by Barrier Systems Inc. is a reinforced steel longitudinal barrier gate designed to span a permanent opening in a concrete barrier system, and it has the ability to pivot open from either fixed end without the use of heavy equipment [5-9]. The AGB Gate system provides a means to close 26, 39, and 52.5 ft openings in rigid longitudinal barrier systems. The exterior faces of the gate comprise three steel channel segments attached to a steel plate on the ends of the barrier segment. The typical overall length of the gate assembly is 52.5 ft, and the effective overall height is 32.6 in. A 52.5-ft long gate section weighs approximately 6,000 lb. The AGB Gate system is patent protected under US patent no. 6,485,224 B1 [7]. The patent covers a traffic barrier that is pivotally attached to a gate by a hinge. A design drawing of the AGB Gate system is shown in Figure 3 and the hinge system can be seen in Figure 4. A rigid cover plate covers the hinge location at the barrier and also acts as a structural member to prevent rotational movement around the hinge due to an impact from an errant vehicle.

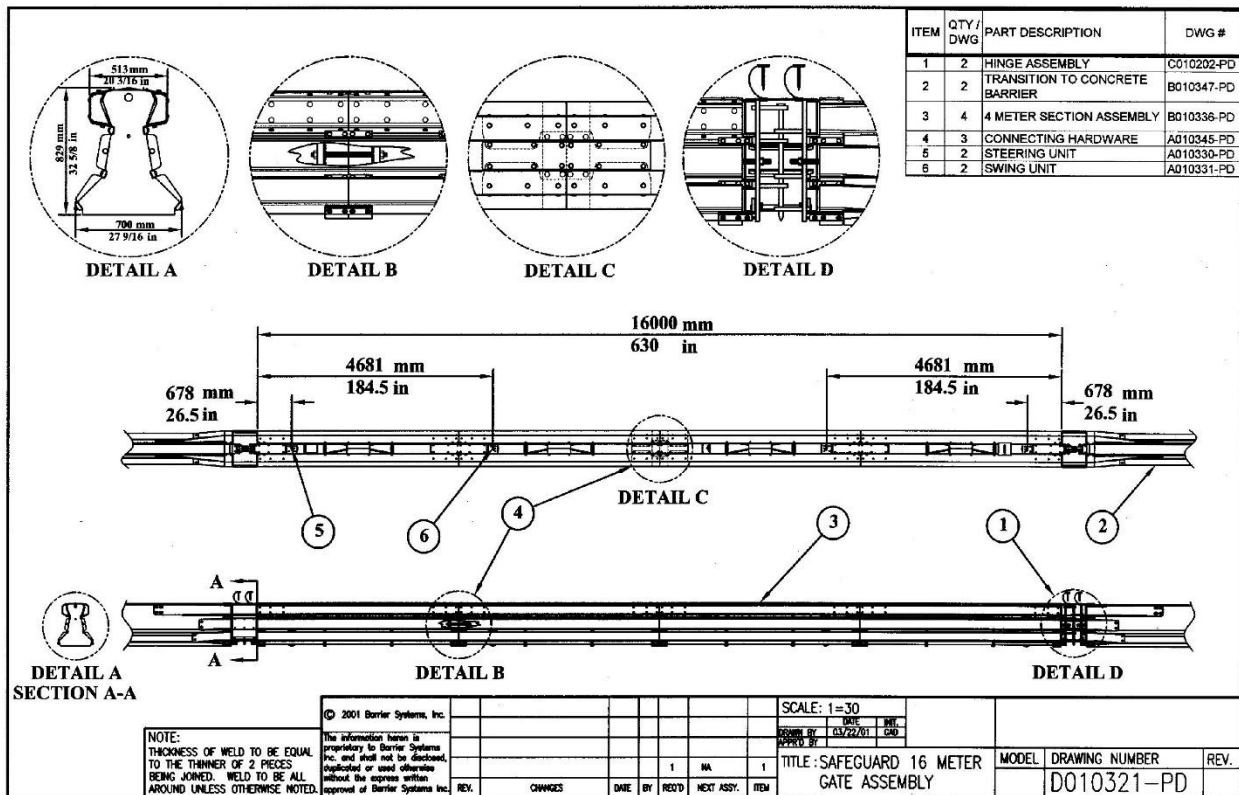


Figure 3. ArmorGuard Gate System [4]

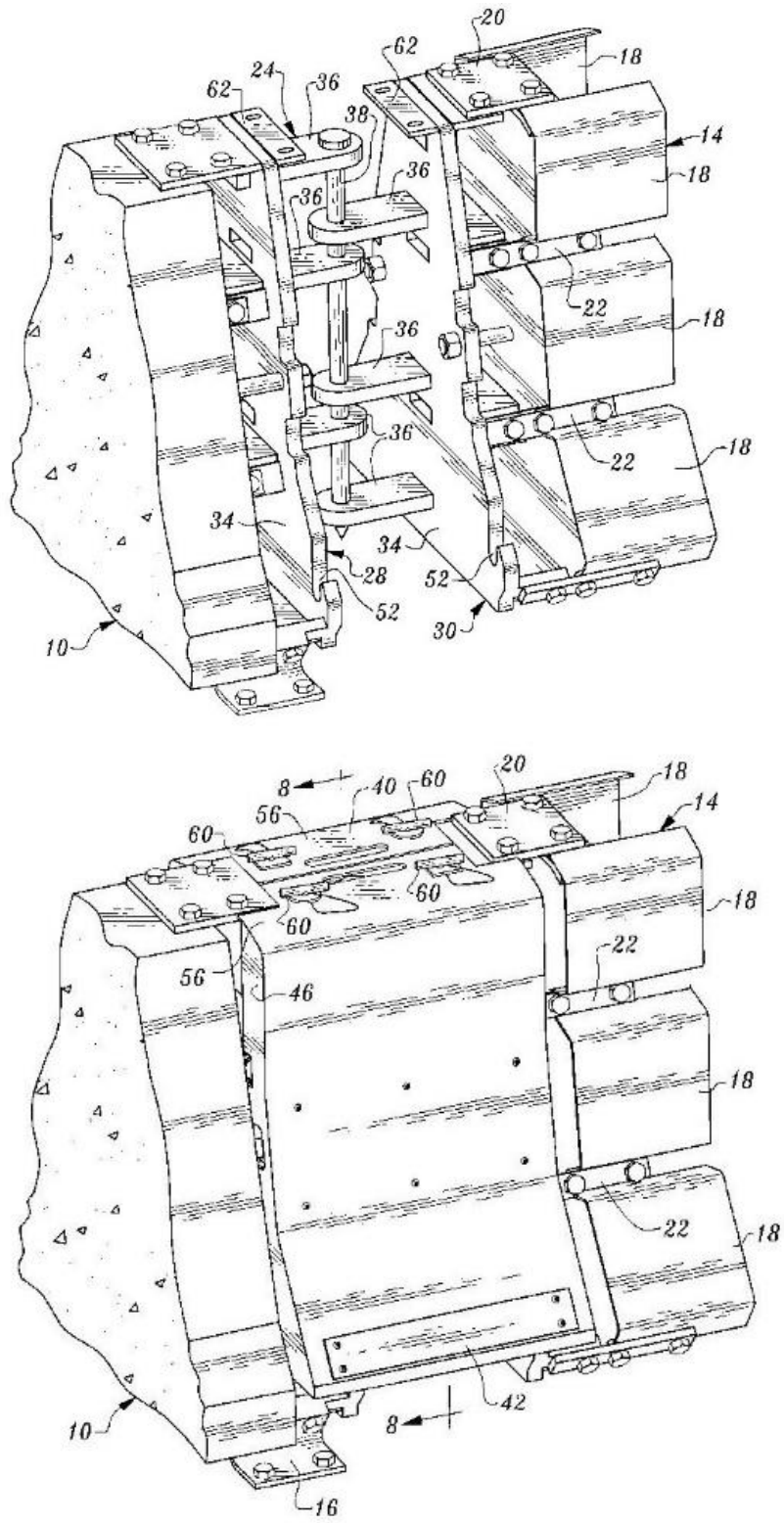


Figure 4. ArmorGuard Gate Hinge System [7]

The AGB gate system is an updated version of the previously described SafeGuard barrier system. Additional evaluation of the AGB Gate system was documented in Federal Highway Administration (FHWA) Acceptance Letter B-173 [9]. Three successful full-scale crash tests were conducted on the AGB Gate system to NCHRP Report 350 TL-3 test designation no. 3-21. The first test, test no. WGB03, was conducted with a 4,409-lb pickup impacting the downstream end of a series of three AGB barrier segments at a speed of 62.2 mph and at an angle of 25 degrees to evaluate the AGB Gate system. The test utilized three AGB barrier segments attached between the adjacent ends of two runs of 10-ft long PCB segments. The full-scale test was successful and resulted in dynamic and permanent set deflections of 105 in.

The second test, test no. WGB04, utilized four AGB barrier segments attached across a gap in a permanent concrete median barrier. In test no. WGB04, a 4,409-lb pickup impacted the final AGB barrier segment upstream from the permanent concrete barrier at a speed of 64.2 mph and at an angle of 25 degrees under NCHRP Report 350 test designation no. 3-21. This full-scale test was successful and resulted in a dynamic deflection of 49 in. and a permanent deflection of 35 in.

The third test, test no. AG8M1, was conducted on a system that consisted of one AGB barrier segment attached to permanent concrete median barriers on both ends. In test no. AG8M1, a 4,409-lb pickup impacted the midpoint of the system at a speed of 63.1 mph and an angle of 25 degrees. The full-scale test was successful, and the barrier system had a dynamic deflection of 28 in. and a permanent deflection of 19 in.

### **2.2.3 MASH TL-3 Emergency Opening System**

In the early 1980s, the Texas Transportation Institute (TTI) developed an emergency opening system (EOS) for the Texas State Department of Highways and Public Transportation [10]. The system comprised two tubular steel beams mounted vertically on top of each other with a separation of 3 in. A W-beam rail was attached to the face of the steel beams and terminated with W-beam terminal connectors to minimize snagging potential. The beams spanned 30 ft between free-standing concrete barrier sections that were modified to transition from a New Jersey safety shape profile to a vertical face. Steel brackets with three  $\frac{7}{8}$ -in. thick horizontal steel plates were anchored to the ends of the concrete barrier sections using eight 1.5-inch diameter anchor bolts. Three full-scale crash tests were successfully conducted to evaluate the impact performance of the system under NCHRP Report 230 [11].

Nearly 30 years later, TTI conducted further testing on modified versions of the EOS to *Manual for Assessing Safety Hardware* (MASH) standards [12-13]. MASH test designation no. 3-10 was performed on the original EOS barrier design with some minor modifications incorporated to reduce the potential for vehicle snagging. The horizontal plates on the steel end bracket were tapered and the curb protruding from the end of the concrete parapet was constructed with a straight taper rather than a rounded nose, as shown in Figure 5. The W-beam sections on the face of the gate were also removed. The test conditions were a 2,420 lb vehicle (designated 1100C) impacting the gate 3.6 ft upstream from the end of the concrete parapet at a nominal impact speed and angle of 62 mph and 25 degrees, respectively. The 1100C test vehicle was contained and redirected, however, the gate failed to comply with MASH due to excessive occupant compartment deformation inside the vehicle caused by vehicle snag on the end of the gate and parapet.



Figure 5. Original MASH TL-3 Emergency Opening System [13]

Several modifications were made to the end of the EOS to help mitigate the severe vehicle snagging. The horizontal steel plates on the end brackets were replaced with tapered sections of 2-in.  $\times$  1/4-in. thick steel tubing, as shown in Figure 6. The ends of the tubular steel beams were cut off and tapered sections of tubing were added. These tubes tapered out 2 in. from the sides of the steel beams and then tapered back down to a width that was less than the width of the end of the concrete parapet to reduce snagging potential from a reverse direction impact. Other details of the EOS, including the concrete buttress details, remained the same as was used in the previous tests. MASH test designation no. 3-10 was performed on the modified design. The modified gate did not perform acceptably due to excessive occupant compartment deformation inside the vehicle [13].



Figure 6. Modified Emergency Opening System [13]

In 2010, researchers at TTI developed and crash tested a new crashworthy median barrier to replace the EOS, as shown in Figure 7 [14]. Various design features were incorporated into the new median barrier gate to help mitigate snagging potential: the vertical spacing between the rail elements was eliminated, stacking the rails on top of one another eliminated the need for welded spacers, and the width of the tubular rail members was increased to match the width of the end of the concrete parapet to which it was attached. The median barrier gate comprised two 29-ft long, 12-in.  $\times$  12-in.  $\times$  1/4-in. A500 Grade B steel tubes. The tubes were stacked vertically on top of one another and bolted together using three 3/4-in. diameter  $\times$  26-in. long ASTM A325 bolts spaced on 80-inch centers. A 2 1/2-in. schedule 40 pipe section was welded inside the ends of the tubes for the connecting pins. The ends of the tubes were reinforced with a tubing support bracket fabricated from ASTM A36 steel plate.

Three crash tests were performed to evaluate the impact performance of different aspects of the median barrier gate to MASH standards. The first test performed on the Texas Department of Transportation (TxDOT) median barrier gate was according to MASH test designation no. 3-20. In this test, the 1100C small car impacted the median barrier gate upstream from its connection to the rigid concrete parapet at a speed of 62.6 mph and an angle of 24.6 degrees. No measurable dynamic or permanent deflection was noted and the test was successful.

The second test was according to MASH test designation no. 3-11 involving a 2270P pickup truck impacting 4.3 ft upstream from the midpoint of the median barrier gate at a speed and angle of 63.1 mph and 24.7 degrees, respectively. The maximum dynamic deflection of the median barrier gate during the test was 1.1 ft and the maximum permanent deformation was 0.8 ft. The test was successful.

The third test performed on the median barrier gate was according to MASH test designation no. 3-21 involving a 2270P pickup truck impacting the median barrier gate upstream from its connection to the rigid concrete parapet at a nominal speed of 63.1 mph and angle 25.5 degrees. The test, conducted to evaluate the strength of the connection between the median

barrier gate and concrete parapet as well as the potential for vehicle snagging in the transition section, was successful. Thus, the new median barrier gate passed all the required evaluation criteria for each test and met the TL-3 impact performance requirements of MASH.



Figure 7. TxDOT Median Barrier Gate [14]

#### **2.2.4 BarrierGuard 800 Median Gate**

The BarrierGuard 800 Barrier System and Gate manufactured by Barrier Systems Inc. is a modular steel barrier gate that is constructed from special sections of BarrierGuard 800 longitudinal barrier segments [14-18]. Schematics of the BarrierGuard 800 gate and joint system are shown in Figures 8 and 9.

The BarrierGuard 800 longitudinal barrier system is patent protected under World International Patent Organization no. WO2007/148110 [17]. The patent specifies a barrier with one or more upright and rail members that form part of the upright members and provide a crash surface. It also specifies a protruding member that projects out of the upright and/or rail members to create a recess or shoulder portion between the protruding members and the crash surface. The connection system between BarrierGuard 800 segments is also patent protected under U.S. Patent no. 2005/ 0249551 A1 [18], which covers a gate system that is connected using a base plate and utilizes parts of a mortise and tenon connection system on both the upper and lower connection joints. It provides a means for fixing the barrier element relative to the carriageway. The BarrierGuard 800 Gate utilizes an internal metal structure and a thrie beam connection to anchor the system to the adjacent concrete barriers. It is constructed of 0.2-in. thick A36 galvanized steel

panels assembled in either 19.7-ft or 39.4-ft sections. Each 39.4-ft long segment weighs approximately 2,381 lb.

The BarrierGuard 800 gate system was tested to meet the evaluation criteria of NCHRP Report 350 TL-3. The full-scale test was conducted on the BarrierGuard 800 gate under NCHRP Report 350 test designation no. 3-21, which involved a 2000P vehicle impacting the device at a speed of 60.8 mph and angle of 25 degree, at 13 ft upstream from the upstream hinge point of the gate. The vehicle was redirected along the length of the barrier and the test was successful. The maximum dynamic deflection was 46 in. and the permanent deflection was 42 in.

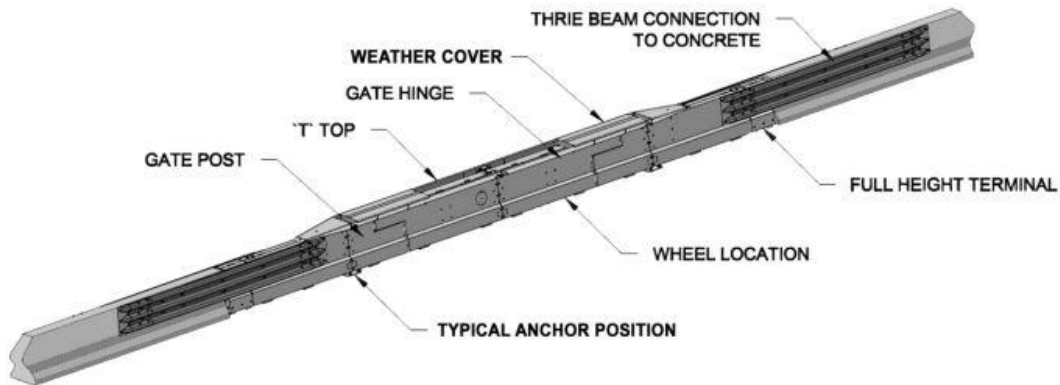


Figure 8. BarrierGuard 800 Gate System [18]

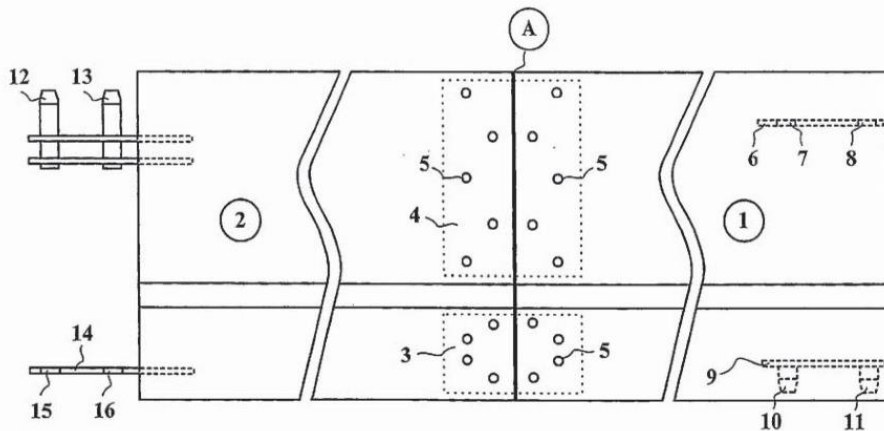


Figure 9. BarrierGuard 800 Joint System [18]

### 2.2.5 BarrierGate System

The BarrierGate system developed by Energy Absorption Systems Inc. is a longitudinal barrier used in conjunction with a concrete safety shape barrier to provide a temporary opening in the continuous barrier for use by emergency vehicles or re-routed traffic [19-22]. The BarrierGate consists of two half gates made with thrie-beam rail elements. In 1993, the BarrierGate system was patented under US patent no. 5,211,503 [21]. The patent specifies for a longitudinal barrier that

has the first and second axially aligned barrier segments separated by a gap that includes two elongated gates. The gate portions are mounted on rails with wheels for axial movement between the open and closed positions. The gates are designed to fit over and straddle the adjacent barrier segments and possess a profile that matches the shape of the barrier segments to eliminate snagging risk. These half gates slide along a track system and are opened by an electrical winch. When the two sections of the gate are closed, the sections form a mortise and tenon joint between the two segments. Drawings of the BarrierGate system are shown in Figure 10.

The BarrierGate system was evaluated under NCHRP Report 350 test designation nos. 3-10, 3-11, and 3-21. In all three tests, the vehicle was redirected with all occupant risk values falling within the acceptable range. The permanent deflection of the barrier for test no. 3-10, 3-11, and 3-21, was 0 in., 21 in., and 27 in., respectively. In all tests, the BarrierGate met the requirements for a TL-3 longitudinal barrier according to the criteria established in NCHRP Report 350.

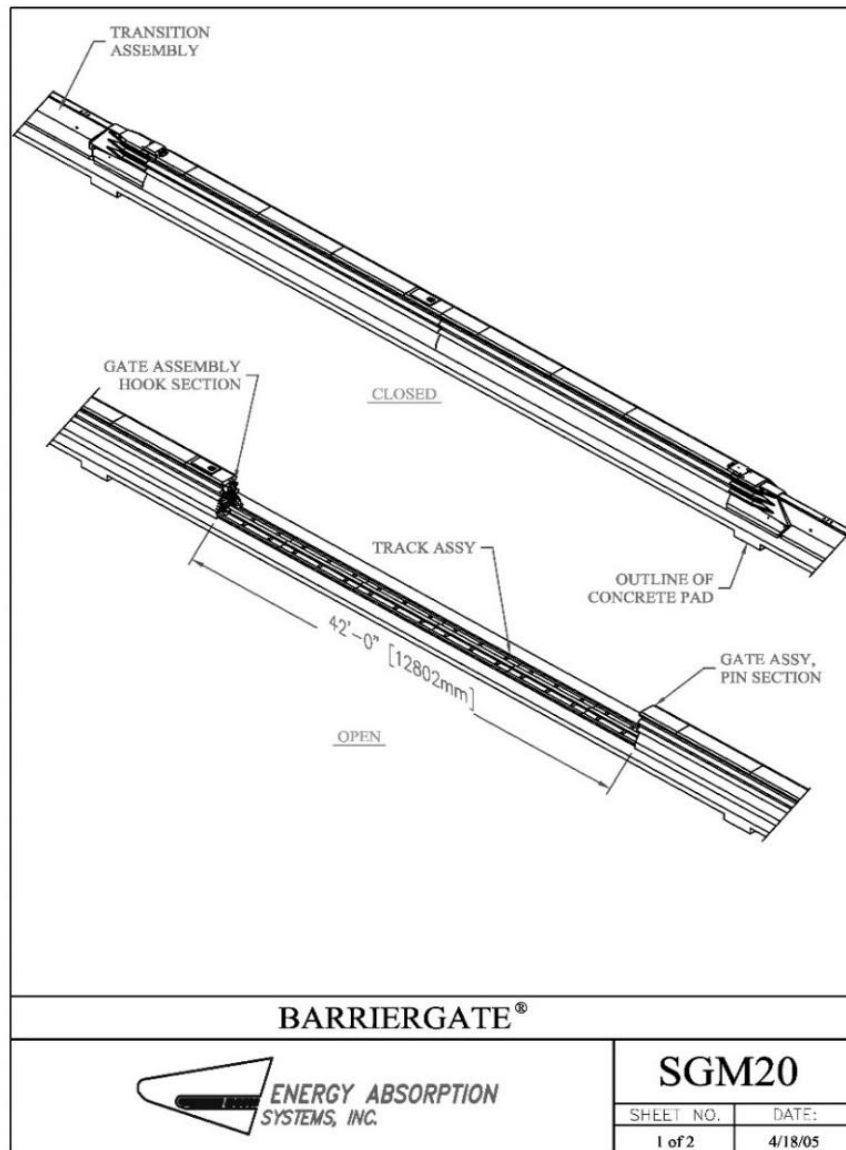


Figure 10. BarrierGate System [22]

## 2.2.6 Vulcan Barrier System and Gate

The Vulcan Barrier Gate from Energy Absorption Systems Inc. is constructed of two or more Vulcan Barrier segments that are pinned together and hinged on their ends, as shown in Figure 11 [23-26]. The Vulcan Barrier System is protected under US patent no. 8,393,822 B2 [24]. The patent outlines a barrier with a structural framework for resisting collapse of the barrier in an impact event and panels that are mounted to opposite sides of the barrier for deflecting vehicles upon barrier impact. The barrier is lightweight with a weight of less than 134 lb/ft. The barrier is stand-alone with no need for additional mass. The sides of the Vulcan Gate are constructed of AASHTO M180 thrie-beam panels. Each of the five steel bulkheads that tie the sides of the Vulcan together incorporate vertically aligned holes to aid in pinning multiple Vulcan segments together. Each segment is equipped with wheels attached to jacks that allow the segments to be lifted and rolled. The adjacent barriers to the gate as well as the transition portions of the gate assembly are anchored to the roadway. Each segment of the Vulcan system has a length of 162 in., a height of 32 in., and a width of 21.5 in.

The Vulcan Barrier is available in effective lengths of 13, 26, and 39 ft. Vulcan barriers use a vertical steel pivot pin to interlink each module allowing the system to follow curves of up to six degrees per four-meter segments. The Vulcan Barrier can be deployed as a free-standing system and is designed to be used with a variety of end terminal options, such as the Triton CET System or QuadGuard® CZ System, as shown in Figure 12. The barrier transition incorporates a lower steel mounting plate with twelve mounting holes for anchoring the transition to a rigid foundation when attaching to adjacent fixed barriers. Optional casters can be installed to simplify deployment and movement. The lightweight and stackable design allows up to 525 ft to be transported on one truck, offering a huge transport savings when compared to traditional concrete barriers [25]. The Vulcan Barrier can also be used as a median gate to allow traffic to be diverted for any reason, as shown in Figure 12.

One full scale crash test was conducted on the Vulcan Barrier Gate system following the guidelines established in NCHRP Report 350 test designation no. 3-21 [23]. In this test, five Vulcan Barriers were extended between two transition sections to rigid ends. During the test, a 2000P vehicle impacted the barriers 9.5 ft upstream from the rigid transition at a speed of 62.0 mph and an angle of 25 degrees. The Vulcan Barrier Gate safely redirected the vehicle with a maximum dynamic deflection of 15.75 in.



Figure 11. Vulcan Barrier Gate Assembly [23]



(a)



(b)



(c)

Figure 12. Vulcan Barrier (a) Portable Steel Longitudinal Barrier [25]; (b) Vulcan Barrier Transition; and (c) Vulcan Gate System [26]

## 2.3 Cover Plates

Several cover plate designs exist for spanning permanent concrete barrier gaps. The drawbacks of the existing cover plate designs include that they were designed for permanent barriers and not PCBs, they have not been full-scale crash tested to current safety standards, and they are only applicable to relatively small gaps. Previous testing of PCBs and joints in permanent concrete barriers has shown that there is potential for the vehicle body and wheels to snag in these barrier gaps and cause vehicle instability. Cover plates are often used to help minimize the potential for vehicle snag by preventing the vehicle from penetrating into the joint between the barriers. Selected cover plates currently in use are discussed in the following sections.

### 2.3.1 California Steel Channel Closure

In 1979, the California Department of Transportation (CALTRANS) investigated a system for spanning gaps in continuous concrete median barriers where storm drain catch basins were located to collect runoff from the median and adjacent freeway lanes [27]. The system was designed for use with a 32-in. tall permanent New Jersey shaped concrete median barrier with a 4-ft gap. Threaded rods measuring  $\frac{7}{8}$ -in. in diameter were cast into the ends of the permanent concrete median barriers at an embedment depth of 5 in. Hanger brackets were cut from pieces of C6x8.2 steel channel and bolted on the ends of the permanent concrete barrier. C6x8.2 beams were bolted to the hangers.

A full-scale crash test was conducted to determine the safety performance of the steel channel beams spanning a 4-ft long gap in a New Jersey concrete median barrier. In test no. 361, a 4,410-lb passenger car impacted the concrete median barrier system 5.2 ft upstream from the face of the 4-ft gap at a speed of 61 mph and an angle of 23 degrees. The gap-spanning hardware sustained minimal damage and the vehicle was safely contained and redirected. Consequently, test no. 361 was determined to be a success according to Transportation Research Circular No. 191 “*Recommended Procedures for Vehicle Crash Testing of Highway Appurtenances*” [28]. Since that testing, the California steel channel closure system has been modified and currently utilizes four C8x11.5 steel channel segments on each side of the barrier that are mounted on steel mounting brackets to be flush with the adjacent concrete barriers, as shown in Figure 13. The system is still specified to span an existing catch basin that requires a maximum of a 4-ft gap between two permanent concrete barriers.

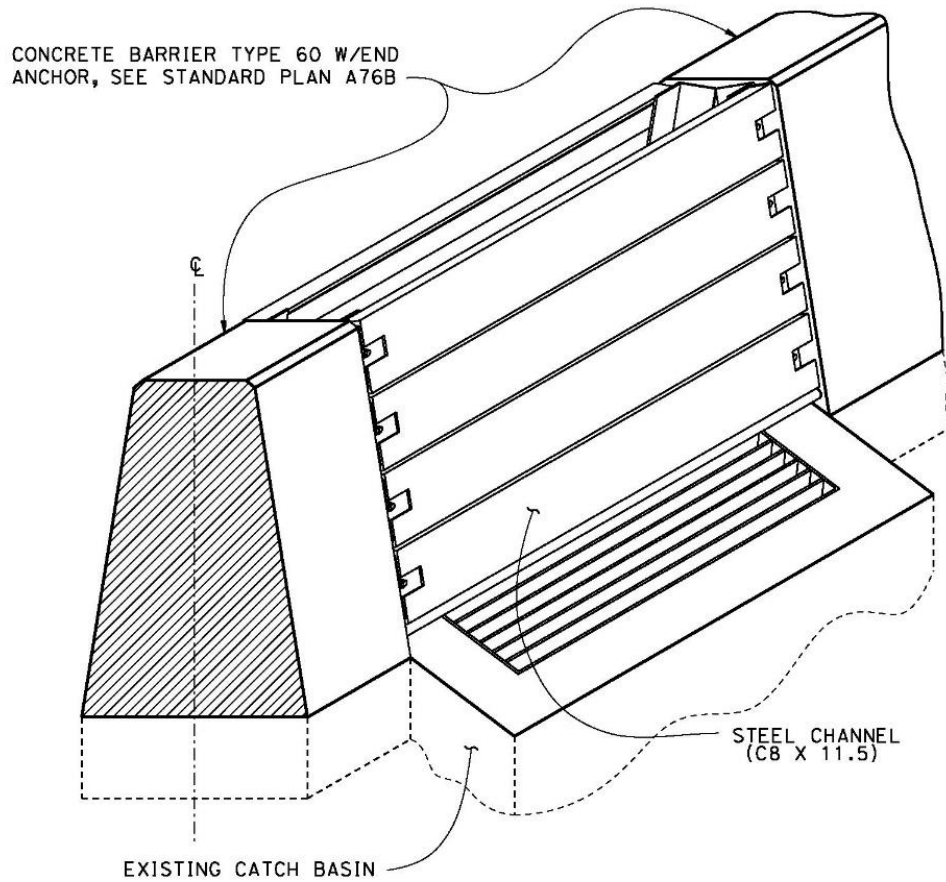
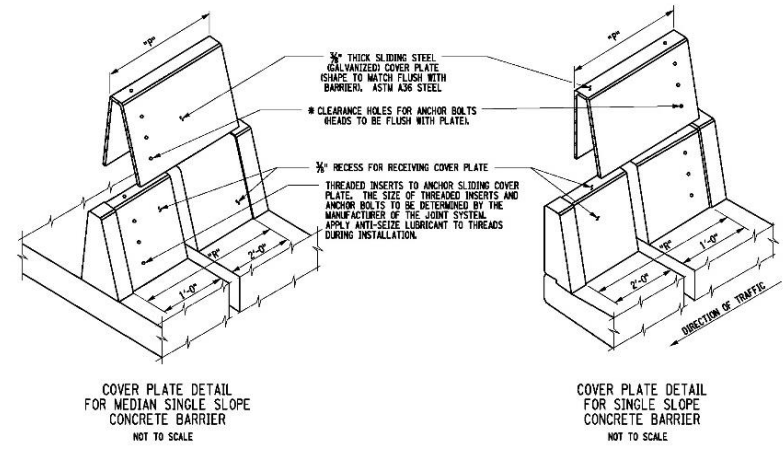


Figure 13. California Steel Channel Closure System. [29]

### 2.3.2 New York Modular Joint System

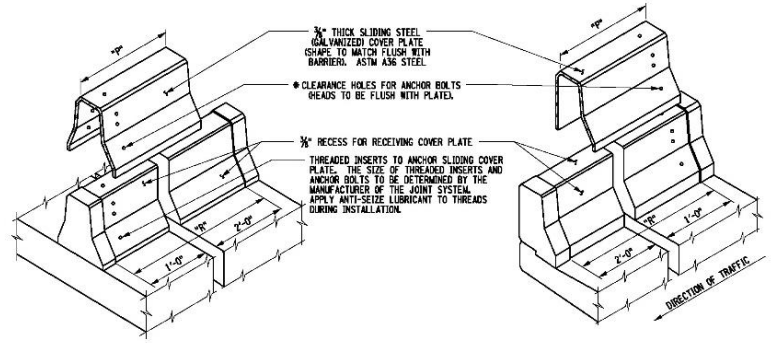
The New York Modular Joint System utilizes a  $\frac{3}{8}$ -in. thick galvanized ASTM A36 steel plate to bridge the gap between barrier sections, as shown in Figure 14 [30]. The cover plate is inserted into a recessed area on the face of the concrete barriers so it is flush with the front face of the barriers. The cover plate is attached to the concrete barriers with anchor bolts inserted into threaded inserts in the concrete barrier. The heads of the bolts are mounted to be flush with the face of the barrier to reduce the potential for vehicle snag on the bolt heads. There are no known crash tests of this system.



COVER PLATE DETAIL FOR MEDIAN SINGLE SLOPE CONCRETE BARRIER  
NOT TO SCALE

COVER PLATE DETAIL FOR SINGLE SLOPE CONCRETE BARRIER  
NOT TO SCALE

• THE SIZE OF THREADED INSERTS AND ANCHOR BOLTS TO BE DETERMINED BY THE MANUFACTURER OF THE JOINT SYSTEM. APPLY ANTI-SEIZE LUBRICANT TO THREADS DURING INSTALLATION.



COVER PLATE DETAIL FOR MEDIAN SAFETY SHAPE  
NOT TO SCALE

COVER PLATE DETAIL FOR SAFETY SHAPE  
NOT TO SCALE

NOTE: COVER PLATES SHALL BE INSTALLED FLUSH WITH THE EDGE OF THE RECESS ON THE BOLTED SIDE TO ALLOW CLEARANCE DURING BRIDGE TEMPERATURE EXPANSION.

FOR DIMENSIONS "P" AND "R", SEE BD-JM12E.

NOTE: DETAILS ON THE DRAWINGS LABELED AS "NOT TO SCALE" ARE INTENTIONALLY DRAWN NOT TO SCALE FOR VISUAL CLARITY. ALL OTHER DETAILS, FOR WHICH NO SCALE IS SHOWN, ARE DRAWN PROPORTIONAL AND ARE FULLY DIMENSIONED.

ISSUED 5/03/08		STATE OF NEW YORK DEPARTMENT OF TRANSPORTATION OFFICE OF STRUCTURES
REVISED		MODULAR JOINT SYSTEM MULTICELL MISCELLANEOUS DETAILS
APPROVED: 1/18/08	ORIGINAL SIGNED BY GEORGE A. CHRISTIAN, P.E. DEPUTY CHIEF ENGINEER (STRUCTURES)	ISSUED UNDER EB 08-002 EFFECTIVE WITH THE LETTING OF 1/08/09

Figure 14. New York Modular Joint System [30]

### 2.3.3 Kansas Expansion Joint

The Kansas expansion joint is utilized to span a thermal expansion joint in anchored PCBs with a span of 4 in. or less. The system utilizes a ½-in. thick steel plate bent to the shape of the concrete barrier and two 1-in. diameter x 28-in. long dowels inserted into the adjacent concrete barriers, as shown in Figure 15. The adjacent concrete barriers have a 1-in. deep recessed portion that allows the steel plate to fit within the exterior profile of the concrete barriers. The steel plate is attached to the concrete barrier on one side of the gap using six 1-in. diameter flat head socket cap screws. The bolt holes in the steel plate are recessed so that the heads of the bolts are flush with the face of the steel plate. The Kansas expansion joint has not been full-scale crash tested to evaluate its safety performance.



Figure 15. Example of Steel Cover Plate at Expansion/Contraction Joints

## 2.4 Additional Patented Systems

While conducting the literature review, additional patents were discovered that could not be matched to products currently in the marketplace. While these systems are not being produced, the patents covering the design aspects of the system were reviewed to provide insight into the development of the system outlined in this report.

### 2.4.1 Removable Barrier

European Patent Office no. 0438267 A1 relates to a removable barrier that is adapted to co-operate with a median barrier on a roadway to form a barrier that can open and allow traffic to pass through. This system allows the two gate segments to slide over the top of the existing barriers to open the gate [33].

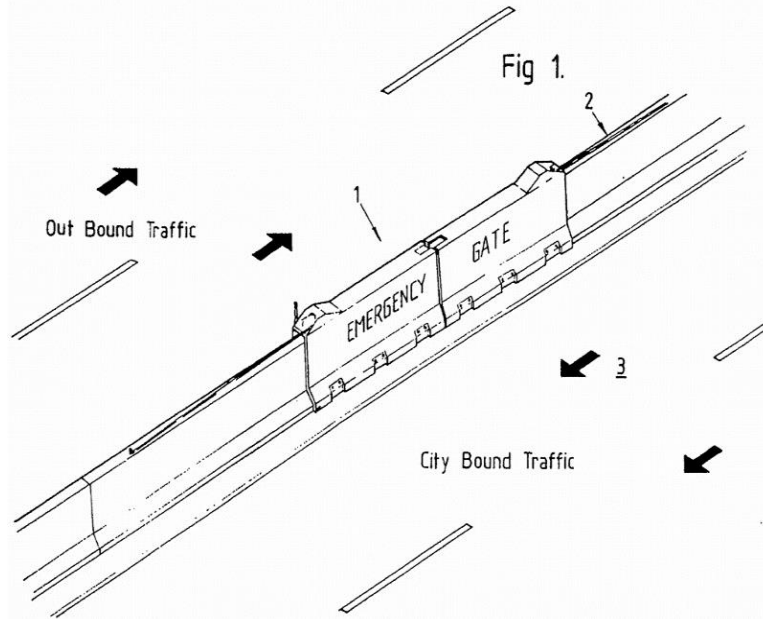


Figure 16. Removable Barrier [33]

### 2.4.2 Modules for Bridging Openings in Road Guard Barriers

World Intellectual Property Organization (WIPO) patent no. WO 86/03239 details a module that can bridge openings that allow for obstacle clearance such as light poles or drainage ditches. The module consists of corrugated panels and one or more stiffener beams attached to one another using bolts and mounting brackets. The stiffener beam is required in one of the panels for providing increased rigidity. The device is mounted to bridge an opening to redirect an impacting vehicle [34].

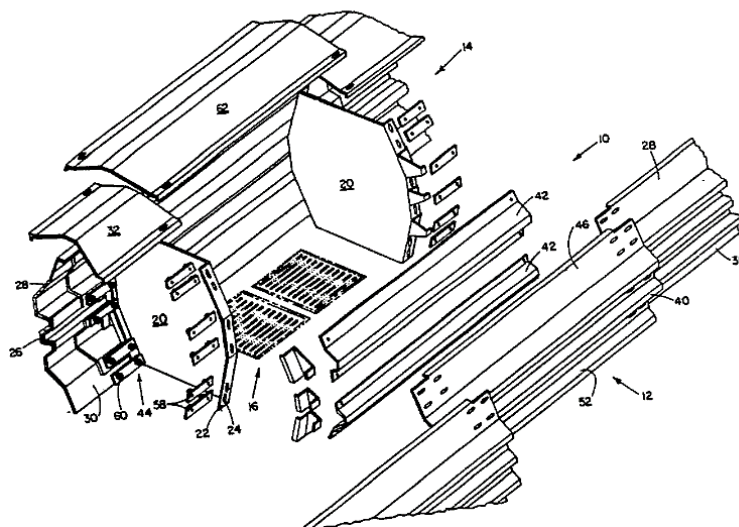


Figure 17. Module for Bridging Openings in Road Guard Barriers [34]

### 2.4.3 Gate Means, Preferably for Use with Barrier Elements

World Intellectual Property Organization patent no. 2005/003465 A1 specifies a gate for use with barrier elements for delimiting of lanes or serving as a longitudinal barrier. The gate element utilizes locking pins that are fixed at protruding loops on the framing elements and adjacent barrier segments. The gate system can be opened from both sides and is able to pivot open up to 180 degrees when one of the pins is removed [35].

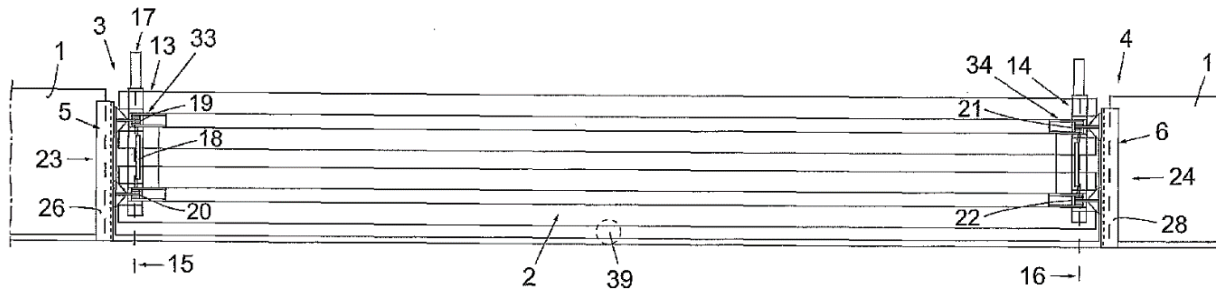


Figure 18. Gate Means, Preferably for Use with Barrier Elements [35]

## 2.5 Miscellaneous Gap-Spanning Systems

### 2.5.1 Metal Transition for Branching Concrete Barriers

TTI conducted two MASH-compliant tests on a metal transition for branching concrete barriers. This metal transition connects a portable concrete barrier to a permanent concrete barrier such that temporary barrier branches off from the permanent barrier and forms a row of portable concrete barriers installed parallel to the permanent barrier [36].

The test installation consisted of a series of pre-cast permanent concrete median barriers, transitional portable concrete barriers (PCBs), and offset PCBs positioned to allow for the installation of a portable variable message sign (PVMS) and its support structure, as shown in Figure 19. A steel transition barrier section provided the connection between the permanent barriers and the offset PCBs. The total length of the test installation was 197 ft. The installation was constructed on a 132-in. wide x 3-in. thick hot mix asphalt concrete. The permanent median barrier was a keyed-in 44-in. tall New Jersey (NJ) Tall Wall barrier. The transitional PCBs were pinned down F-shape concrete barrier segments with cross-bolted connections. These transitional PCBs were connected to the permanent NJ Tall Wall barrier using a fabricated steel transition attachment that was 429 in. long x 31.6 in. tall. It provided a smooth transition between the permanent concrete median barriers (CMBs) and the first transitional PCB. The traffic side face of the transition was a smooth panel that conformed to the profile of the concrete barriers. This panel was reinforced with four HSS tubes and lateral supports [36].

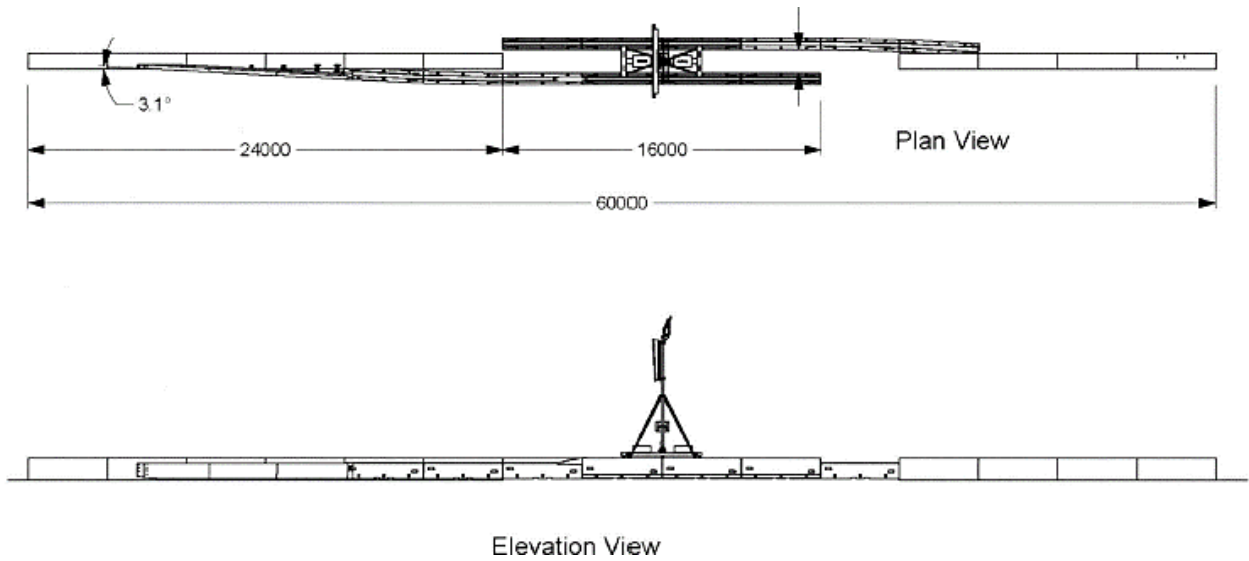


Figure 19. Layout of the Branching Transition and Barrier Mounted Sign Installation [36]

Two MASH-compliant tests were conducted on this configuration. In the first test, a 2,462-lb small car impacted the steel transition at a speed and angle of 62.4 mph and 25.1 degrees, respectively, and was contained and redirected by the transition. This test yielded a maximum dynamic deflection of 1.2 in. and the maximum roll and pitch angles were 23 degrees and 11 degrees, respectively. The device performed acceptably according to MASH test designation no. 3-20 criteria. The second test was conducted according to MASH test designation no. 3-21 and consisted of a 2270P pickup truck impacting the steel transition at a speed and angle of 62 mph and 24.9 degrees, respectively. This test yielded a maximum dynamic deflection of 1.6 in. and the maximum roll and pitch angles were 16 degrees and 18 degrees, respectively. The device performed acceptably according to MASH test designation no. 3-21 criteria.

### **3 DEVELOPMENT OF DESIGN CONCEPTS**

#### **3.1 Design Criteria**

Prior to the development of design concepts for gap-spanning hardware, discussions were held between the researchers and sponsors to define the design criteria for the prototype PCB gap-spanning hardware. Within the project objective, the following design criteria were identified:

1. The system should be designed for the 12.5-ft long, F-shape PCB with pin-and-loop connections developed through the Midwest Pooled Fund Program.
2. The system should be capable of accommodating variable gap lengths ranging from 6 in. to 12.5 ft.
3. The system should be crashworthy under MASH TL-3 impact conditions.
4. The design needed to provide proper load transfer between the barriers adjacent to the gap. Free-standing PCB systems rely on load transfer between barrier segments to function properly. Thus, the gap treatment hardware needed to provide a means of transferring shear and tensile loads across the gap, thus providing for a continuous barrier system.
5. The design also needed to provide sufficient lateral stiffness and strength to capture errant vehicles and prevent vehicle snag on the adjacent PCB segment. Vehicle snag can result in vehicle instabilities, excessive Occupant Ridedown Acceleration (ORA) and Occupant Impact Velocity (OIV) values, and/or hardware failures.
6. It was desired that the gap between adjacent runs of PCBs be accommodated without overlapping barrier segments in order to minimize the overall width of the system.
7. It was desired that the design required no special PCB segments or modified PCB end sections.
8. It was desired that the design limited the number of components and used standard components when possible.
9. It was desired that the design required minimal field fabrication.

#### **3.2 Design Concepts**

A variety of concepts were brainstormed for treating the gaps between adjacent runs of PCBs. A series of design concepts were generated and drawn as schematics for further evaluation. The schematics of design concepts are shown in Figures 20 through 33. The seven concepts for treating gaps between adjacent PCB segments were as follows:

1. Concept No. 1 – Internal Modular System 1
2. Concept No. 2 – Internal Modular System 2
3. Concept No. 3 – External Modular Cover Plates
4. Concept No. 4 – Thrie Beam and Toe Plate
5. Concept No. 5 – Cover Plate
6. Concept No. 6 – Cover Plate and Beam
7. Concept No. 7 – Two-Piece Cover Plate

### 3.2.1 Concept No. 1 – Internal Modular System 1

An internal modular system concept for addressing gaps in adjacent PCBs was developed which consisted of short barrier segments of various lengths to bridge the gap between PCBs, as shown in Figures 20 and 21. The segments would be made from concrete or steel and would employ a pin-and-loop connection between each segment similar to an F-shape PCB. A family or kit of various barrier lengths would be necessary to ensure that gap lengths from 10 in. to 12.5 ft could be accommodated. Although there is no anchoring to the face of the PCBs, segment joints spaced closely together may potentially pose a snag hazard. This concept design has no components external to the gap and does not require anchoring to the PCBs, but the large number of closely spaced joints may cause excessive barrier deflections in the gap region. A minimum gap of 10 in. between PCBs would be necessary to utilize this system concept.

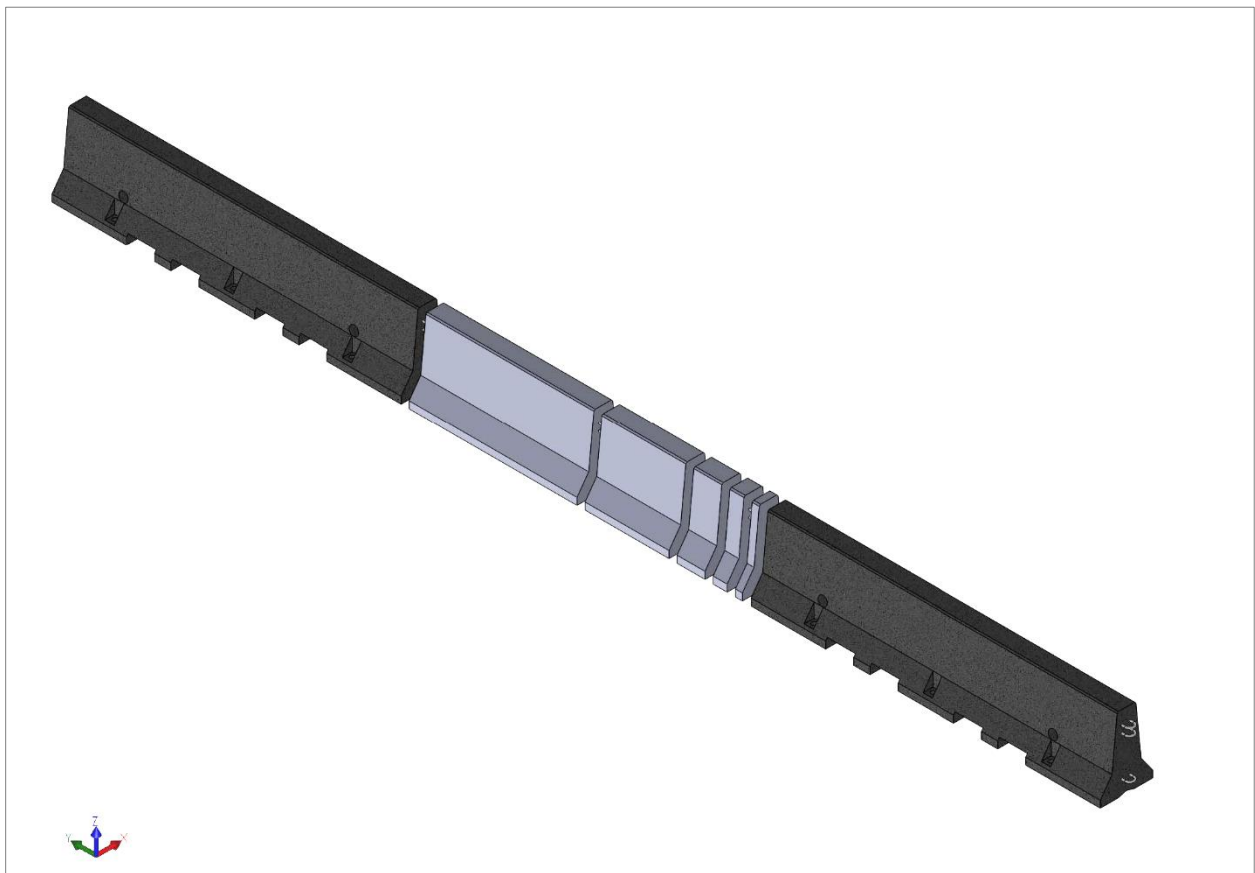


Figure 20. Concept No. 1 – Internal Modular System 1

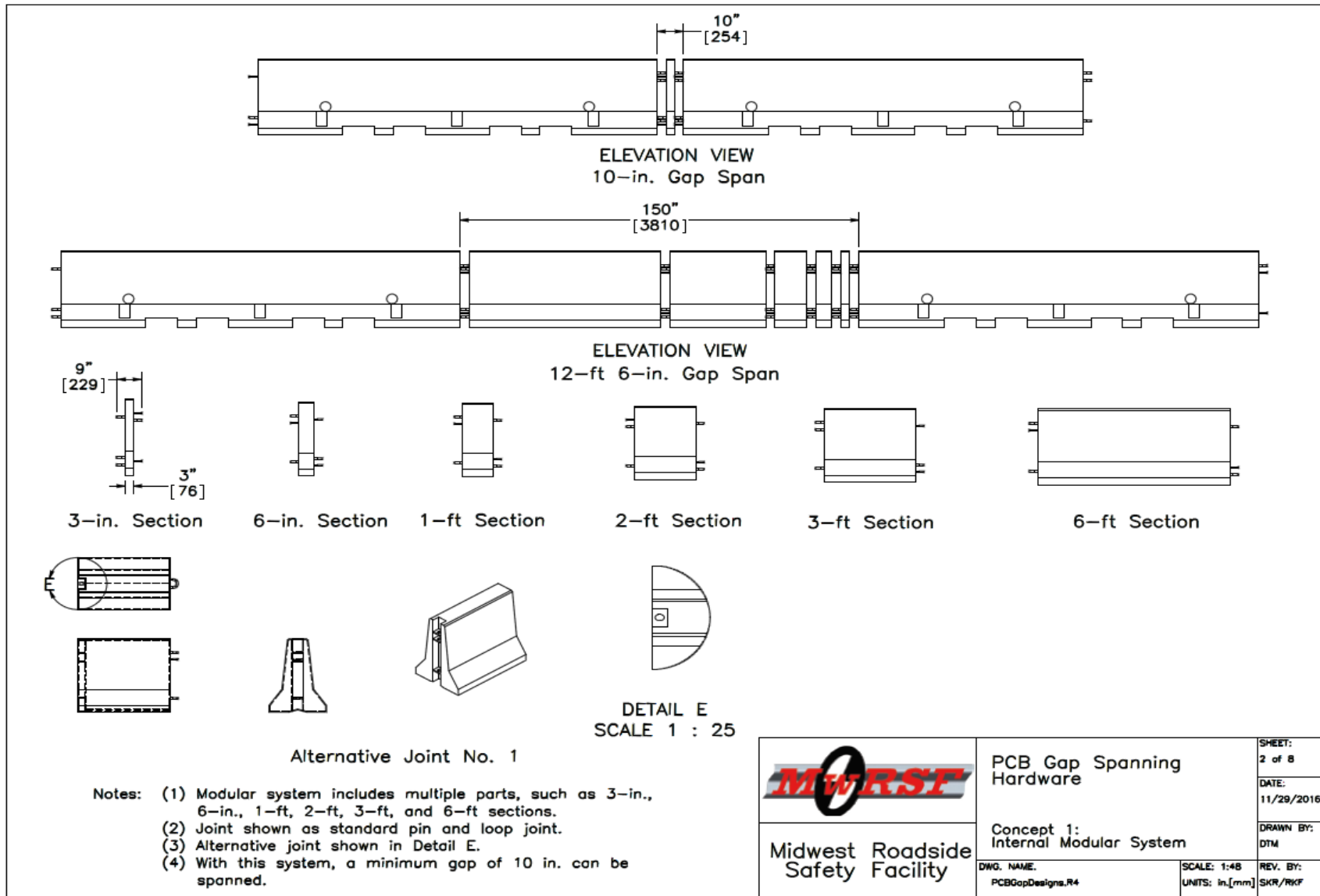


Figure 21. Design Details, Concept No. 1 – Internal Modular System 1

### 3.2.2 Concept No. 2 – Internal Modular System 2

The second concept for an internal modular system for addressing gaps in adjacent PCBs was modular like the first concept except that individual steel segments were bolted together to create a continuous steel barrier spanning the PCB gaps, as shown in Figures 22 and 23. Like the previous concept, a family or kit of various segment lengths would be necessary to ensure that all gap lengths between 10 in. and 12.5 ft could be accommodated. A pin-and-loop connection was used to connect the modular system's steel barriers to the adjacent PCBs. This concept would reduce vehicle snag as there were no extra joints and no external hardware mounted on the face of the PCBs. A minimum gap of 10 in. would be necessary to utilize this system concept. The steel segments would need to be assembled while laying on their sides to expose the underside and inside of the hollow segments. This concept design was deemed relatively labor intensive to install as each steel segment required several bolted joints.

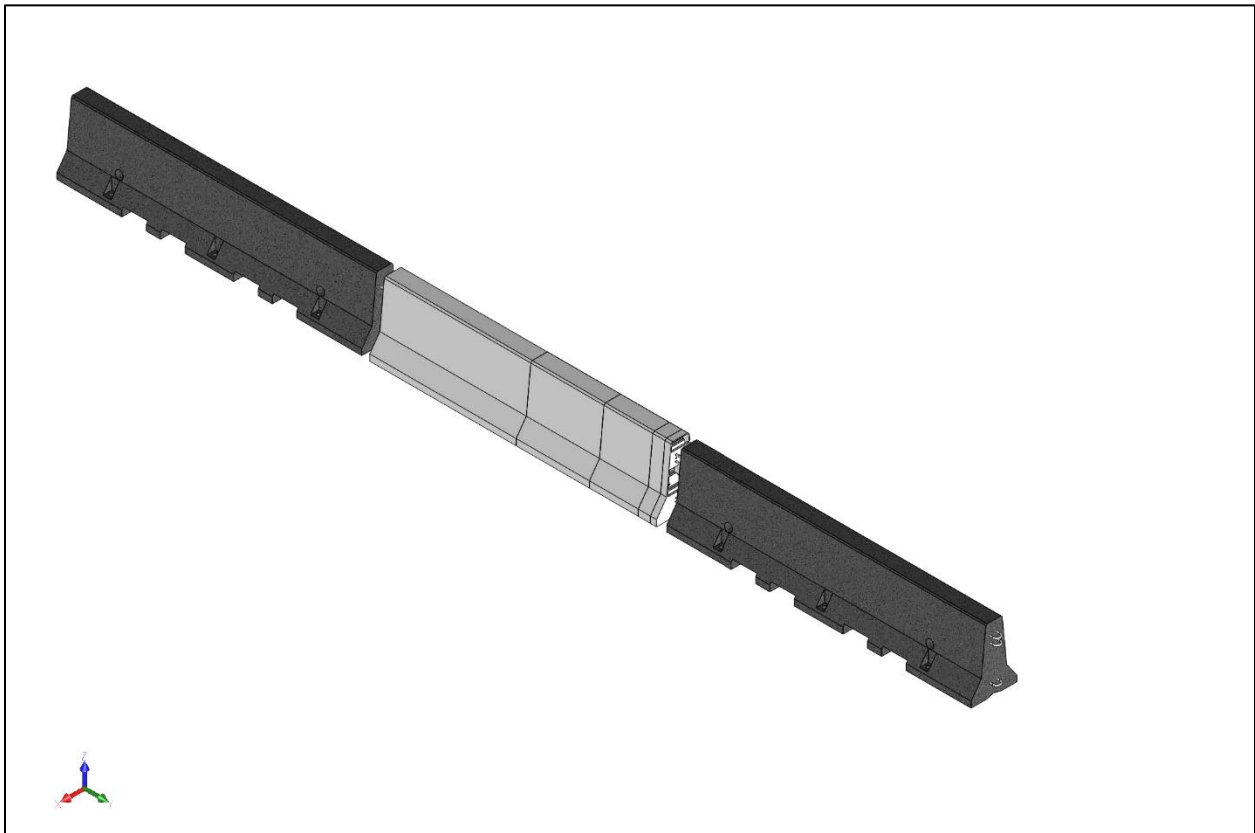


Figure 22. Concept No. 2 – Internal Modular System 2

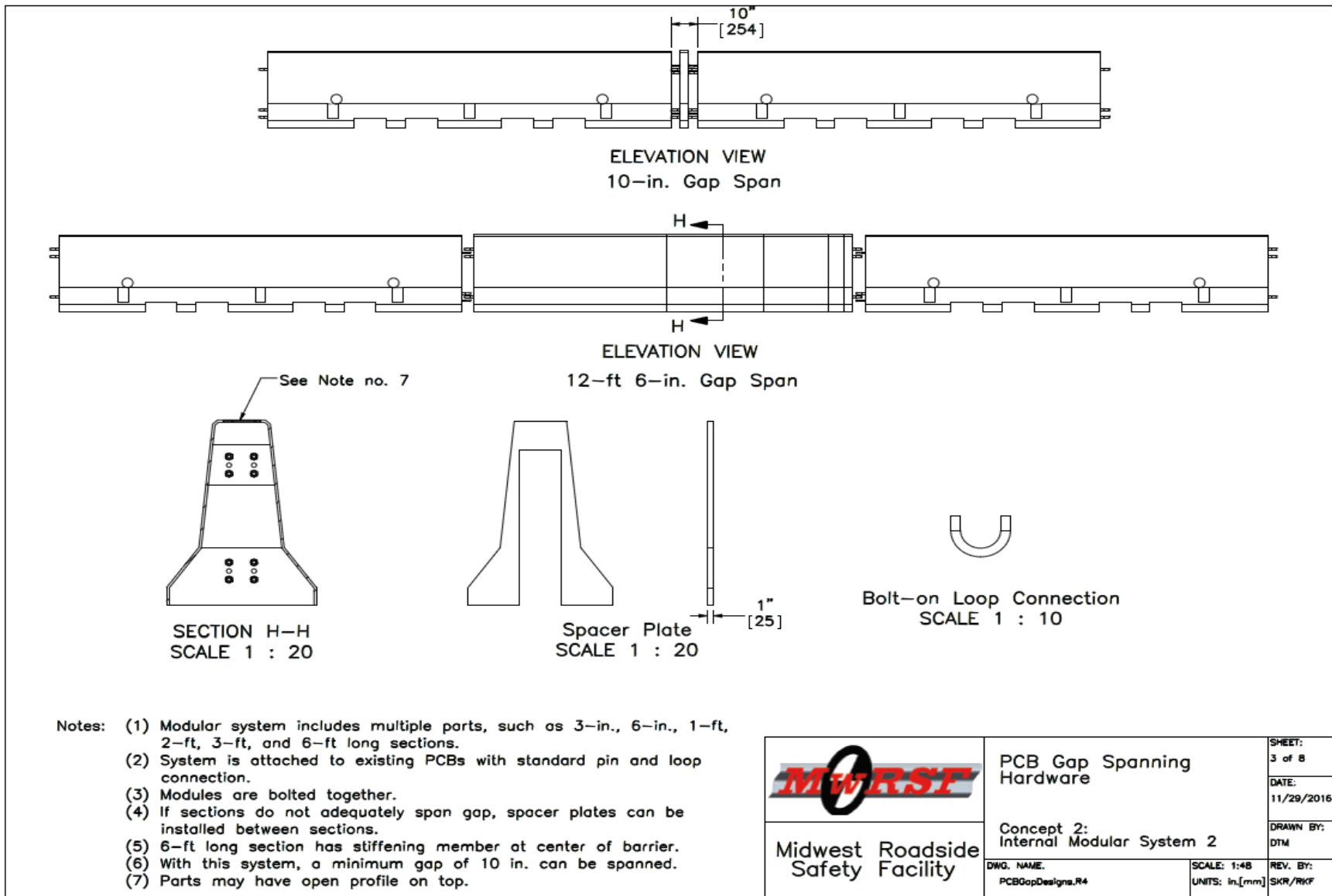


Figure 23. Design Details, Concept No. 2 – Internal Modular System 2

### 3.2.3 Concept No. 3 – External Modular Cover Plates

A concept for an external modular system for addressing gaps in adjacent PCBs was developed that consisted of steel cover plates and internal stiffeners bolted together, as shown in Figures 24 and 25. These components could be repeated to span the variable gap sizes between PCB segments. The internal stiffener assemblies had cross sections matching the F-shape PCB segments. The steel cover plates were designed to match the profile of the F-shape PCBs. On both sides of the gap, the cover plates were anchored to the face of the PCBs to provide tensile and shear load transfer. In this concept, multiple assemblies with plates, stiffeners, and bolts were required. The individual components are relatively small and would be easy to transport. The size and thickness of the cover plates and the stiffener plates would be determined through analysis and evaluation of the hardware. Assembly of the system would require bolting together the various steel components as well as anchoring the cover plates to the PCB segments on each end of the gap.

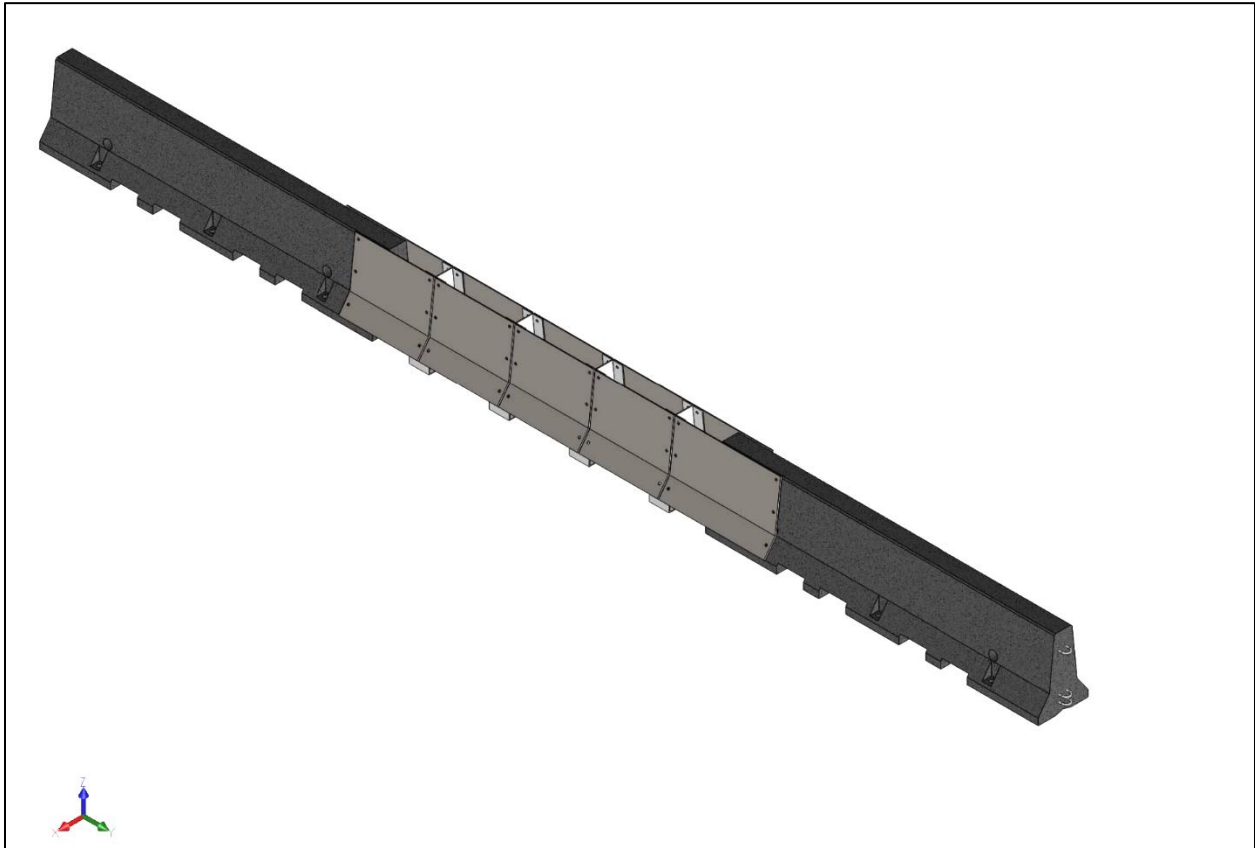


Figure 24. Concept No. 3 – External Modular Cover Plate

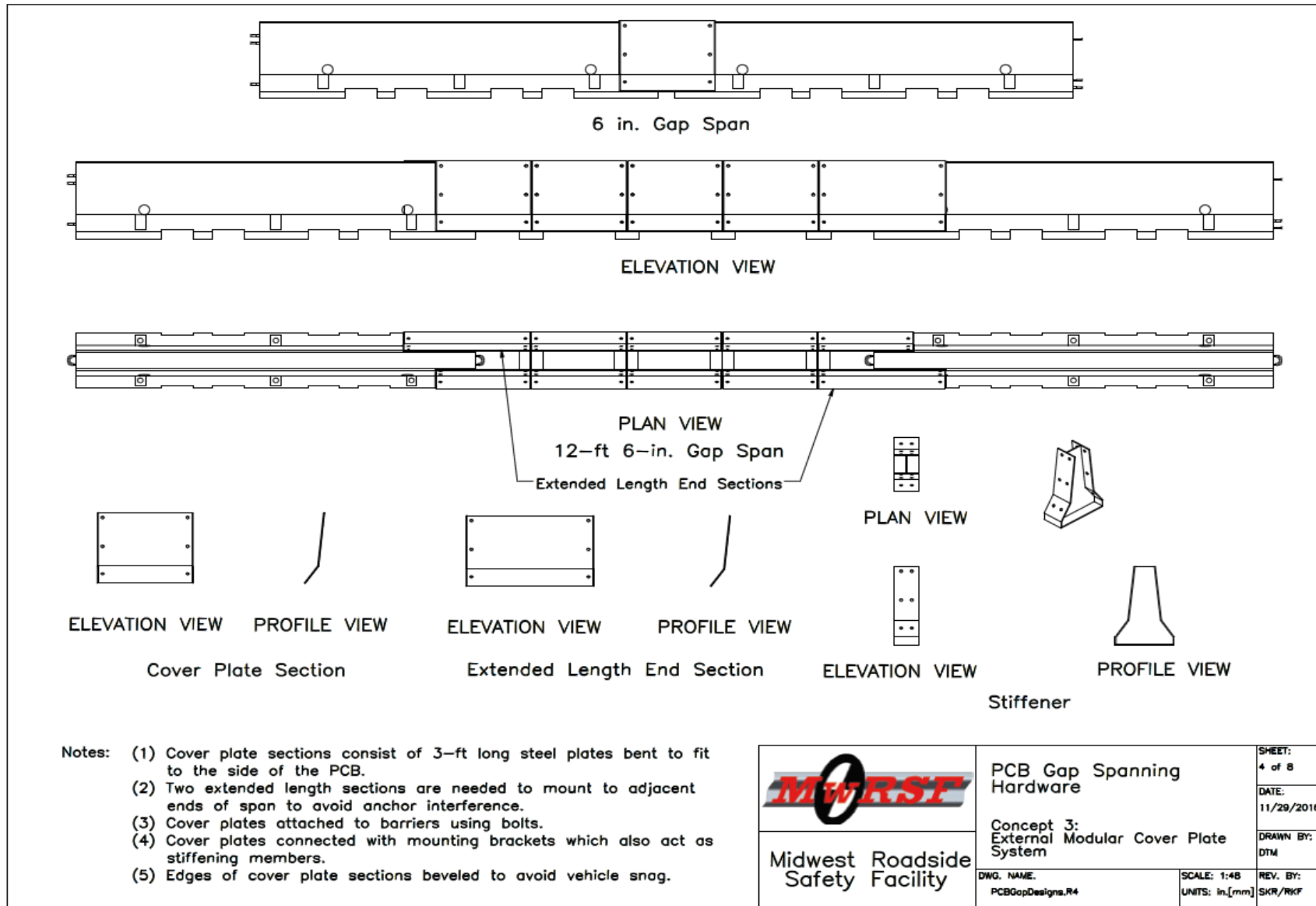


Figure 25. Design Details, Concept No. 3 – External Modular Cover Plate

### 3.2.4 Concept No. 4 – Thrie Beam and Toe Plate

The fourth concept for addressing gaps in adjacent PCBs consisted of two nested thrie-beam rail sections attached to the front and back sides of the PCBs adjacent to the gap with thrie beam terminal connectors and wedge bolt anchors, as shown in Figures 26 and 27. Steel stiffeners were inserted between the parallel rail sections to strengthen rails and prevent large deformations of the thrie beam when longer gap lengths were encountered. The number of stiffeners installed between thrie-beam rails could be adjusted depending on the gap length. To minimize vehicle wheel snag during impacts, steel toe plates were added below the thrie beam and attached to the lower slope, or toe, of the PCBs. This concept effectively creates a long rigid segment within a PCB installation, which may stiffen the system in that region and reduce barrier deflections. Thus, evaluation of the concept requires analysis of impacts upstream from the gap to investigate barrier loading, deflections, and pocketing in this stiffness transition region. This concept utilized mostly existing hardware components with the exception of the toe plates and stiffeners. Assembly of the system would require bolting together the various steel components as well as anchoring the thrie beam and toe plate to the PCB segments on each end of the gap.



Figure 26. Concept No. 4 – Thrie Beam and Toe Plate

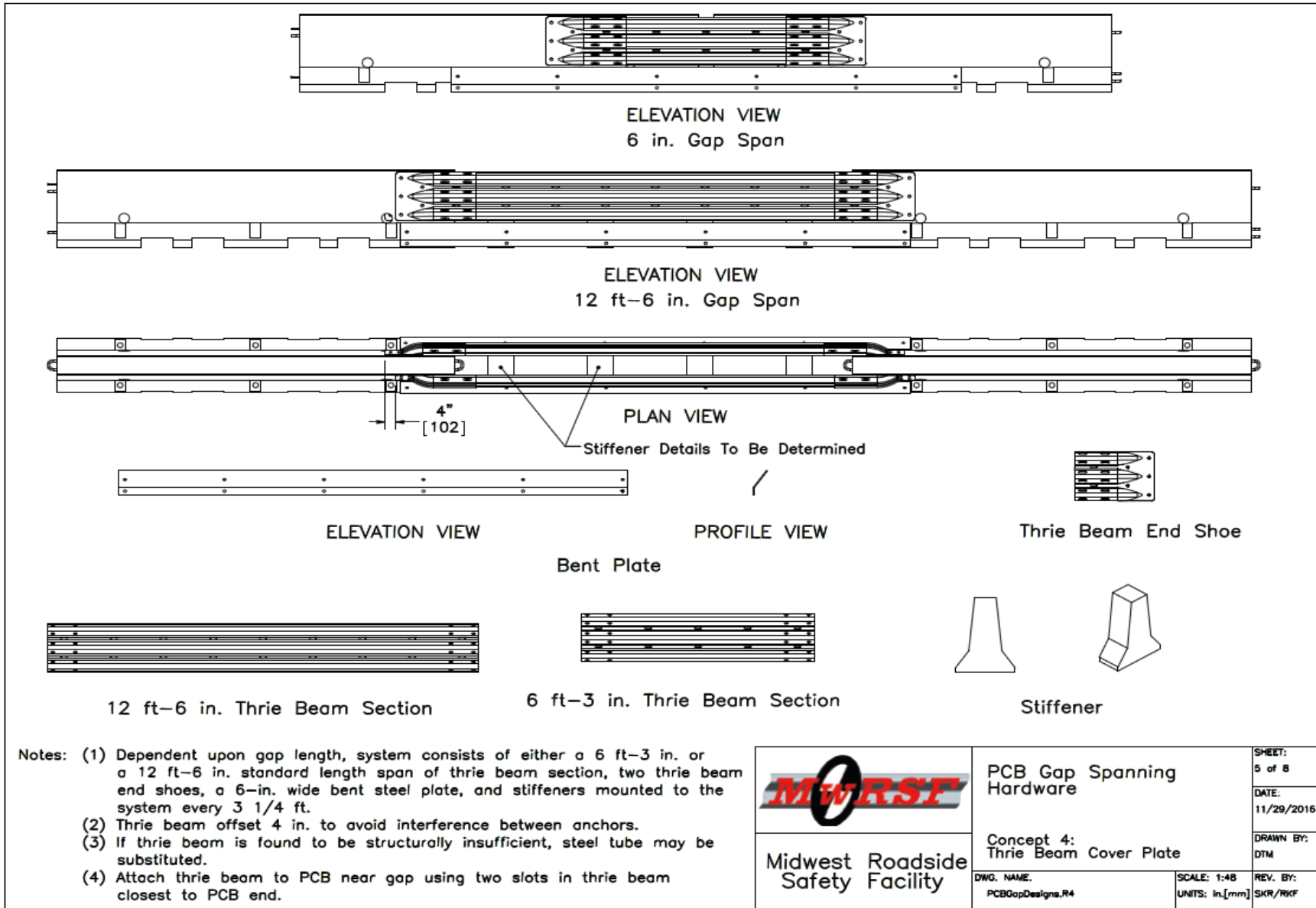


Figure 27. Design Details, Concept No. 4 – Thrie Beam and Toe Plate

### 3.2.5 Concept No. 5 – Cover Plate

The fifth concept for addressing gaps between adjacent PCB segments consisted of a single steel cover plate spanning the gap between adjacent PCBs, as shown in Figures 28 and 29. The cover plate matched the F-shape profile of the PCBs and fit over the top of the PCB segments. The steel section for this concept would likely need to be 15 ft to 17 ft long and fabricated by welding steel plates together. The cover plate was anchored to the face of PCBs on each end of the gap and would be chamfered to prevent vehicle snag. Internal stiffeners would likely be required when longer gap lengths are encountered to provide proper lateral strength. This concept effectively created a long rigid segment within a PCB installation, which may stiffen the system in that region and reduce barrier deflections. Thus, evaluation of the concept would require analysis of impacts upstream from the gap to investigate barrier loading, deflections, and pocketing. This concept requires minimal assembly, but the large cover plate segment may be relatively difficult to transport and handle during installation. Assembly issues may arise from construction tolerances if the PCBs are not cast to the exact width specified, thereby leaving gaps between the PCB face and the cover plate or not allowing the cover plate to fit over the PCB.

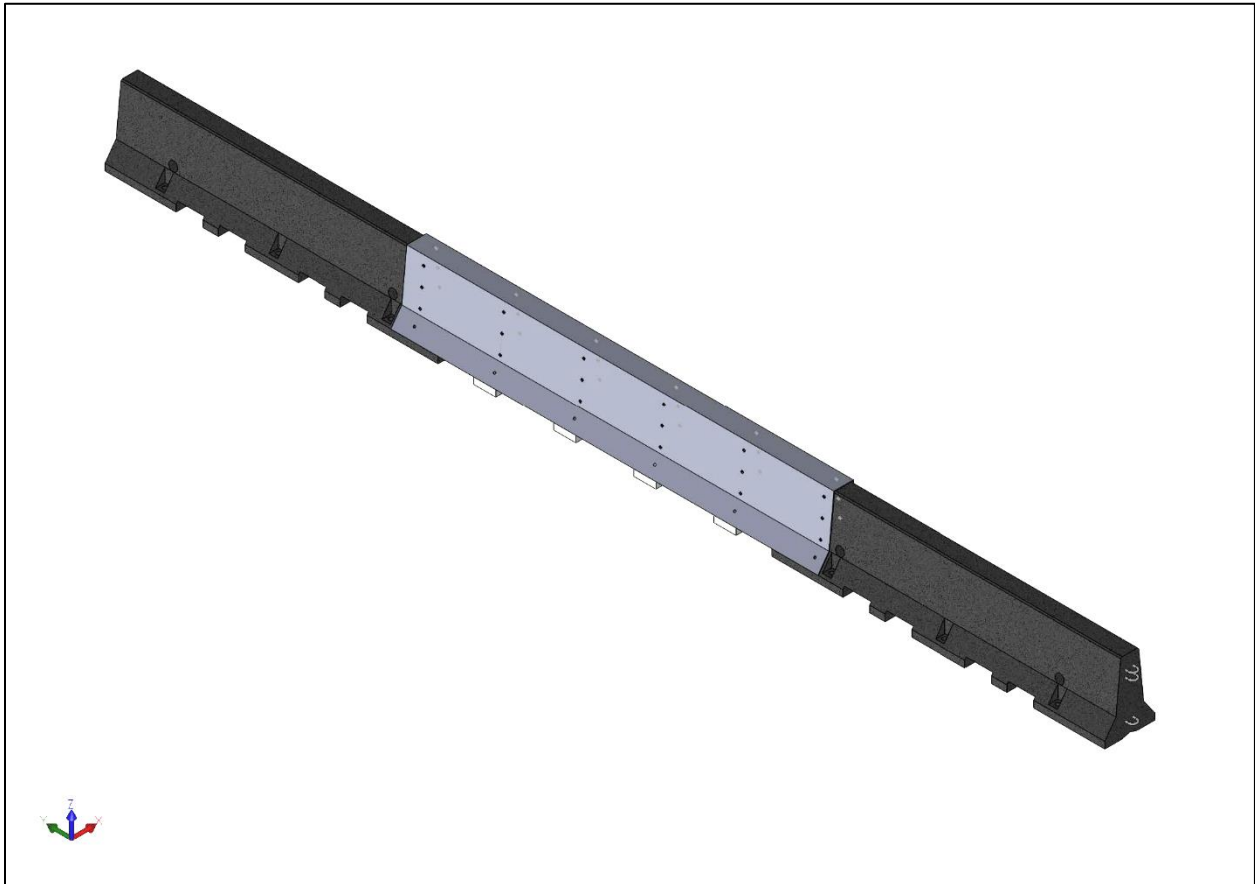


Figure 28. Concept No. 5 – Cover Plate

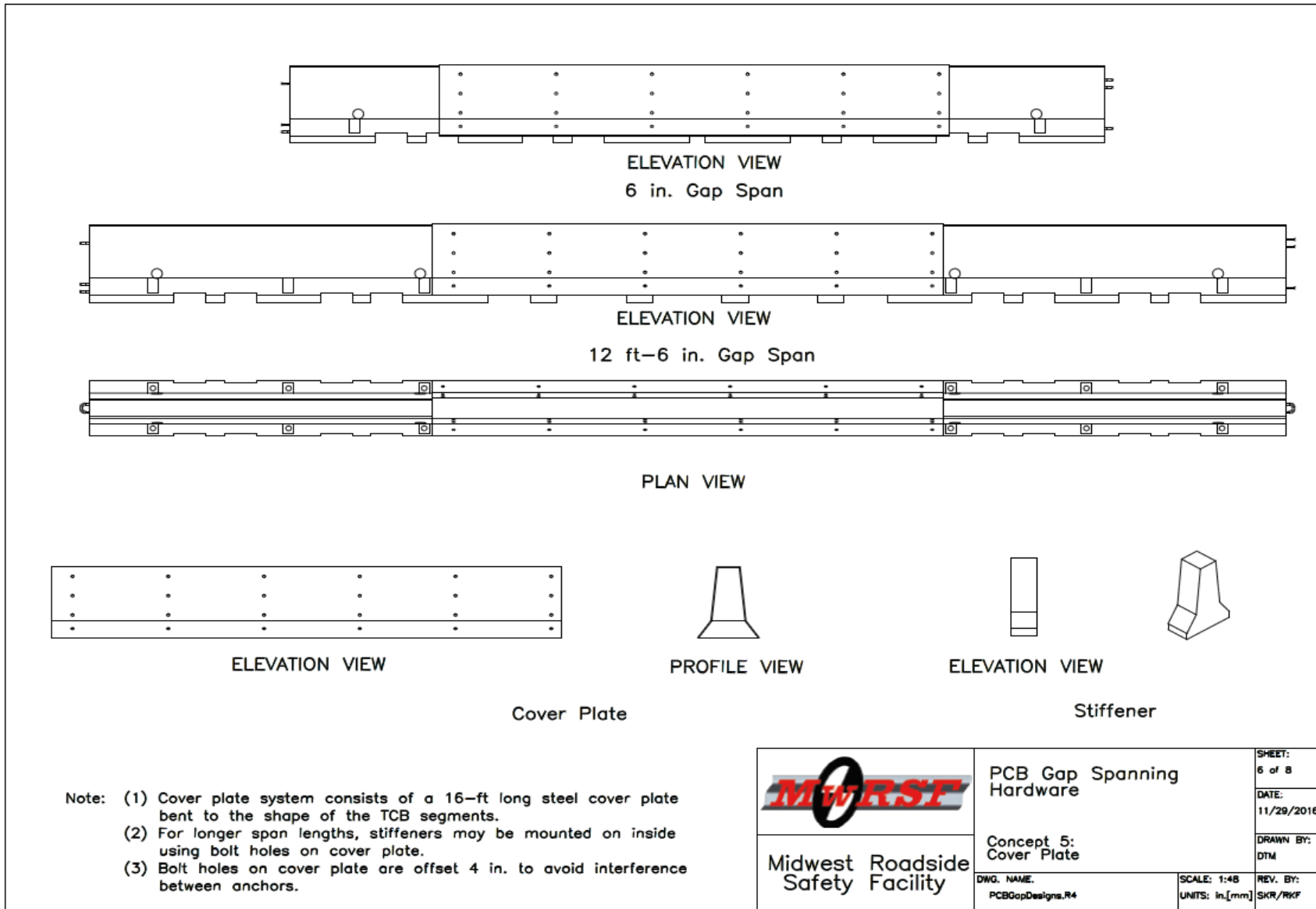


Figure 29. Design Details, Concept No. 5 – Cover Plate

### 3.2.6 Concept No. 6 – Cover Plate and Beam

Concept no. 6 was similar to concept no. 5 except that a steel tube was welded to both sides of the cover plate, as shown in Figures 30 and 31. The steel tube increased the strength of cover plate and would eliminate the need for internal stiffeners. Also, as witnessed during the testing of a retrofit reduced-deflection PCB for the Wisconsin Department of Transportation [38], the tube would provide increased vehicle stability by limiting vehicle climb during impacts. Other advantages and disadvantages of concept no. 6 were similar to concept no. 5.



Figure 30. Concept No. 6 – Cover Plate and Beam

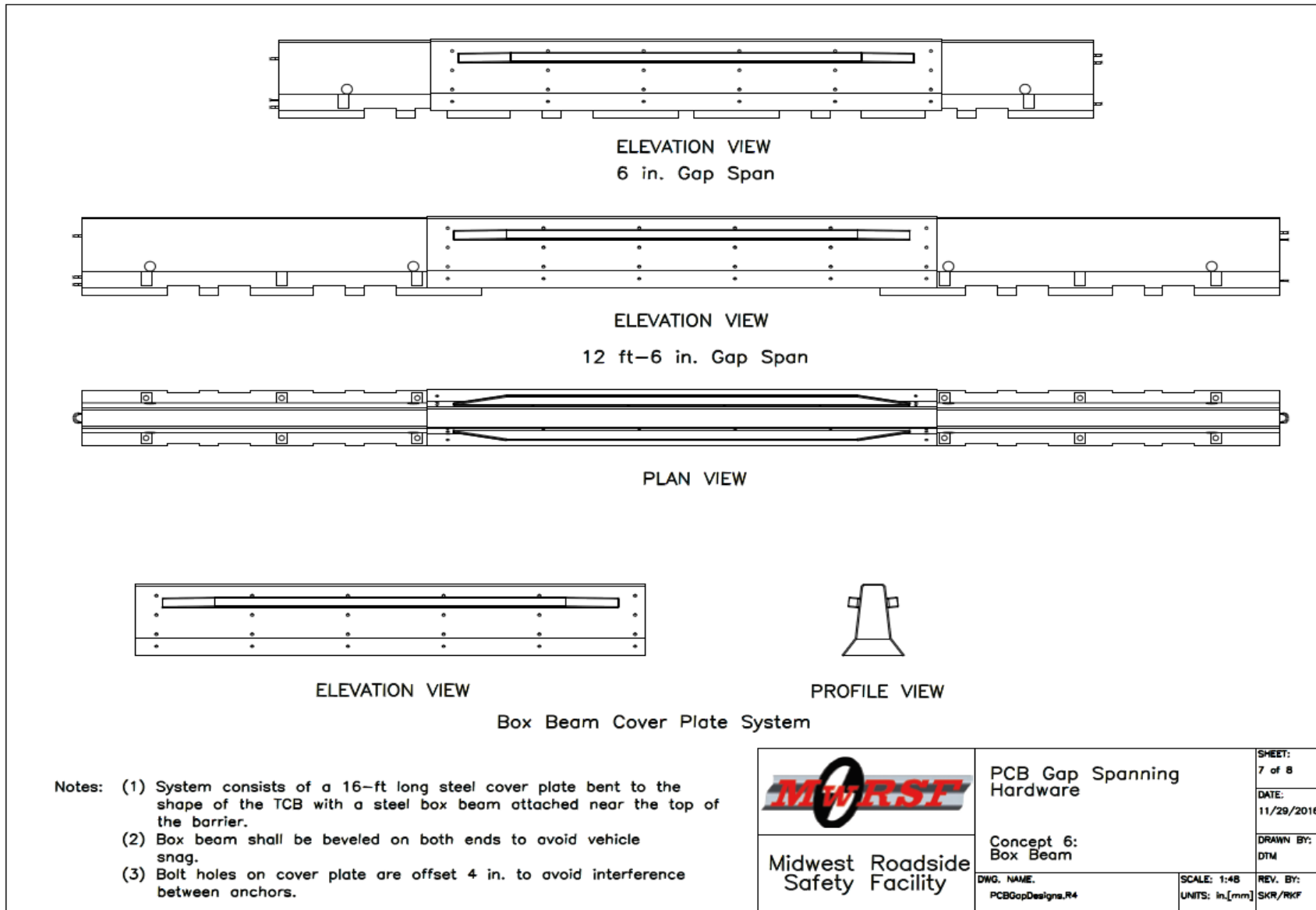


Figure 31. Design Details, Concept No. 6 – Cover Plate and Beam

### 3.2.7 Concept No. 7 – Two-Piece Cover Plate

Concept no. 7 was a variation of the single cover plate concept (concept no. 5) constructed by splitting the cover plate into two pieces and inserting a standard pin and loop joint between the two cover plate assemblies, as shown in Figures 32 and 33. The cover plate was connected to PCB segments using concrete anchor bolts. If a gap were less than 6.25 ft, only one cover plate would be required to extend from one PCB segment and connect to another using the standard pin and loop connection. If a gap were longer than 6.25 ft, two cover plates would be needed. The smaller size of the steel segments makes them easier to transport and install as compared to the single cover plate concepts (concept nos. 5 and 6). Moreover, with a joint placed in the middle of long segments, the performance of the PCB system should be less affected than it would be for concept nos. 5 and 6. Assembly issues may arise from construction tolerances if the PCBs are not cast to the exact width specified, thereby leaving gaps between the PCB face and the cover plate or not allowing the cover plate to fit over the PCB.



Figure 32. Concept No. 7 – Two-Piece Cover Plate

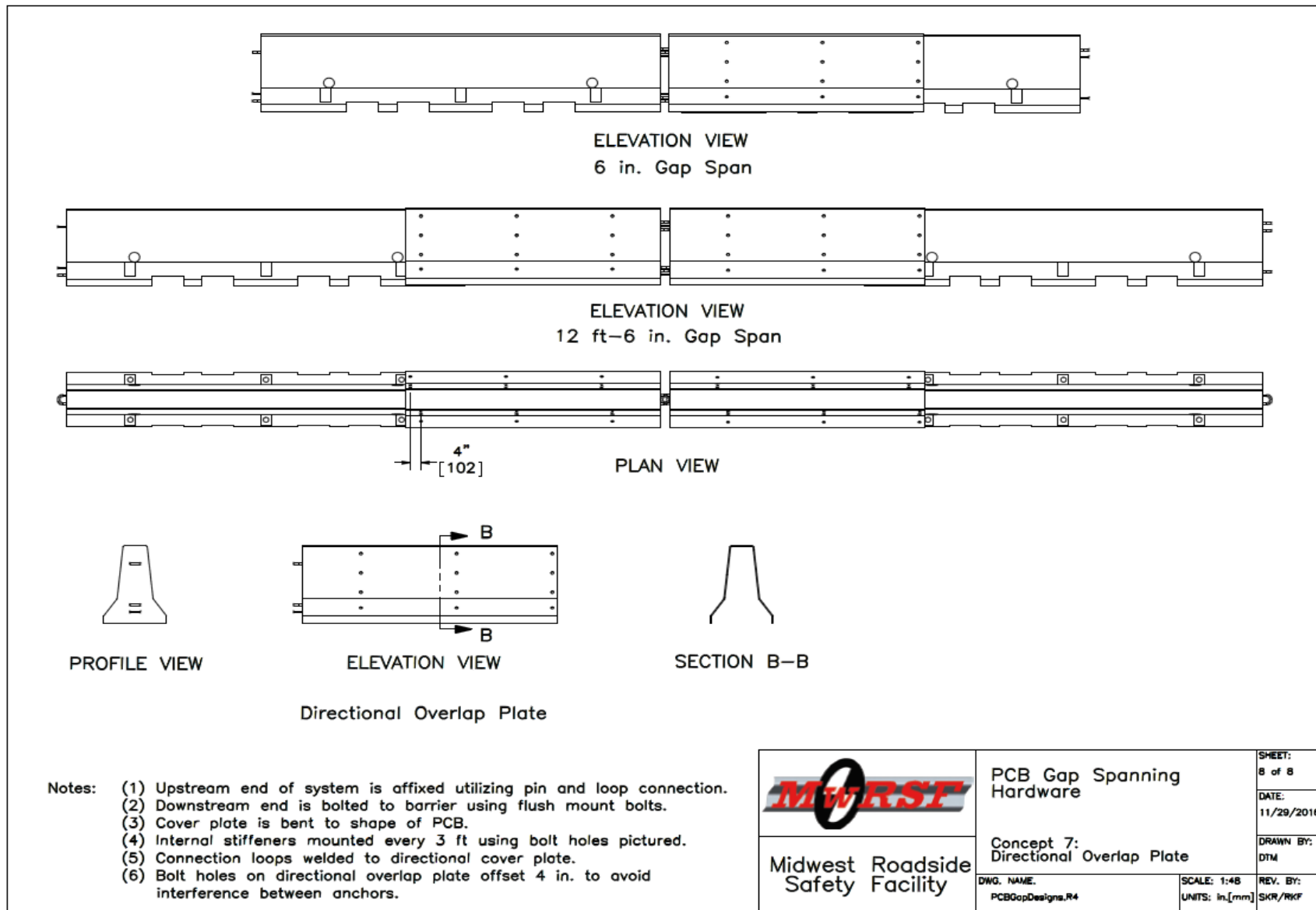


Figure 33. Design Details, Concept No. 7 – Two-Piece Cover Plate

### **3.3 Design Concept Selection**

Seven design concepts for PCB gap-spanning hardware were identified as possible systems for guarding longitudinal gaps in adjacent runs of PCBs. These design concepts were presented to the Midwest Pooled Fund Program member states for feedback. Following the discussion, the design concepts were ranked based on feasibility, likelihood of success in passing MASH TL-3 impact safety criteria, and ease of installation. A survey was developed and sent out to the Midwest Pooled Fund Program member states to seek their input on desired design concept(s) for further evaluation. According to the survey results, concept no. 7 (two-piece cover plate) was the most preferred option and concept no. 4 (three beam and toe plate) was ranked as the second most preferred option. Thus, concept nos. 7 and 4 were selected for further evaluation. LS-DYNA [37] computer simulation was used to further develop the preferred design concepts for PCB gap-spanning hardware to meet MASH 2016 TL-3 impact safety standards.

## **4 SIMULATION OF CONCEPT NO. 7 – TWO-PIECE COVER PLATE**

LS-DYNA [37] computer simulations were conducted to design, refine, and evaluate concept no. 7 with a two-piece cover plate. Details on the analysis are presented in the subsequent sections.

### **4.1 Evaluation Criteria**

Evaluation criteria for PCB gap-spanning hardware were based on three appraisal areas: (1) structural adequacy; (2) occupant risk; and (3) vehicle trajectory after collision.

Criteria for structural adequacy were intended to evaluate the ability of the PCB system and gap-spanning hardware to contain and redirect impacting vehicles. Controlled lateral deflection of the barrier was acceptable. Thus, the gap spanning hardware needed to provide adequate structural capacity to transfer impact loading effectively across the gap in the barriers, maintain its structural integrity, and effectively redirect impacting vehicles.

Occupant risk metrics, which evaluate the degree of hazard to the occupants in the impacting vehicle, included the longitudinal and lateral occupant impact velocities (OIVs) as well as longitudinal and lateral occupant ridedown accelerations (ORAs). According to MASH 2016, longitudinal and lateral OIVs should fall below the maximum allowable value of 40 ft/s, and longitudinal and lateral ORAs should fall below the maximum allowable value of 20.49 g's [1]. Occupant compartment damage was not measured in this study. To date, there have been no extensive validation efforts that have focused on the occupant compartment of the Chevrolet Silverado pickup model.

Post-impact vehicle trajectory is a measure of the potential of the vehicle to result in a secondary collision with other vehicles and/or fixed objects, thereby increasing the risk of injury to the occupants of the impacting vehicle and/or other vehicles. In addition, other concerns including vehicle snag and vehicle climbing were examined. The gap-spanning system should capture and smoothly redirect the vehicle. Also, the vehicle should not penetrate, underride, or override the gap-spanning system while remaining upright during and after the impact event. Roll, pitch, and yaw angular displacements were used to evaluate vehicle stability. According to MASH 2016, the maximum roll and pitch angles should not exceed 75 degrees [1]. It was also determined that wheel snag on the upstream end of the PCB system could affect vehicle behavior and cause rapid deceleration and or vehicle instability. Thus, snag was documented for each simulation.

### **4.2 Initial Design Details**

The two-piece cover plate design consisted of two separate cover plate sections with a standard pin and loop joint between the assemblies. The cover plate was connected to the PCB segments using concrete anchor bolts. If a gap were less than 6.25 ft, only one cover plate would be required to extend from one PCB segment and connect to another using the standard pin and loop connection. If a gap were longer than 6.25 ft, two cover plates would be needed. Preliminary design details for the computer simulation effort are shown in Figures 34 and 35.

The initial cover plate design was specified as ¼-in. thick ASTM A1011 Grade 50 steel plate. Variation of the cover plate thickness would be investigated during the LS-DYNA analysis.

Each cover plate had the same basic geometry of the F-shape PCB and extended from the top of the PCB segment to the top of the 3-in. tall toe of the PCB. The overall plate dimensions were made slightly larger than the F-shape PCB to allow it to fit over top of the PCB segments adjacent to the barrier gap. No internal stiffeners or spacers were included in the design concept initially, but they could be added as needed. Each cover plate was 9 ft long to allow for the required overlap of the PCB segments to accommodate anchoring of the plate to the adjacent PCB segments. The cover plate would be anchored to the face of the PCB at each end of the gap but would be chamfered to prevent snag. The cover plate was designed with multiple holes to accommodate anchorage of the cover plate to the adjacent PCBs with variable gap lengths. Four sets of holes for anchor locations spaced at 76 in. were incorporated into the plate initially, as shown in Figure 35. The top and bottom rows of anchor holes were positioned at a height of  $16\frac{7}{16}$  in. and  $3\frac{5}{8}$  in. from the lower edge of the cover plate, respectively, as shown in Figure 35. It was anticipated that a minimum of eight anchors (four on each side of the PCB) would be required to attach the design concept to each PCB segment.

An end plate was constructed on one end of the cover plate that closed the section. The end plate was constructed of ASTM A1011 Grade 50 steel, and the thickness was initially  $\frac{5}{8}$  in. The end plate also allowed for the placement of connection loops for use in the pin and loop connection to the adjacent PCB. The connecting loops were designed to match the configuration used by the F-shape PCB. Thus, A706 steel connection loops with a  $\frac{3}{4}$ -in. diameter were utilized. A schematic of the end plate is shown in Figure 35.

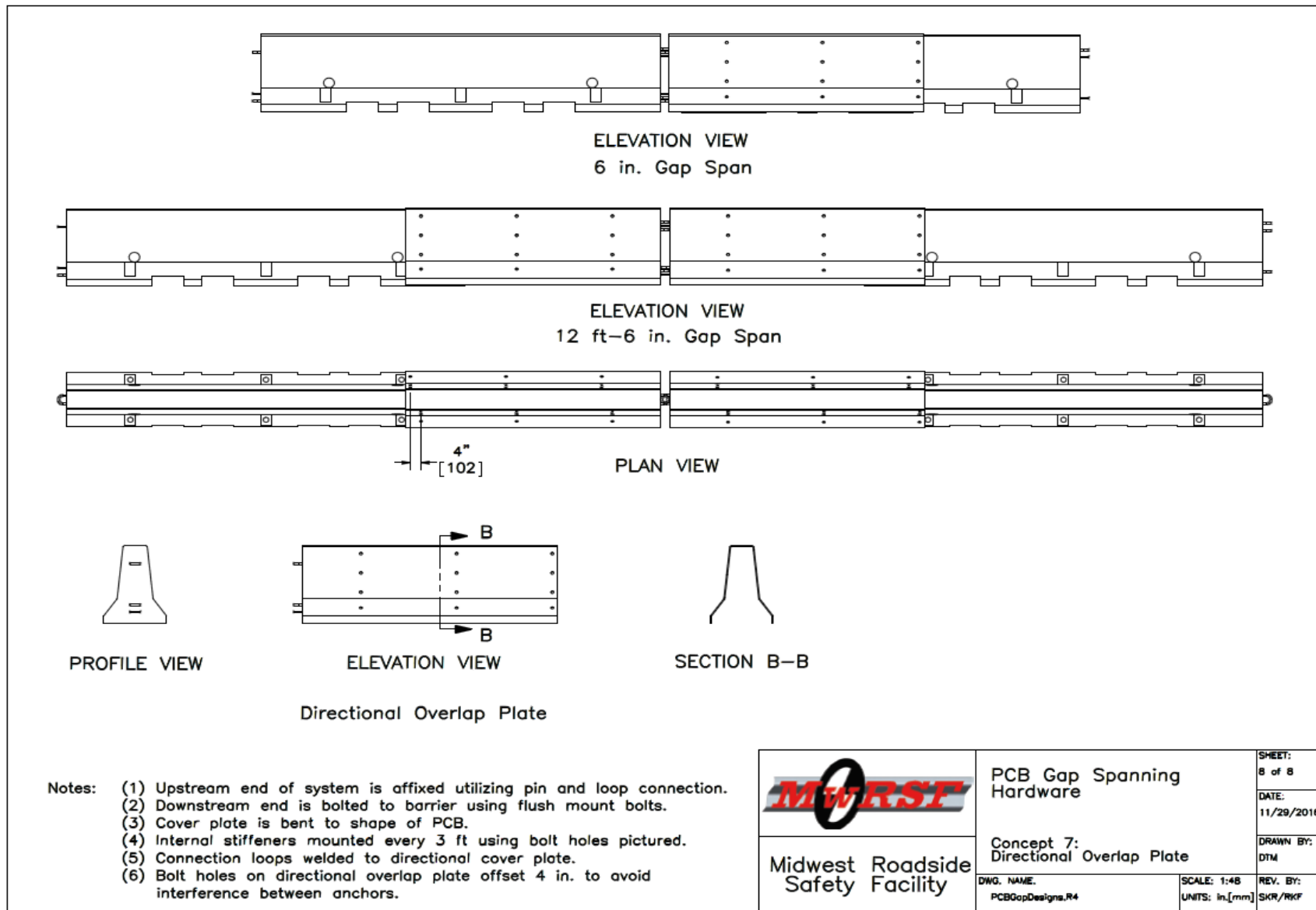


Figure 34. Design Details, Concept No. 7

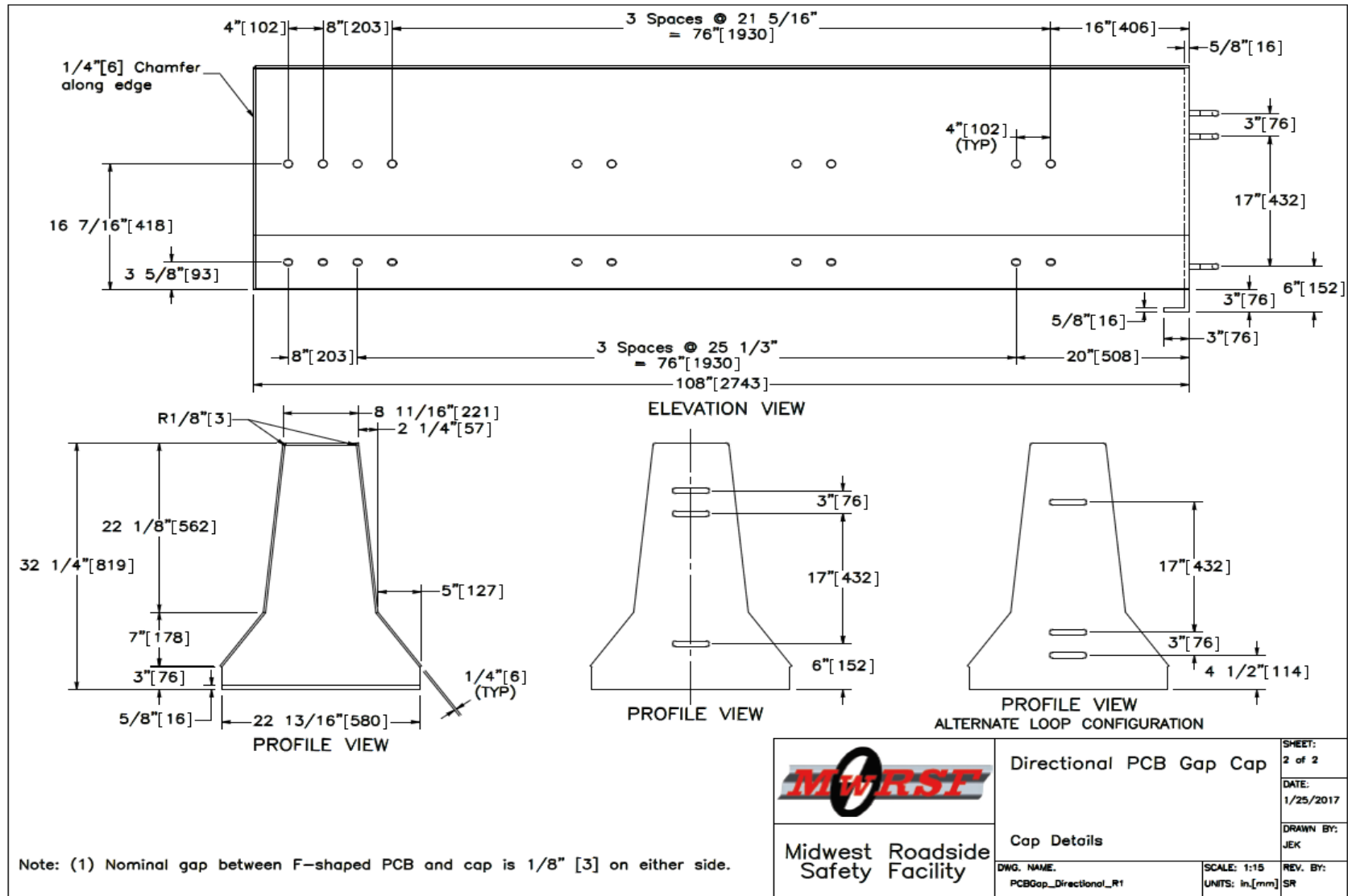


Figure 35. Design Details, Concept No. 7

### 4.3 Simulation Model

The model of the F-shape PCB used to simulate the design concepts was developed previously at MwRSF [38-39]. The model consisted of the F-shape barrier, the end connection loops, and the connection pins, as shown in Figure 36. The main body of the F-shape barrier model was created using shell elements with a rigid material definition. The rigid material definition allowed the proper mass and rotational inertias to be defined for the barrier even though it was essentially hollow. The barrier segments were assigned a mass of 4,976 lb based on measurements taken from actual barrier segments. The rotational inertias were determined based on SolidWorks models of the PCB segment. The SolidWorks models tended to overestimate the mass and rotational inertia of the PCB segment as the solid model included the mass of the concrete body and the reinforcing steel but did not account for the volume of concrete lost due to the reinforcing steel. Thus, the rotational inertias determined by the software were scaled down based on the ratio of the actual measured mass of the barrier segment to the software-estimated mass of the segment. The use of the shell elements improved the overall contact of the barrier and the vehicle. In addition, the use of shell elements made it easier to fillet the corners and edges of the barrier. By rounding off the barrier edges, the edge contacts and penetrations were reduced, thus further improving the contact interface.

The loops in the barrier model consisted of two sets of three rebar loops. The connection loops were modeled with a rigid material as previous testing of the barrier in various configurations showed little to no deformation of the connection loops. The connection pin was modeled with the MAT\_PIECEWISE\_LINEAR\_PLASTICITY material in LS-DYNA with the appropriate properties for A36 steel. The baseline barrier system model incorporated a total of 16 barrier segments for a total barrier length of 200 ft.

The simulated F-shape barrier model was impacted under the MASH 2016 TL-3 impact conditions for test designation no. 3-11. It was then compared to actual tests on free-standing, F-shape barriers (test no. 2214TB-2) to ensure that it provided reasonable estimates of the barrier evaluation parameters prior to implementing PCB cover plate design concepts. Details of the comparison can be found in Bielenberg et al. [39].

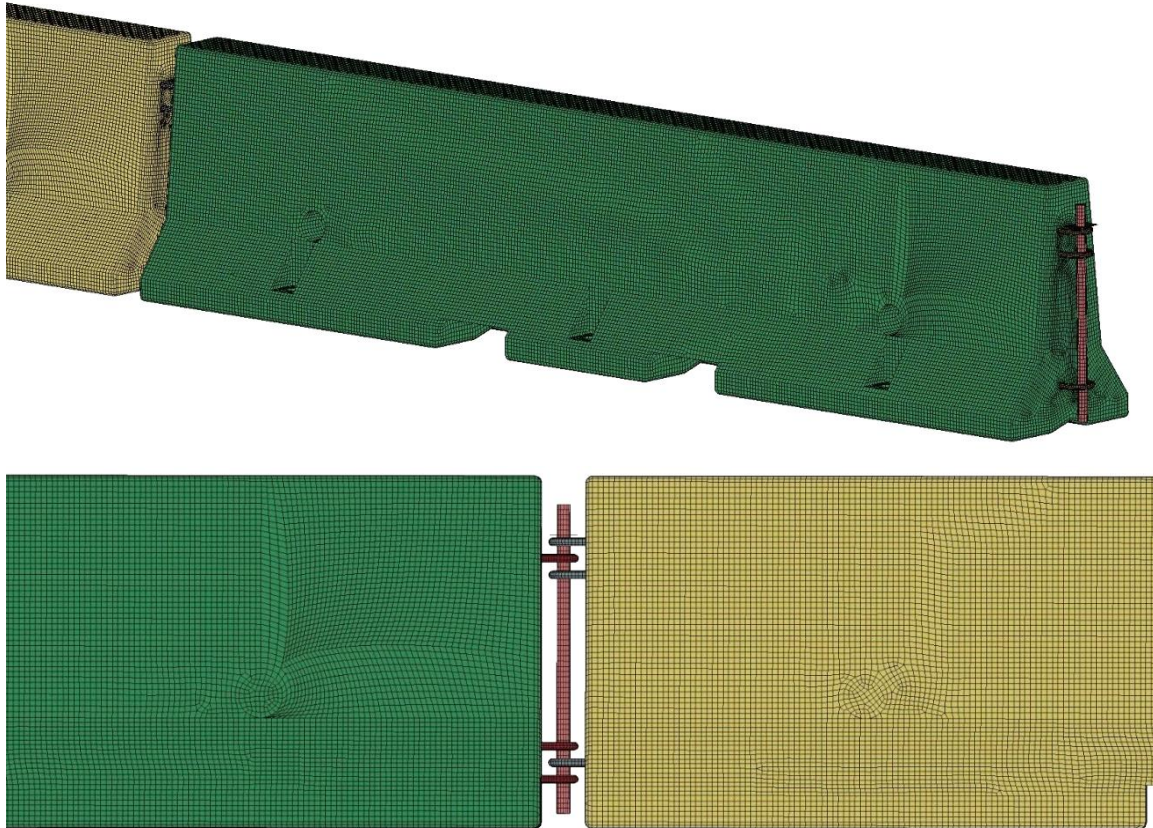


Figure 36. F-Shape PCB Barrier Model

To create a 12.5-ft long gap, a single PCB segment in the middle of the system was removed and two cover plate assemblies were added. A 3D geometric model of the cover plates was developed in SolidWorks and imported into HyperMesh for pre-processing and meshing of the cover plate model. The cover plate model along with the barrier is shown in Figure 37. The cover plate cap and end plate were created using the shell elements with MAT\_24\_PIECEWISE\_LINEAR\_PLASTICITY to represent the ASTM A1011 Grade 50 steel material properties. Anchorage of the cover plate to the PCB was accomplished by defining elements on the cover plate at the anchor locations as the same part as the rigid PCB, thus fixing the cover plate to the PCB at those locations.

The loops were added using solid elements and rigid material properties. The nodes of the loops and end of the cover plate cap were merged. Cylindrical steel pins were added to connect the adjacent cover plates together using MAT-24 with A36 steel material properties. Incremental stiffeners were added later in the analysis of the two-piece cover plate concept as an alternative method of reinforcing the cap design along the gap length. Further details on these stiffeners will be provided in a subsequent section. A list of PCB two-piece cover plate parts and associated LS-DYNA parameters are shown in Table 1.

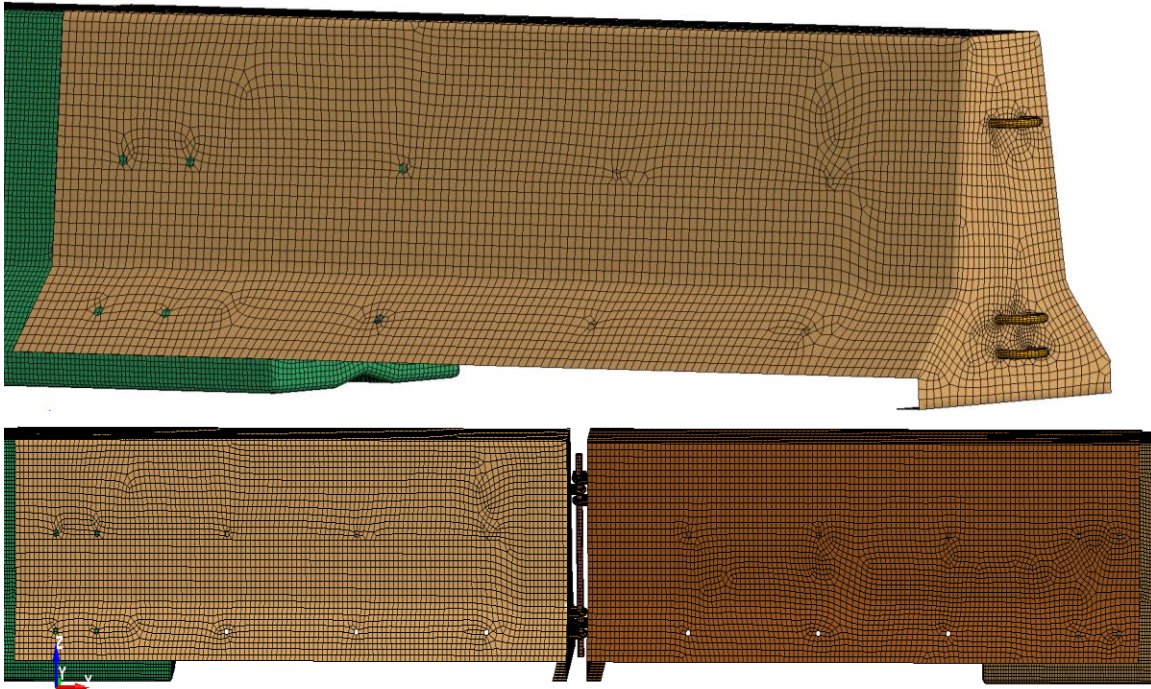


Figure 37. Two-Piece Cover Plate Model

Table 1. Two-Piece Cover Plate Parts and LS-DYNA Parameters

<b>Part Description</b>	<b>Material Type</b>	<b>Material Formulation</b>	<b>Element Type</b>	<b>Element Formulation</b>	<b>Element Thickness (in.)</b>
F-Shape PCB	Concrete	MAT-20 Rigid	Shell	Belytschko-Tsay, Type 2	0.07
Barrier Loops	ASTM A706	MAT-20 Rigid	Solid	Constant Stress Solid Element	N/A
Connection Pin	ASTM A36	MAT-24 Piecewise-Linear-Plasticity	Solid	Fully Integrated, S/R Solid	N/A
Connection Pin Plate	ASTM A36	MAT-24 Piecewise-Linear-Plasticity	Shell	Belytschko-Tsay, Type 2	1/2
Cover Plate	ASTM A1011 Grade 50	MAT-24 Piecewise-Linear-Plasticity	Shell	Fully Integrated Shell Element Type 16	1/4
End Plate	ASTM A1011 Grade 50	MAT-24 Piecewise-Linear-Plasticity	Shell	Fully Integrated Shell Element Type 16	1/2
Stiffeners	ASTM A1011 Grade 50	MAT-24 Piecewise-Linear-Plasticity	Shell	Fully Integrated Shell Element Type 16	1/4

N/A – Not Applicable

#### 4.4 Model Analysis – Cover Plate Cap Thickness

To investigate the PCB gap two-piece cover plate design concept, the LS-DYNA model of fifteen, freestanding, F-Shape PCBs along with a two-piece cover plate gap-spanning hardware was simulated with a 2270P vehicle impacting the system at a speed of 62 mph and at an angle of 25 degrees. The PCB gap cover plate system was evaluated under MASH test designation no. 3-11 impact conditions as 2270P impacts were considered more critical than 1100C impacts due to the expected higher impact load. In these simulations, the 2270P Chevrolet Silverado V2 model impacted a barrier system with a 12.5-ft long gap and the two-piece cover plates connected with pins and loops. The vehicle impacted the system either 4.3 ft upstream from the center of the cover plate joint or 8.8 ft upstream from the center of the cover plate joint. These points were selected to maximize the loading on the joint between the two-piece cover plates and the mid-span of the two-piece cover plate section. Five cap thicknesses including  $\frac{1}{2}$  in.,  $\frac{3}{8}$  in.,  $\frac{1}{4}$  in.,  $\frac{3}{16}$  in., and  $\frac{1}{8}$  in. were modeled to evaluate the two-piece cover plate design. The results of the simulation of various cover plate configurations were analyzed and used to refine the design concept. Sequential photographs with a cap thickness of  $\frac{1}{4}$  in. at an impact point of 4.3 ft upstream from the cover plate joint are shown in Figure 38. A summary of the simulation results for the various configurations is shown in Tables 2 and 3 at two impact points of 4.3 ft and 8.8 ft upstream from cap joint, respectively.

All the simulations models met MASH criteria for ORA and OIV evaluations. However, review of the simulation models found that localized crushing of the cover plates was prominent for the thinner cover plate designs. Local lateral deformation of the cover plates was measured along the adjacent edges of the cover plate, as shown in Table 2 and Figure 39. The magnitude of these lateral deformations to the cover plates raised concerns of vehicle snag and instability. It was desired by the researchers to limit local lateral deformations to around 3 in. Increased cover plate thicknesses of  $\frac{3}{8}$  in. and  $\frac{1}{2}$  in. reduced the local lateral deformation and crushing of the cover plate, but the added thickness would also significantly raise the cost and weight of the design. As such, it was desired to limit the local deformations of the cover plates without significantly increasing the plate thickness.

Deformation of the cover plates near the base of the end plates was also noted in this initial simulation analysis. This deformation could also lead to tire and wheel snag and potential vehicle instability. As such it was desired to improve this behavior as well

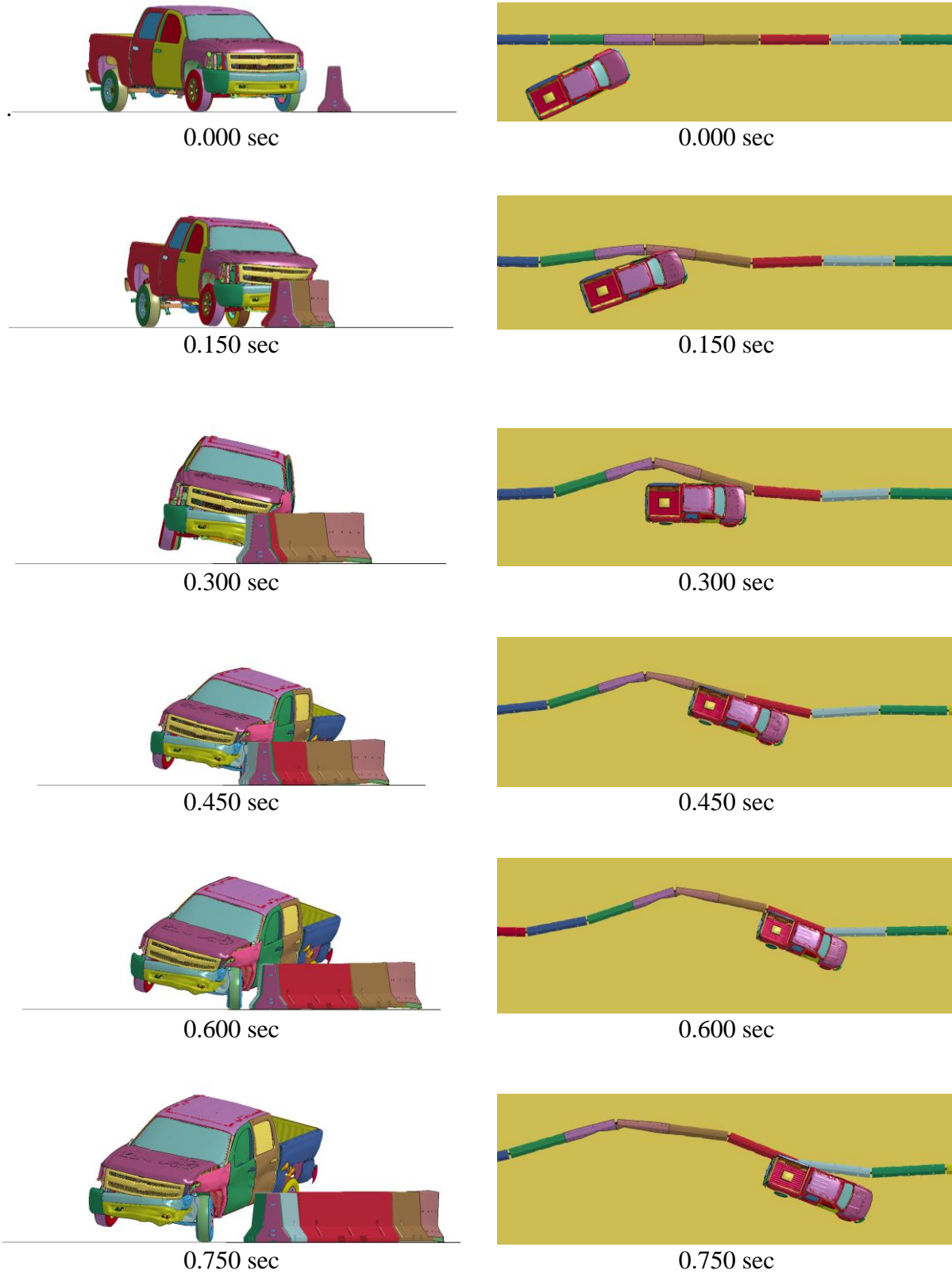


Figure 38. Sequential Images, Impact Point at 4.3 ft Upstream from Cover Plate Joint with Cap Thickness of 1/4 in.

Table 2. Summary of Simulation Results: Varied Cap Thicknesses, Impact Point 4.3 ft Upstream from Cap Joint

Cap Thickness (in.)	Local Lateral Cap Deformation (in.)	Max Lateral Barrier Deflection (in.)	Lateral OIV (ft/s)	Long. OIV (ft/s)	Lateral ORA (g's)	Long. ORA (g's)	Max Roll (deg.)	Max Pitch (deg.)
1/8	18.7	132.1	-12.5	-23.3	-13.2	-10.0	-20.5	9.0
3/16	12.9	116.6	-12.5	-19.7	-12.8	-7.5	-57.6	17.2
1/4	9.5	103.5	-13.8	-18.4	-12.4	6.6	-18.3	9.6
3/8	3.1	84.2	-14.4	-16.4	-16.8	-5.2	-19.9	15.0
1/2	0.5	78.3	-14.1	-15.0	-17.6	-4.9	-20.9	13.6
MASH Limits	N/A	N/A	≤ 40	≤ 40	≤ 20.49	≤ 20.49	< 75	< 75

N/A – Not Applicable

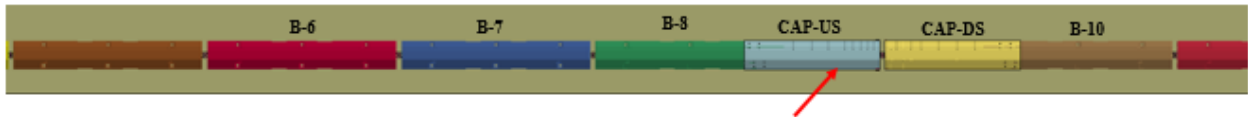
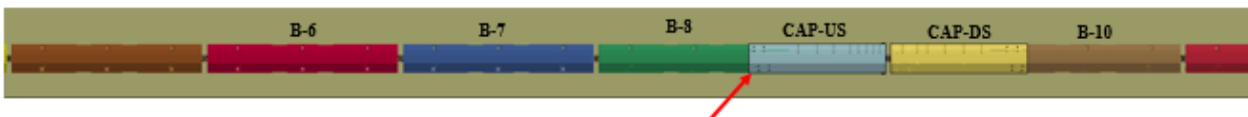


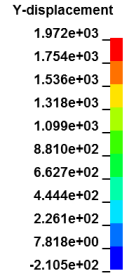
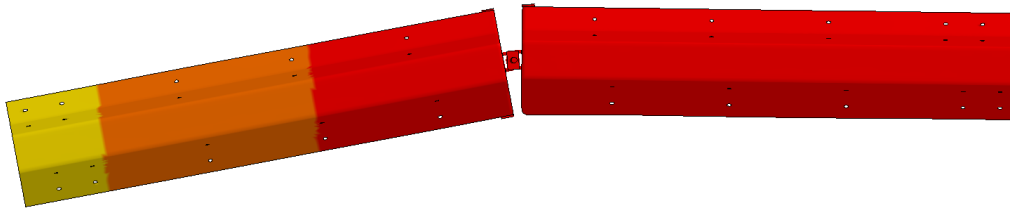
Table 3. Summary of Simulation Results: Varied Cap Thicknesses, Impact Point 8.8 ft Upstream from Cap Joint

Cap Thickness (in.)	Local Lateral Cap Deformation (in.)	Max Lateral Barrier Deflection (in.)	Lateral OIV (ft/s)	Long. OIV (ft/s)	Lateral ORA (g's)	Long. ORA (g's)	Max Roll (deg.)	Max Pitch (deg.)
1/8	11.6	116.9	-14.8	-11.8	-9.8	-14.4	-15.1	18.7
3/16	13.8	110.9	-15.1	-10.5	-10.4	-7.5	-16.9	11.1
1/4	8.6	95.2	-15.0	-10.2	-12.5	-5.3	-16.5	8.7
3/8	5.7	79.1	-15.4	-10.2	-14.9	-4.9	-15.6	9.2
1/2	3.4	71.2	-15.7	-11.2	-12.5	-5.3	-15.7	9.1
MASH Limits	N/A	N/A	≤ 40	≤ 40	≤ 20.49	≤ 20.49	< 75	< 75

N/A – Not Applicable

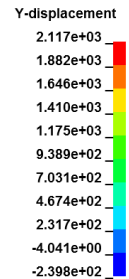
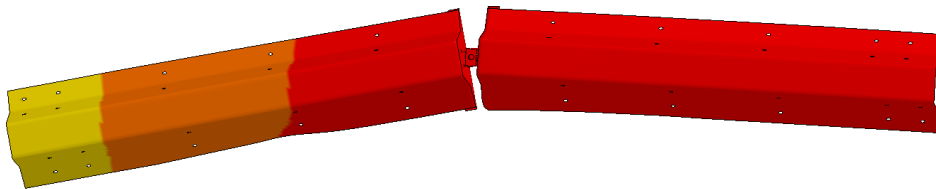


PCB GAP COVER PLATE  
Time = 840  
Contours of Y-displacement  
min=-210.471, at node# 918664  
max=1972.41, at node# 1496590



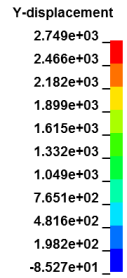
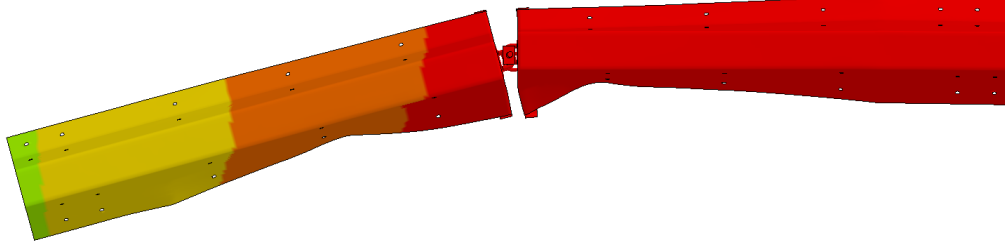
1/2-in. Thick Cap

PCB GAP COVER PLATE  
Time = 800  
Contours of Y-displacement  
min=-239.764, at node# 918647  
max=2117.46, at node# 1476312



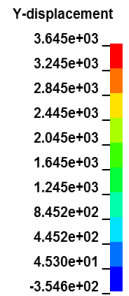
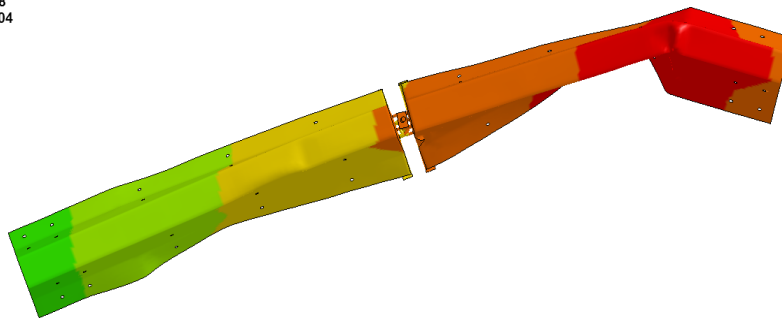
3/8-in. Thick Cap

PCB Gap Cover Plate  
Time = 1200  
Contours of Y-displacement  
min=-85.2711, at node# 918664  
max=2749.32, at node# 1455262



1/4-in. Thick Cap

PCB GAP COVER PLATE  
Time = 835  
Contours of Y-displacement  
min=-354.627, at node# 916428  
max=3644.65, at node# 1455204



1/8-in. Thick Cap

Figure 39. Lateral Displacement and Plastic Hinge Formation for Impact Point 4.3 ft Upstream from Cap Joint

## 4.5 Refinement of Two-Piece Cover Plate Design

Excessive deformations of the cover plate led to further investigation of stiffening techniques and modifications to the cover plate. Several design modifications were evaluated including adding an end plate stiffener tube and utilizing incremental cap stiffeners. Computer simulations of each of the proposed modification and the results are discussed in the subsequent sections.

### 4.5.1 Addition of End Plate Stiffener Tube

The simulation results of the original design suggested that the bottom of the ends plates experienced excessive deformations. To stiffen the end plate, an HSS3x3x $\frac{5}{8}$  tube box stiffener was added to the bottom of the plates, as shown in Figure 40. The tube was located along the bottom edge of the end plate.

Although adding a box tube to the end plate reduced the overall deformation, the localized crush was shifted slightly toward the middle of the cover plate. Stiffening the lower portion of the plate did not resolve the plastic deformation, as shown in Figure 41.

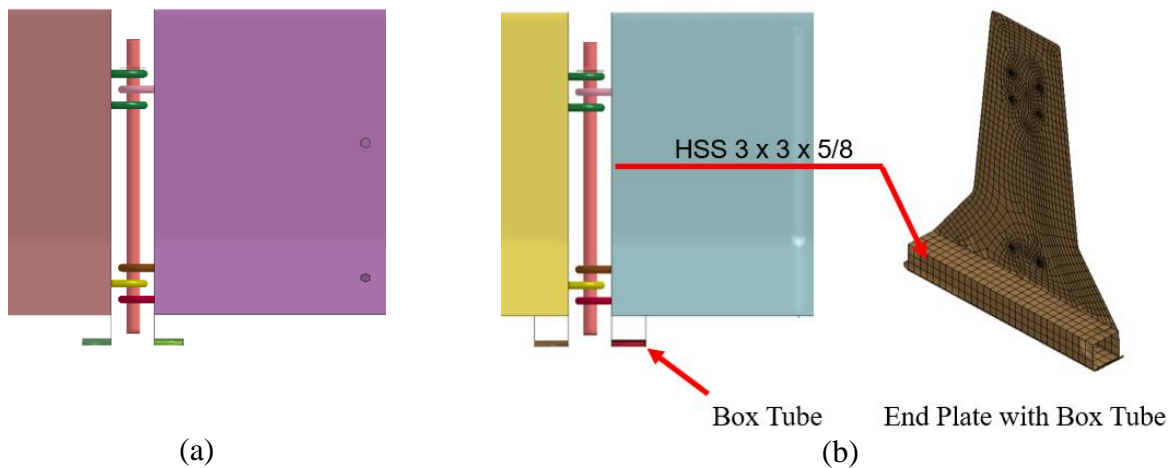


Figure 40. Model of (a) Baseline Cover Plate and (b) Modified Design with Stiffener Box Tube

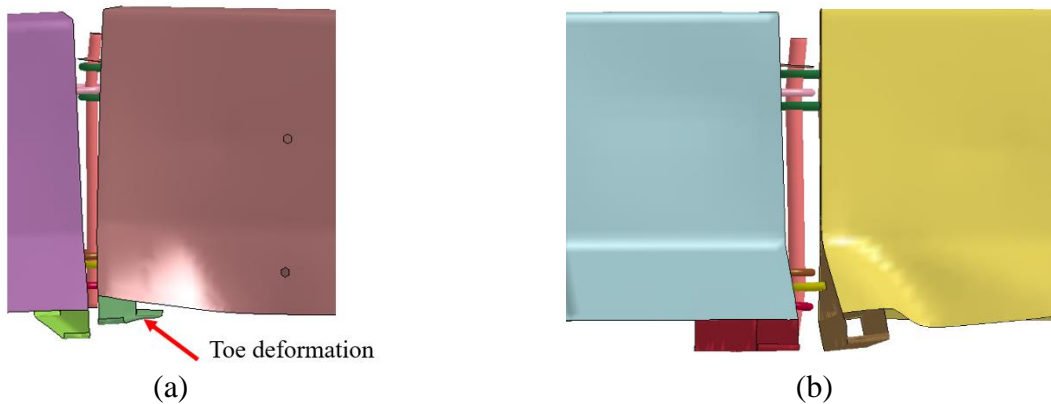


Figure 41. Simulated Damage in (a) Baseline Cover Plate and (b) Modified Design with Stiffener Box Tube

#### 4.5.2 Cap Thickness and Incremental Cap Stiffeners

Internal plate stiffeners with various thicknesses and spacings were added to the PCB gap spanning cover plate system to reduce localized deformation of the cover plate and improve the structural performance. Design variations of three and six stiffeners were modeled with various stiffener thicknesses including  $\frac{3}{8}$  in.,  $\frac{1}{4}$  in., and  $\frac{3}{16}$  in. The stiffeners were modeled using shell elements and connected to the cap by merging nodes to simulate welding of the stiffeners and cap. The stiffeners were modeled with the MAT\_PIECEWISE LINEAR\_PLASTICITY material in LS-DYNA with ASTM A1011 Grade 50 Steel properties. Cover plate thicknesses were also varied between  $\frac{3}{8}$  in.,  $\frac{1}{4}$  in.,  $\frac{3}{16}$  in., and  $\frac{1}{8}$  in. The cover plate with three stiffeners and box tube at the toe in a 12.5-ft long gap configuration are shown in Figure 42.

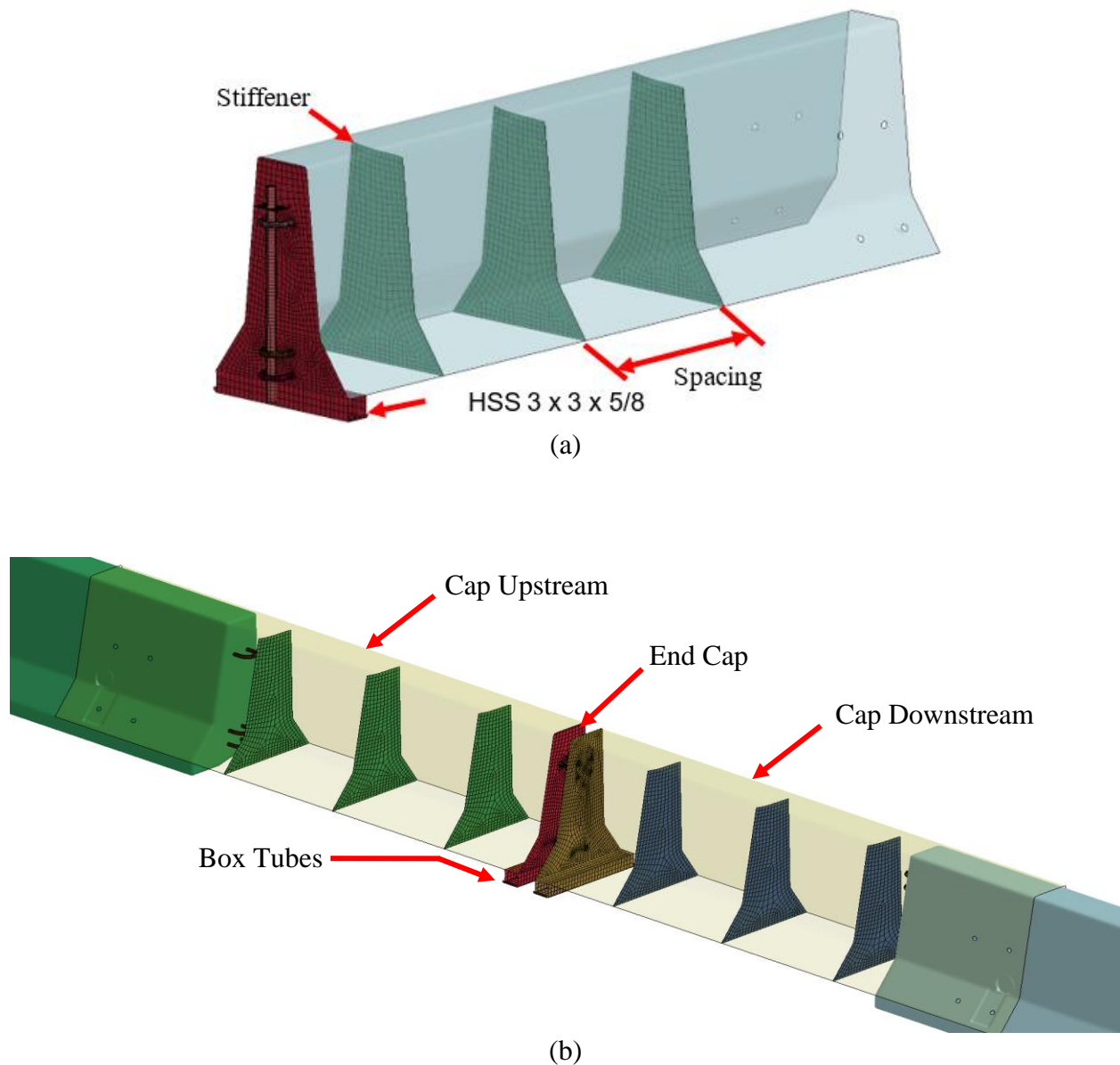


Figure 42. Model of (a) Cover Plate with Three Stiffeners and Box Tube, (b) 12.5-ft Long Gap-Spanning Configuration

A summary of simulation results for the modified two-piece cover plate designs with varied thicknesses of the cap and stiffeners with an impact point of 4.3 ft upstream from the cover plate joint is shown in Table 4. The variations of internal cap reinforcement utilizing three and six stiffeners had a spacing of  $25\frac{3}{8}$  in. and 14 in., respectively. The cases with three stiffeners and a  $\frac{5}{8}$ -in. thick end plate resulted in an excellent improvement in deformations for both  $\frac{3}{16}$ -in. and  $\frac{1}{4}$ -in. thick cap configurations. The proposed design modification, including (1) increasing cap thickness, (2) adding a box tube at end plate base, and (3) adding incremental stiffeners, sufficiently reduced lateral crush and showed promise as a system for connecting PCB segments on opposite sides of a gap. The final deformed shapes of caps with three stiffeners are shown in Figure 43. The simulation results suggested that  $\frac{3}{16}$ -in. and  $\frac{1}{4}$ -in. thick caps with three  $\frac{1}{4}$ -in. thick stiffeners had a maximum lateral crush of 3.9 in. and 2.8 in., respectively, as shown in Table 4, and would be expected to provide the desired structural capacity of the cover plate sections in terms of localized deformations. Cap thickness was further examined relative to loading of the pin and loop joint in a subsequent section. However, the researchers determined that a  $\frac{1}{4}$ -in. thick cap was the best option for the design as it provided the best combination of weight and reduced local deformations. Additional simulations for impacts upstream and downstream from the cover plate as well as on smaller gap widths requiring only one cover plate assembly were desired to further evaluate the structural capacity and the potential for vehicle snag and stability. Simulations were also conducted to evaluate the end plate thickness. These models are discussed in subsequent sections.

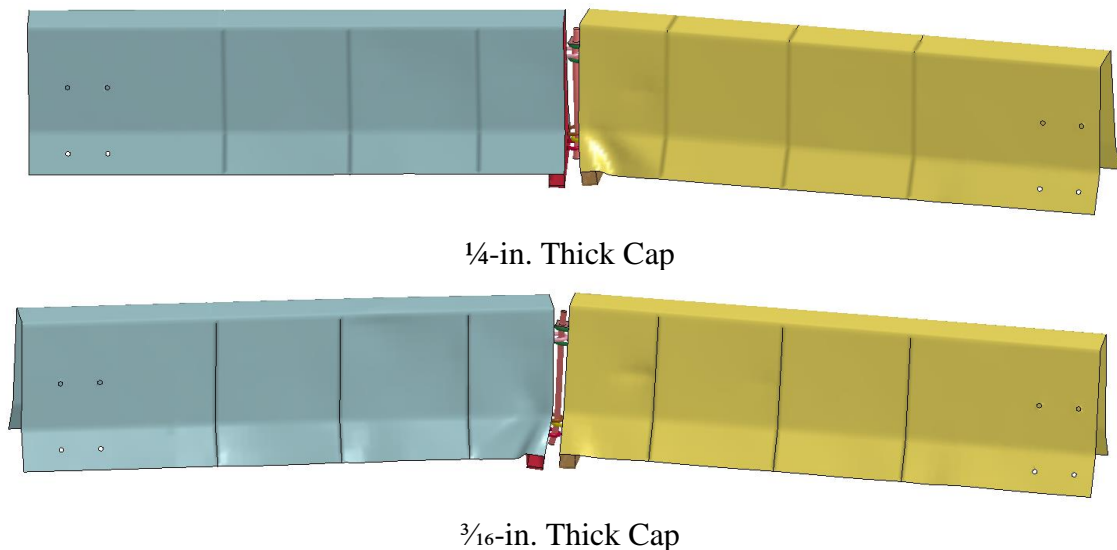


Figure 43. Simulation with Three Stiffeners, Impact Point 4.3 ft Upstream from Cover Plate Joint

Table 4. Summary of Simulation Results: Varied Cap Thicknesses with Stiffeners, Impact Point 4.3 ft Upstream from Cap

Cap Thicknesses (in.)	Stiffener Thickness (in.)	Stiffener Spacing (in.)	Local Lateral Cap Deformation (in.)	Max Lateral Barrier Deflection (in.)	Lateral OIV (ft/s)	Long. OIV (ft/s)	Lateral ORA (g's)	Long. ORA (g's)	Roll (deg.)	Pitch (deg.)
3/8	3/8	25 3/8	0.5	72.0	-13.7	-17.7	-13.5	-5.4	-20.2	11.4
1/4	1/4	14	0.8	82.8	-13.7	-18.2	-12.2	-6.1	-16.3	10.3
	1/4	-	0.6	80.0	-13.4	-17.7	-12.5	-6.7	-17.0	10.8
	1/4	25 3/8	2.8	89.3	-14.1	-18.0	-15.5	-5.2	-18.8	11.6
3/16	1/4	25 3/8	3.9	96.2	-14.1	-19.0	-15.8	-6.6	-33.7	17.0
	3/16	25 3/8	3.9	96.1	-13.7	-21.6	-14.5	-6.7	-18.0	11.1
	3/16	14	0.7	89.8	-13.7	-20.3	-13.5	-7.0	-17.3	10.0
	3/16	-	1.0	89.0	-14.1	-17.7	-13.4	-6.4	-16.4	11.5
1/8	1/8	14	5.6	81.9*	-13.3	-24.6	-7.3	-7.8	-10.84	4.2
	1/8	-	5.8	115.2	-13.7	-23.3	-14.5	-7.7	-14.1	12.7

\* Maximum value was not reached prior to conclusion of simulation.

### 4.5.3 End Plate Thickness and Loop Configuration

Additional simulations were conducted to investigate the thickness of the end plate and ensure adequate structural strength and minimal deformation. The initial models of the two-piece cover plate concept were simulated with a  $\frac{5}{8}$ -in. thick end plate. However, little to no deformation of the end plate was noted in those models, and it was desired to reduce the thickness of the end plate if possible. Modified two-piece cover plate models were simulated with a  $\frac{1}{2}$ -in. thick end plate and with various cover plate thicknesses including  $\frac{1}{8}$  in.,  $\frac{1}{4}$  in.,  $\frac{3}{16}$  in., and  $\frac{3}{8}$  in.

For the upstream end plate of the two-piece cover plate concept, the highest effective stresses were observed at top single loop location, and for the downstream end plate the highest effective stresses were observed at the bottom single loop location, as shown in Figure 44. In these locations, the von-mises stresses exceeded 50 ksi, corresponding to plastic deformation. The simulation results suggested that the end plates would experience plastic deformations.

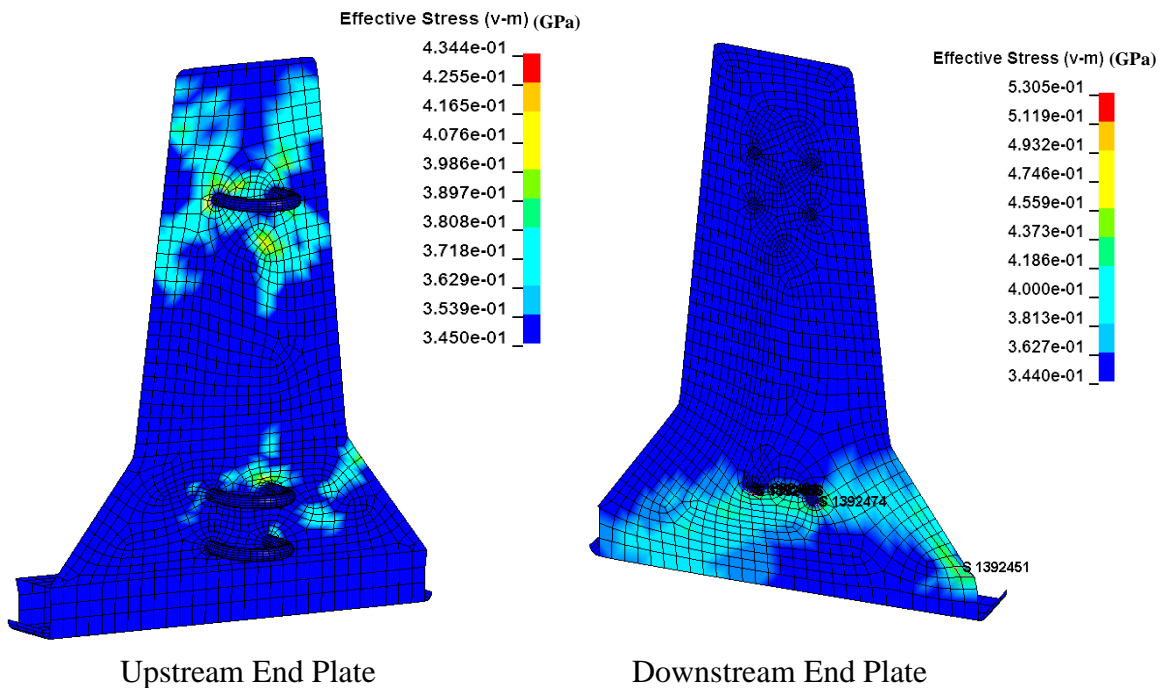


Figure 44. Von Mises Stress,  $\frac{1}{2}$ -in. Thick End Plate

To further evaluate the use of a  $\frac{1}{2}$ -in. thick end plate, the model with a  $\frac{1}{2}$ -in. thick end plate was evaluated in terms of the localized deflections at the connection loop locations. The localized dynamic and permanent deformations were observed to be 1.4 in. and 0.9 in., respectively. These local deformations of the end plate were undesirable. Thus, the thickness of the end plate was reverted to the original  $\frac{5}{8}$ -in. thickness.

The capacity of the connection loops was also evaluated. The connecting loops with diameter of  $\frac{3}{4}$  in. were modeled, as shown in Figure 45. Force transducers were used to obtain the contact forces between the pin and loop, as shown in Table 5. The simulation results suggested that  $\frac{3}{4}$ -in. diameter connection loops would perform acceptably. The yield capacity of  $\frac{3}{4}$ -in. loops was estimated to be 53 kips, which was larger than all the loop forces observed in the simulations.

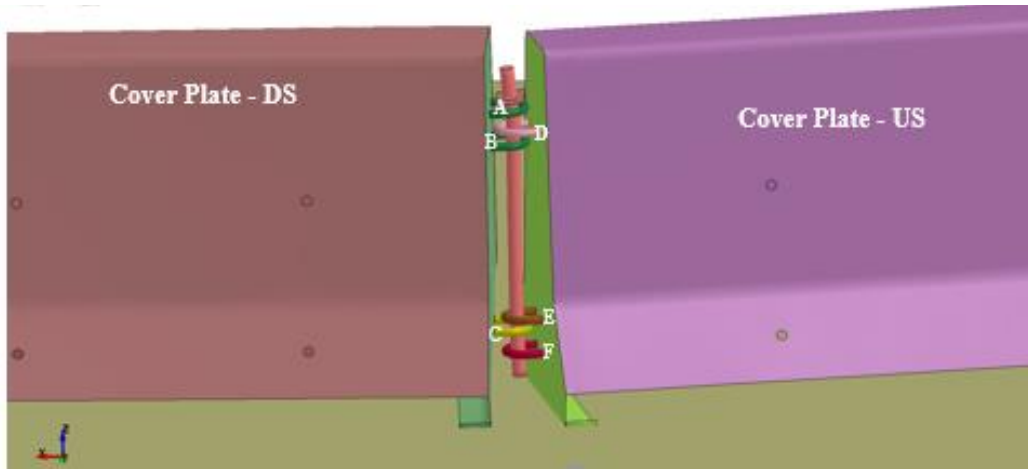


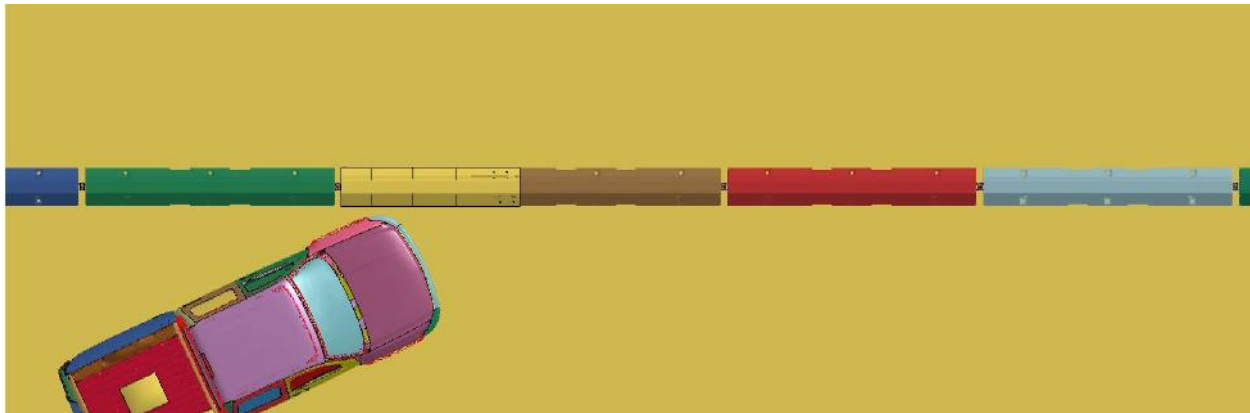
Figure 45. Pin and Loop Connection Configuration

Table 5. Loop Contact Forces for Different Cap Thicknesses

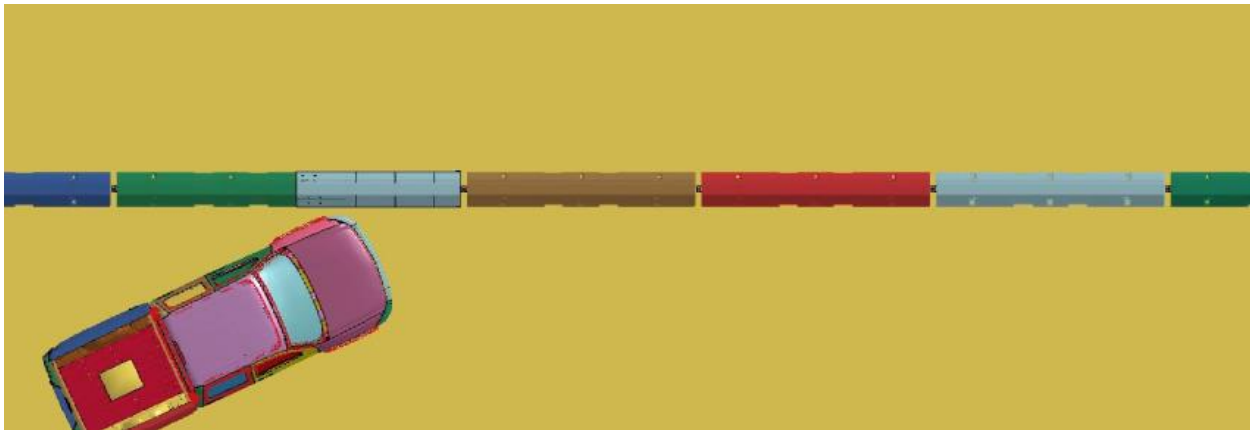
Cap Thickness (in.)	End Plate Thickness (in.)	Longitudinal Loop Contact Force (kips)	Resultant Loop Contact Force (kips)
1/8	1/2	45.4	45.6
3/16	1/2	43.8	44.6
1/4	1/2	45.9	46.0
3/8	1/2	50.5	50.6

#### 4.6 Single 1/4-in. Thick Cover Plate Over 6.25-ft Long Gap

A simulation analysis was conducted to investigate the design performance at for a 6.25-ft gap length with a single 1/4-in. thick cover plate and three stiffeners. This analysis was conducted to ensure that gaps using only a single cover plate assembly would function properly. For a 6.25-ft long gap, two different cover plate configurations were simulated: (a) anchored to the downstream PCB and pinned to the upstream PCB, and (b) anchored to the upstream PCB and pinned to the downstream PCB, as shown in Figure 46.



(a) Anchored to Downstream PCB and Pinned to Upstream PCB



(b) Anchored to Upstream PCB and Pinned to Downstream PCB

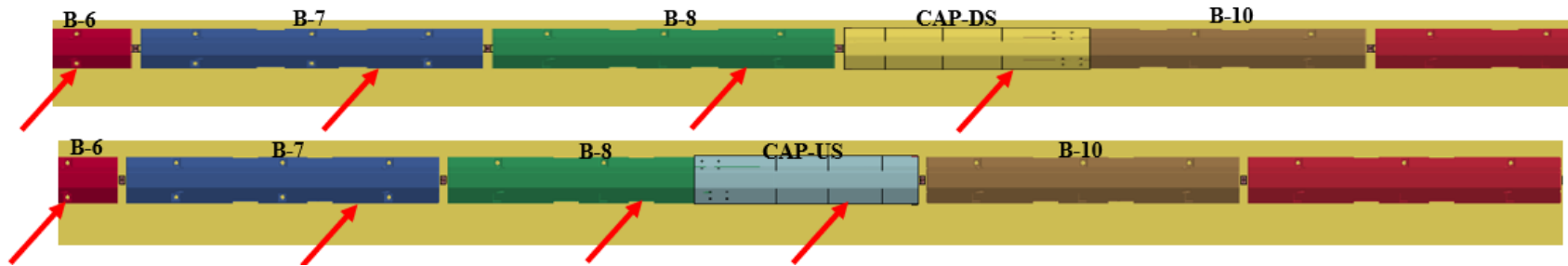
Figure 46. Two Variations of 6.25-ft Gap Model with Single Cap

A summary of the simulation results of the two 6.25-ft gap configurations is shown in Table 6. Simulations were conducted at various impact points on and upstream from the cover plate. In the table, simulation nos. 1 through 4 were associated with configuration (a) and simulation nos. 5 through 8 were associated with configuration (b). Results of the simulation found that cover plate deformations, barrier deflections, and occupant risk indices were all similar to those of the analysis performed on the larger barrier gap with two cover plates.

Table 6. Summary of Simulation Results: Single ¼-in. Thick Cover Plate

Sim. No.	Design Concept	Impact Point	Local Lateral Cap Deformation (in.)	Max Lateral Barrier Deflection (in.)	Lateral OIV (ft/s)	Long. OIV (ft/s)	Lateral ORA (g's)	Long. ORA (g's)	Roll (deg.)	Pitch (deg.)
1	Single ¼-in. Cap DS	4.3 ft Upstream from Joint of CAP DS and B 10	1.6	79.9	-14.4	-19.4	-15.0	-5.5	-19.9	15.7
2	Single ¼-in. Cap DS	4.3 ft from Downstream End of CAP DS	1.0	80.9	-18.7	-13.8	-16.9	-6.3	-12.3	33.0
3	Single ¼-in. Cap DS	4.3 ft Upstream from Joint of B7 and B8	1.3	80.4	-16.7	-12.5	-17.7	-5.1	-20.6	9.3
4	Single ¼-in. Cap DS	4.3 ft Upstream from Joint of B6 and B7	0.7	79.1	-16.0	-14.4	-15.8	-7.7	-22.3	15.6
5	Single ¼-in. Cap US	4.3 ft Upstream from Joint of CAP US and B 0	2.2	91.6	-16.1	-14.7	-15.2	-6.1	-19.0	14.0
6	Single ¼-in. Cap US	4.3 ft from Upstream End of CAP US	0.7	67.9	-18.7	-13.8	-12.4	-4.3	-16.2	11.0
7	Single ¼-in. Cap US	4.3 ft Upstream from Joint of B7 and B8	0.9	69.9	-16.4	-14.8	-16.8	-5.9	-17.5	10.9
8	Single ¼-in. Cap US	4.3 ft Upstream from Joint of B6 and B7	1.2	78.2	-16.0	-14.8	-17.6	-7.1	-23.4	11.3
MASH Limits		N/A	N/A	N/A	≤ 40	≤ 40	≤ 20.49	≤ 20.49	< 75	< 75

N/A – Not Applicable



56

#### 4.7 Multiple Impact Points Analysis – Test Designation No. 3-11

A final series of MASH test designation no. 3-11 simulations were conducted to evaluate various impacts on the maximum 12.5-ft long barrier gap using the two-piece cover plate concept with both  $\frac{3}{16}$ -in. and  $\frac{1}{4}$ -in. thick cover plates, three internal stiffener plates, and  $\frac{5}{8}$ -in. thick end plates with box tube reinforcement. Simulations were conducted with impact points upstream from the gap-spanning hardware as well as multiple impact points along the cover plates that had not been investigated previously, as shown in Figure 47. Impacts upstream from the cover plates were simulated to evaluate the transition in stiffness from standard PCBs to the gap-spanning hardware system. Additional impacts to the cover plates were simulated to evaluate the structural capacity of cover plates, especially at the joint and the cover plate-to-PCB transition.

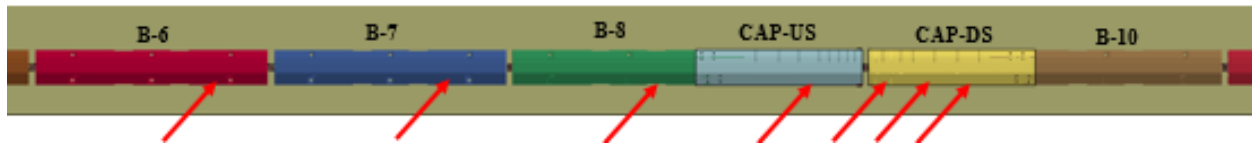


Figure 47. Simulated Impact Points

Results from the simulation analysis are summarized in Table 7. Review of the simulations found that both cap thickness options successfully redirected the impacting pickup truck and met occupant risk criteria for all the selected impact points. However, simulations with the  $\frac{3}{16}$ -in. thick cover plate indicated more localized deformation and corresponding increases in vehicle pitch and roll values. This raised concerns with respect to the thinner cover plate option. Thus, the  $\frac{3}{16}$ -in. thick cover plate design was eliminated from further consideration.

Table 7. Summary of Simulation Results: Evaluation of Multiple Impact Point Investigation

Impact Point	Local Lateral Cap Deformation (in.)	Max Lateral Barrier Deflection (in.)	Lateral OIV (ft/s)	Long. OIV (ft/s)	Lateral ORA (g's)	Long. ORA (g's)	Roll (deg.)	Pitch (deg.)	Yaw (deg.)
<b>Case 1: 3/16-in. Thick Cover Plate with Three 1/4-in. Thick Stiffeners</b>									
4.3 ft Upstream from Joint of B6 and B7	0.3	79.8	-16.0	-14.4	-17.8	-5.7	-20.9	12.9	-44.4
4.3 ft Upstream from Joint of B7 and B8	0.8	73.9	-16.0	-14.8	-16.4	-5.5	-16.6	10.8	-39.5
4.3 ft from Upstream End of CAP-US	1.5	74.4	-18.4	-12.5	-11.9	-4.3	-15.3	7.6	-45.6
4.3 ft Upstream from Joint of CAP-US and CAP-DS	3.9	96.2	-14.1	-19.0	-15.8	-6.6	-33.7	17.0	-49.2
1 ft Downstream from Joint of CAP-US and CAP-DS	1.6	88.3	-15.7	-20.9	-15.0	-6.3	-10.0	11.7	-53.5
4.3 ft from Upstream End of B-10	1.3	96.6	-17.0	-17.7	-13.8	-6.3	-11.4	11.6	-65.3
4.3 ft from Downstream End of CAP-DS	3.0	96.6	-18.0	-15.0	-16.9	-5.4	-11.1	10.5	-61.6
<b>Case 2: 1/4-in. Thick Cover Plate with Three 1/4-in. Thick Stiffeners</b>									
4.3 ft Upstream from Joint of B6 and B7	0.4	78.0	-16.0	-14.8	-18.9	-5.7	-23.0	10.4	-45.5
4.3 ft Upstream from Joint of B7 and B8	1.0	72.2	-16.0	-14.8	-16.8	-5.5	-16.9	10.4	-38.7
4.3 ft from Upstream End of CAP-US	0.6	73.2	-18.4	-12.8	-12.5	6.3	-14.3	8.6	-44.8
4.3 ft Upstream from Joint of CAP-US and CAP-DS	2.8	89.3	-14.1	-18.0	-15.5	-5.2	-18.8	11.6	-46.2
1 ft Downstream from Joint of CAP-US and CAP-DS	2.2	89.9	-17.4	-14.4	-15.5	-7.4	-12.2	12.7	-52.8
4.3 ft from Upstream End of B-10	1.4	89.8	-17.7	-13.8	-13.9	-6.0	-12.8	8.9	-55.7
4.3 ft from Downstream End of CAP-DS	1.4	96.3	-18.8	-13.5	-15.2	-8.9	-13.4	12.5	-47.4

#### 4.8 Summary and Conclusions

Concept no. 7, the two-piece cover plate, was evaluated using LS-DYNA. Computer simulations were conducted with a 2270P vehicle impacting the PCB cover plate installation with varying cap thicknesses, quantities and spacings of stiffeners, end plate configurations, gap lengths, and impact points. After evaluation of the simulation results, a two-piece cover plate design with a 1/4-in. thick steel cap and three 1/4-in. thick stiffeners showed the desired performance. The end plate consisted of a 5/8-in. thick plate with an HSS3x3x5/8 box tube at the base and incorporated a pin-and-loop connection, as shown in Figure 48. The pin and loop connection consisted of a standard 1 1/4-in. diameter A36 steel connection pin and 3/4-in. diameter reinforcing bar loops.

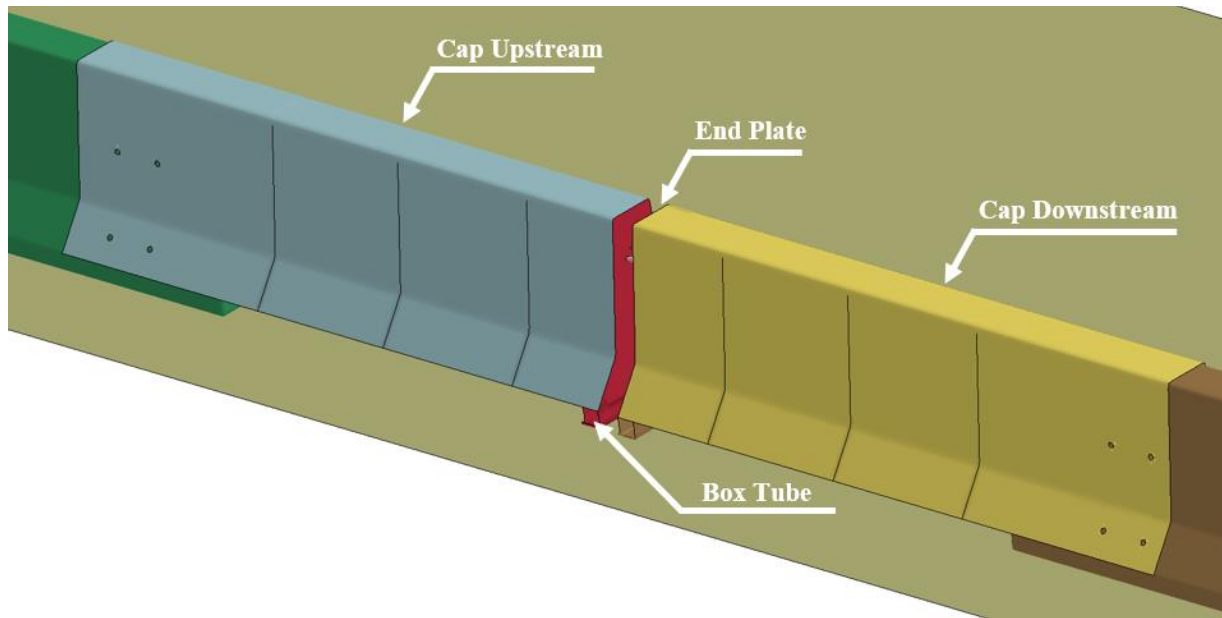


Figure 48. Final Design of Two-Piece Cover Plate for PCB Gaps, 12.5-ft Gap

## **5 SIMULATION OF CONCEPT NO. 4 – THRIE BEAM AND TOE PLATE**

LS-DYNA computer simulations were conducted to design, refine, and evaluate concept no. 4 which consisted of thrie-beam panels and a toe plate supported by internal stiffeners. The simulation results for various design configurations were analyzed and used to identify the most desired design for the development of a prototype gap-spanning system for full-scale crash testing. The same evaluation criteria used to in the design approach for concept no. 7 were used for concept no. 4.

### **5.1 Initial Design Details**

In concept no. 4, thrie-beam rail elements were placed on both sides of the PCBs and anchored with standard terminal connectors, or end shoes. Internal stiffeners were incorporated to increase the lateral stiffness and strength of the hardware for long gaps. It was anticipated that thrie beam nesting might be required to further strengthen the sides of the concept. A toe plate was placed adjacent to the lower sloped face of the PCB segments to mitigate the wheel snag on the toe of the PCB. The initial thrie beam and toe plate concept design details are shown in Figures 49 through 52. Note that further updates to these initial details were made during the development and simulation process.

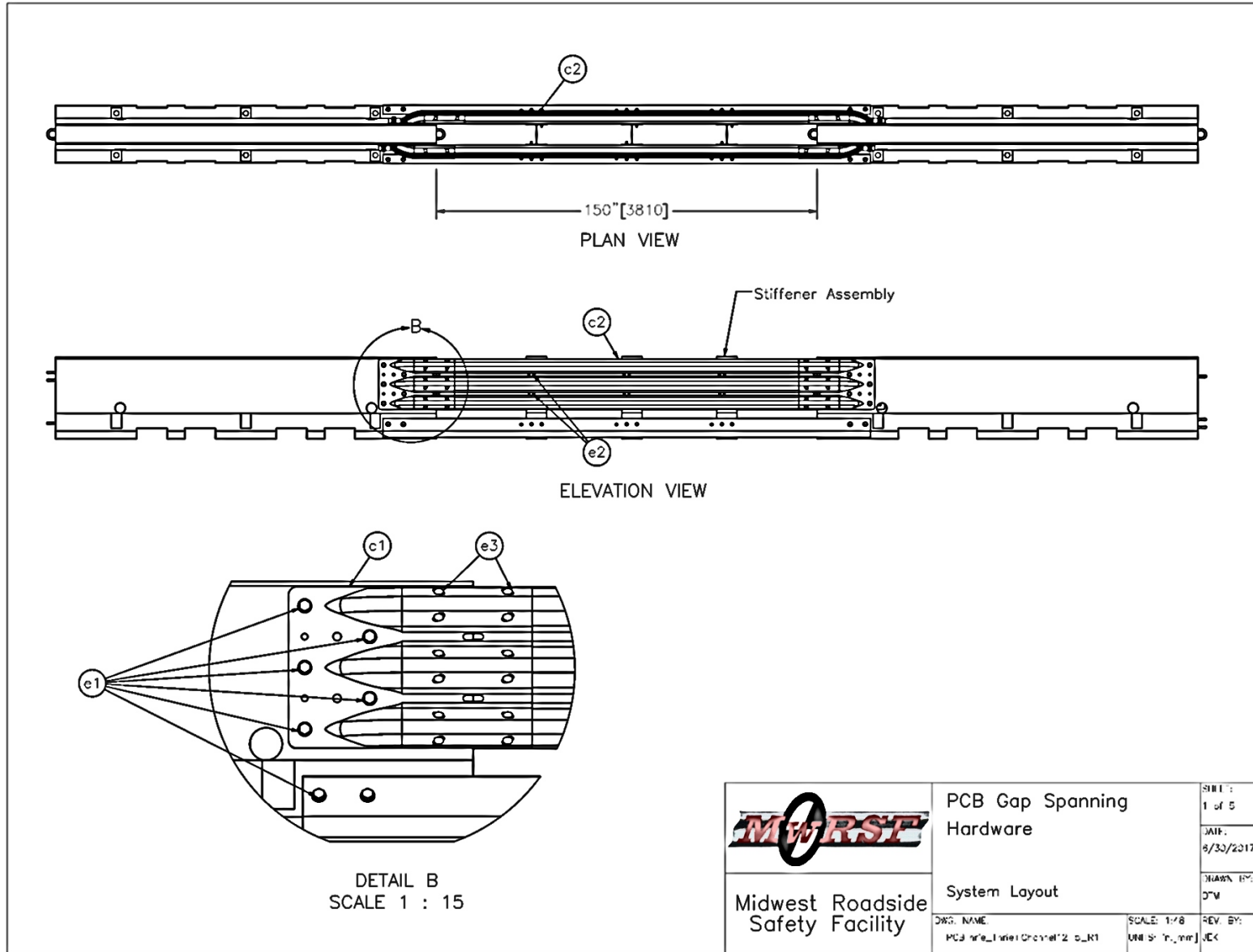


Figure 49. Concept No. 4: Thrie Beam and Toe Plate

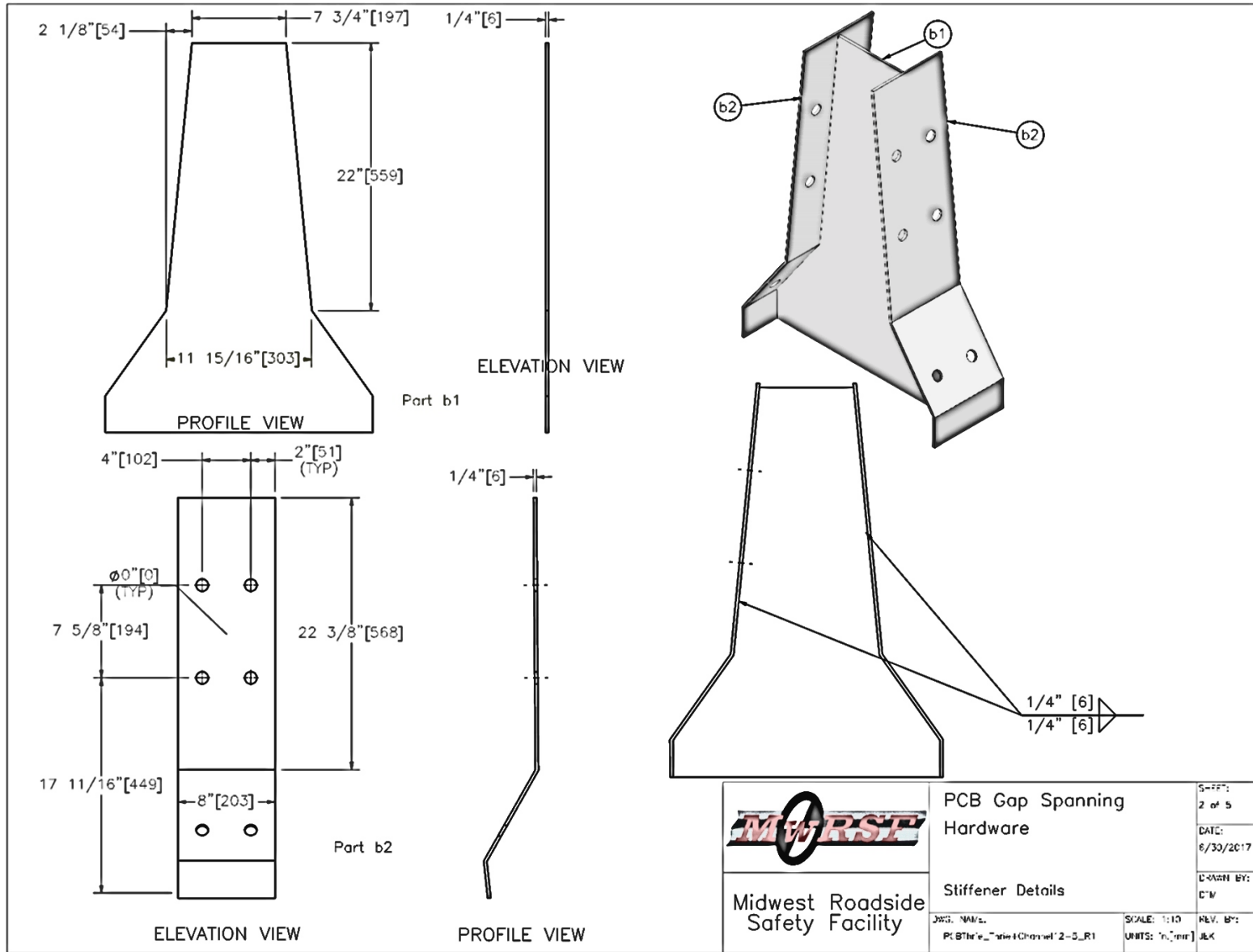


Figure 50. Concept No. 4: Thrie Beam and Toe Plate, Stiffener Details

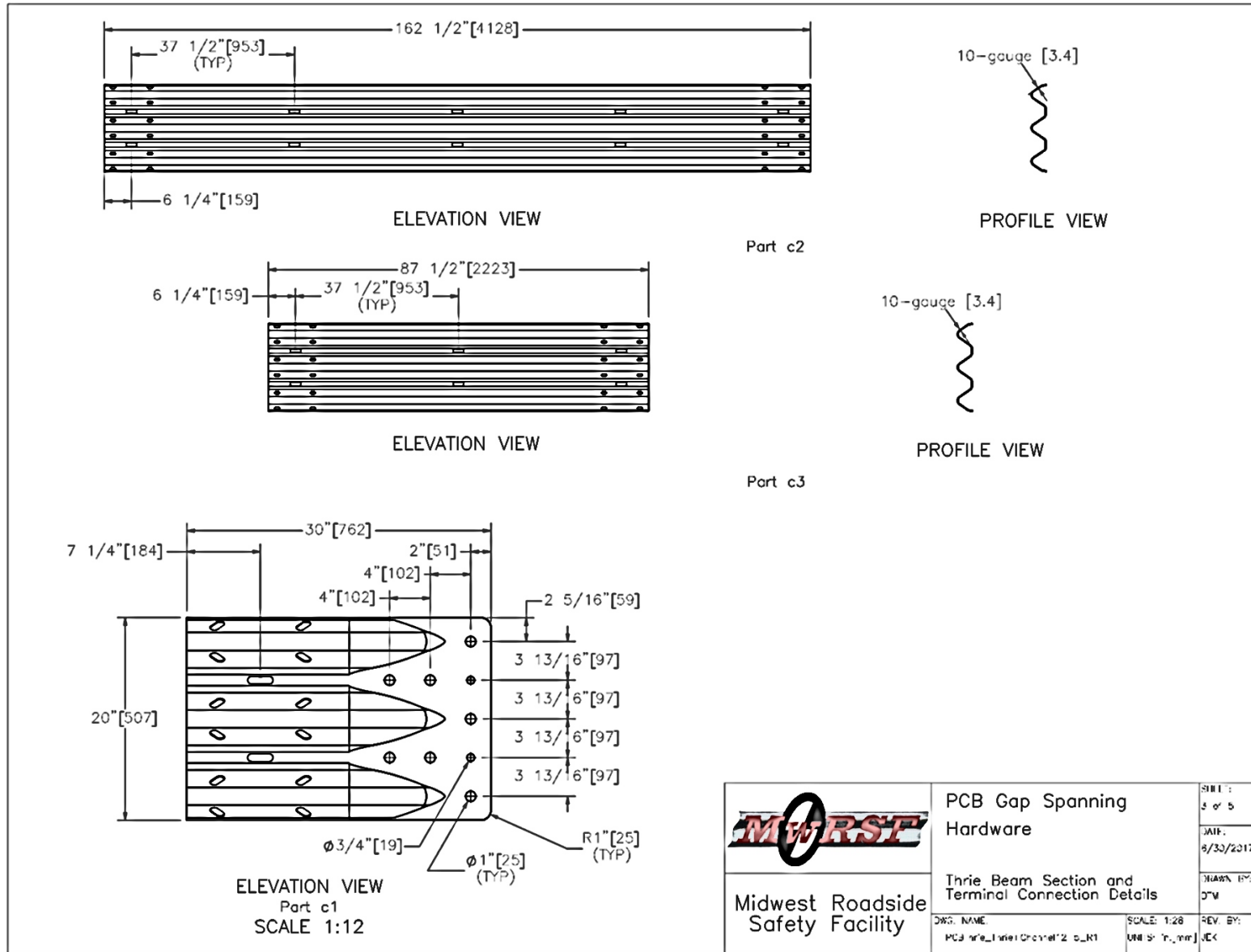


Figure 51. Concept No. 4: Thrie Beam and Toe Plate, Thrie Beam and Terminal Connector Details

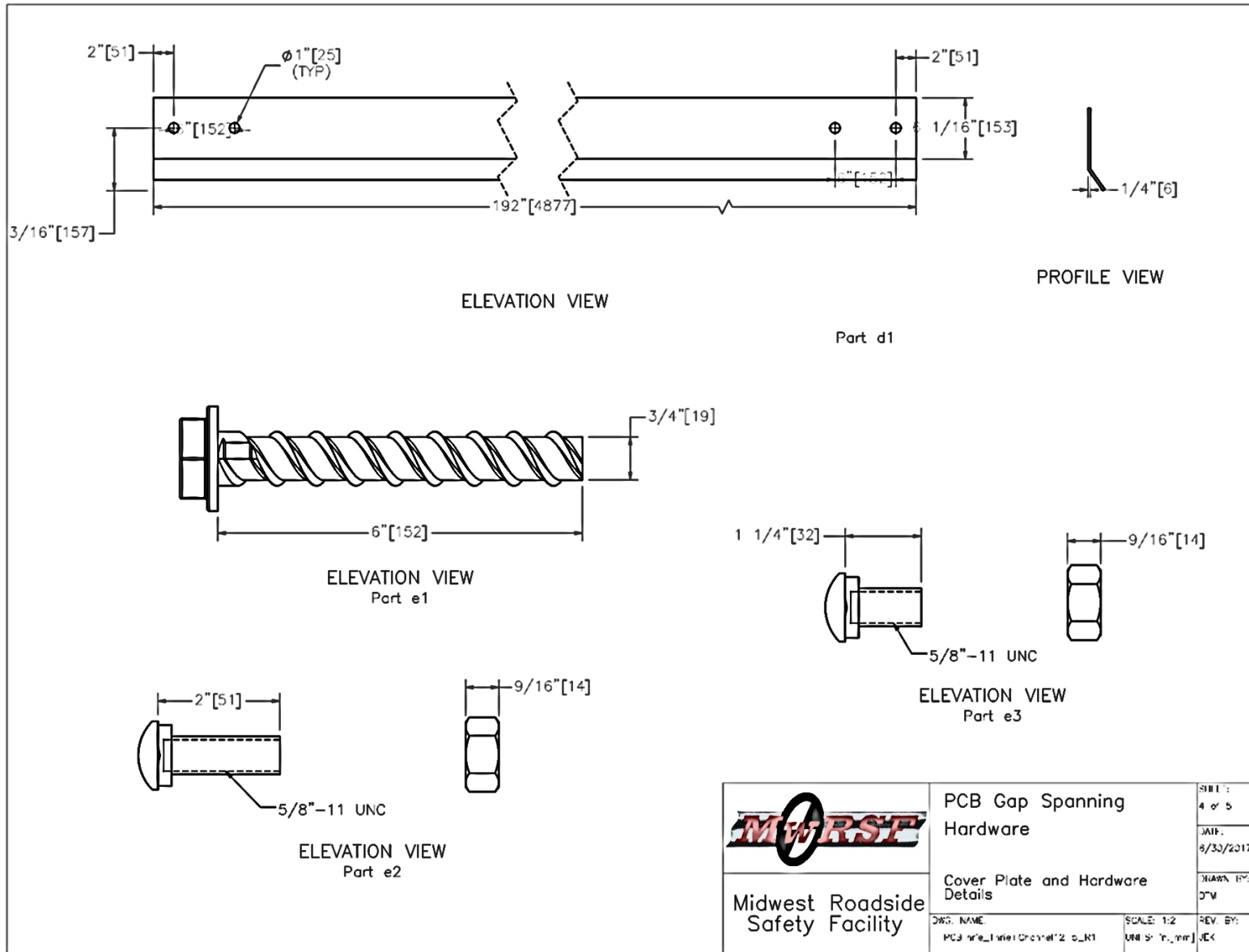


Figure 52. Concept No. 4: Thrie Beam and Toe Plate, Toe Plate and Hardware Details

## 5.2 Simulation Model

The 12-gauge thrie-beam rail was modeled using deformable shell elements with a mesh measuring approximately 1 in. x  $\frac{3}{8}$  in. An elastic-plastic material model MAT\_24\_PIECEWISE\_LINEAR\_PLASTICITY was used to simulate the AASHTO M180 galvanized steel thrie-beam rail. Rectangular areas of the thrie beam around the slotted holes measuring 4.8 in. x 2.6 in. were refined with a finer mesh. The refined mesh in this region improved the contact between the thrie-beam rail and connecting bolts. Due to the difficulty in predicting rupture in thrie beam, rail rupture and tearing were not simulated. Two 10-gauge thrie-beam end shoes were used to attach each thrie-beam rail to the PCB segments, as shown in Figure 53.

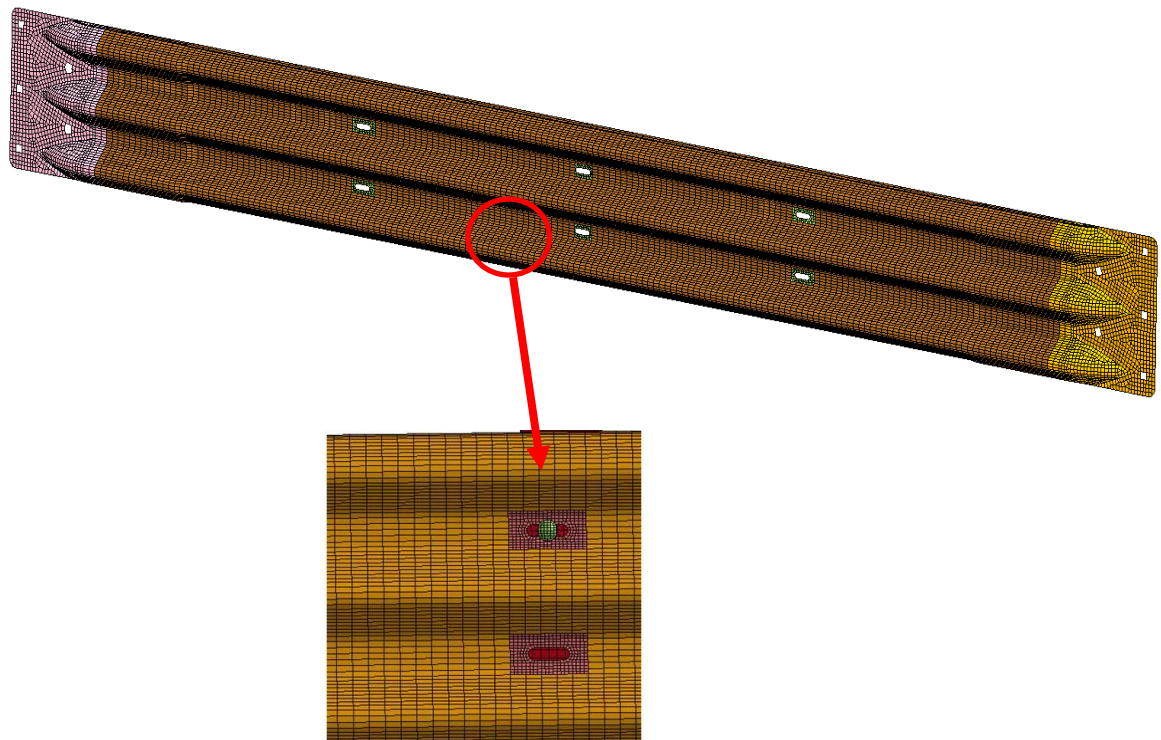


Figure 53. Thrie Beam Model

Some simulated design configurations included nested 12-gauge thrie beam. This modification from a single 12-gauge rail section to two nested rail sections was incorporated by doubling the thickness of each thrie-beam rail section as well as the bolt hole areas. Rail splices were modeled by merging adjacent nodes. The refined rail meshes near slot locations were tied to the coarser rail mesh using \*TIED\_NODE-CONSTRAINED. The connection hardware, including the bolts, nuts, and stiffener plates, were modeled explicitly in the model. Bolts were modeled using a rigid material model. Bolt preload was achieved using a discrete spring element in LS-DYNA. The internal stiffeners were added to the model to reduce the localized deformation of the thrie beam and toe plate and improve the overall structural performance. The stiffeners were modeled with ASTM A1011 grade 50 steel properties. In the bolt hole areas, the stiffeners were meshed with a similar mesh size as the thrie beam and toe plate parts to allow for a smooth contact interface. A list of the thrie beam and toe plate model components and their associated LS-DYNA parameters is shown in Table 8.

Table 8. Summary of PCB GAP Thrie Beam Model Parts and LS-DYNA Parameters

Part Description	Material Type	Material	Element Type	Element Type	Element Thickness
Thrie-Beam Guardrail Section	AASHTO M180	MAT-24 Piecewise-Linear-Plasticity	Shell	Fully Integrated Shell Element Type 16	12-gauge 10-gauge
End Shoe	AASHTO M180	MAT-24 Piecewise-Linear-Plasticity	Shell	Fully Integrated Shell Element Type 16	10-gauge
Toe Plate	ASTM A1011 Grade 50	MAT-24 Piecewise-Linear-Plasticity	Shell	Fully Integrated Shell Element Type 16	¼ in.
Stiffeners	ASTM A1011 Grade 50	MAT-24 Piecewise-Linear-Plasticity	Shell	Fully Integrated Shell Element Type 16	¼ in.
Bolt Spring	ASTM A307	MAT-11 Spring Non-Linear Elastic	Discrete	Translational Spring/Damper	N/A
Bolts	ASTM A307	MAT-20 Rigid	Solid	Constant Stress Solid Element	N/A
Nuts	ASTM A307	MAT-20 Rigid	Solid	Constant Stress Solid Element	N/A

N/A – Not Applicable

For improved sliding performance of the system, the stiffener geometry utilized a base plate at the ground line, as shown in Figure 54. Anchorage of the thrie beam end shoes and the toe plate to the PCB was accomplished by defining elements on those parts at the anchor locations as the same part as the rigid PCB, thus fixing them to the PCB at those locations. The overall assembly details of the thrie beam and toe plate model are shown in Figure 55.

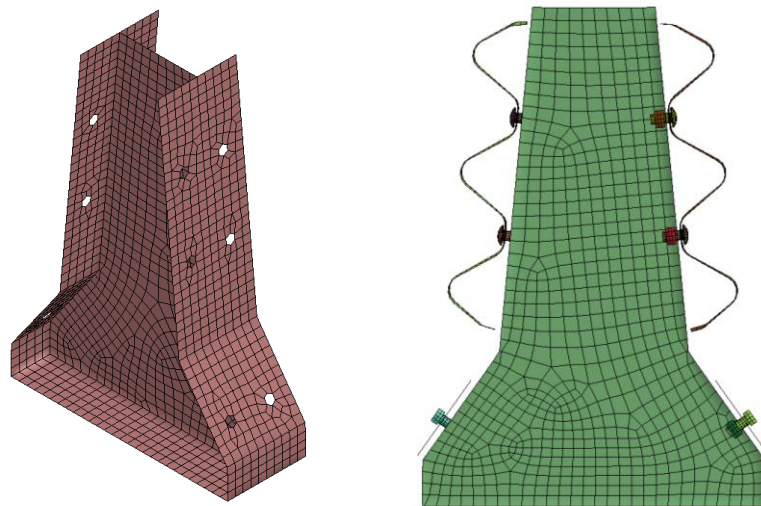


Figure 54. Thrie Beam Stiffener Model

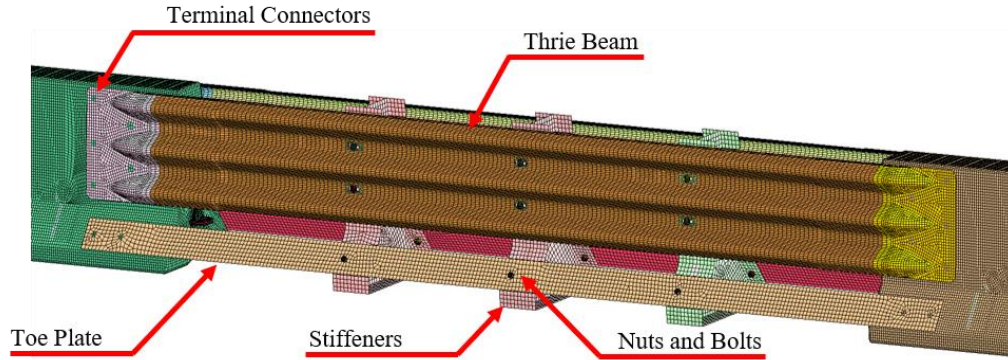


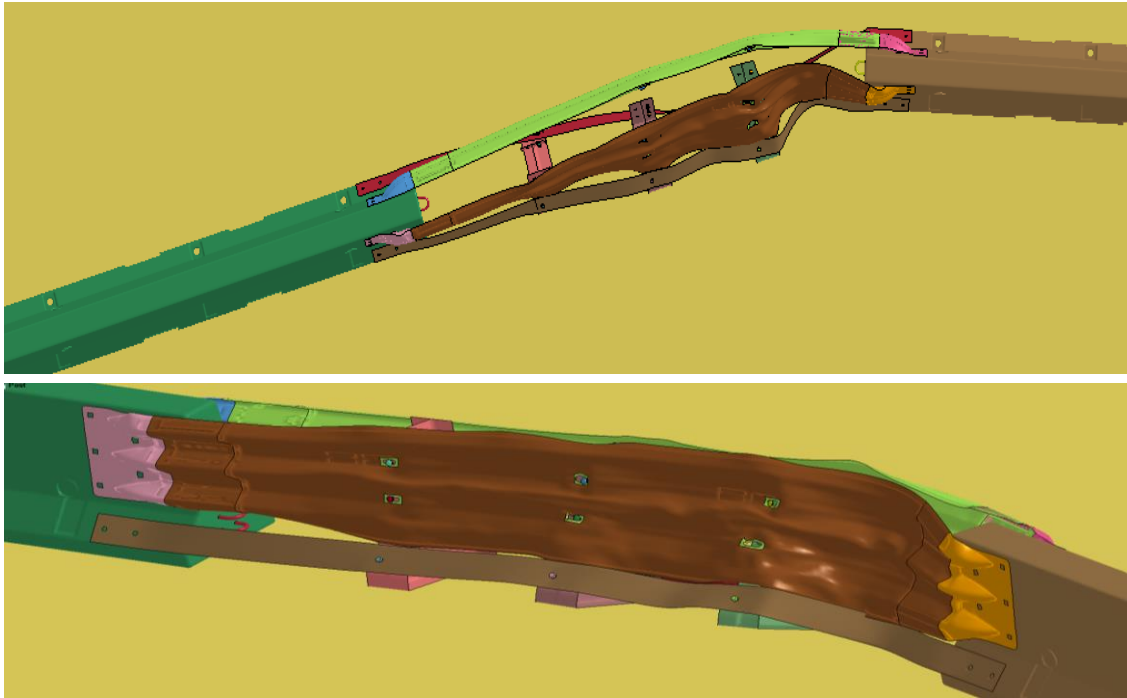
Figure 55. Thrie Beam and Toe Plate Model

### 5.3 Simulations of Thrie Beam and Toe Plate Model with Rail Variations

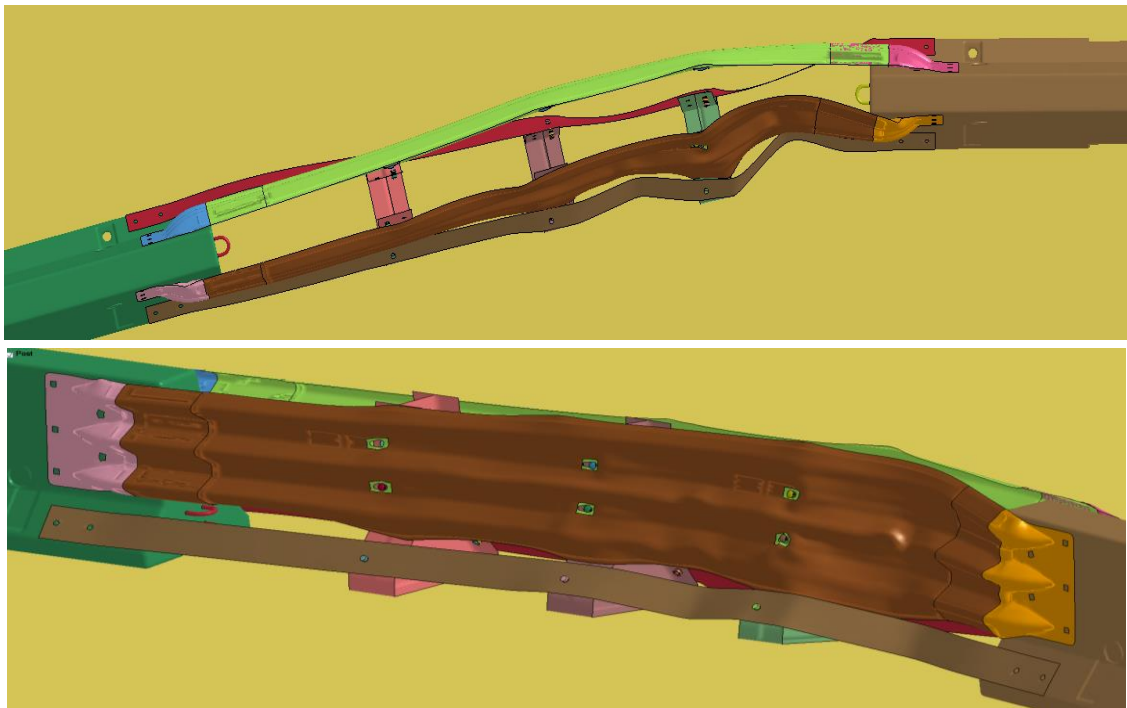
The simulation model was modified with four different thrie-beam rail variations to determine a suitable thrie-beam rail section for the design of gap spanning hardware. Simulations were conducted with variations of single 12-gauge, single 10-gauge, nested 12-gauge, and nested 10-gauge thrie-beam rail. The rail thickness variations were evaluated based on MASH safety performance criteria and their structural deformation and integrity.

#### 5.3.1 Single Thrie-beam rail

The thrie beam and toe plate design was simulated with either a single 12-gauge or a single 10-gauge rail, three ¼-in. thick internal stiffeners, and ¼-in. thick toe plates. The performance of both single rail configurations was deemed unacceptable as excessive deformation and hinging was observed when impacted 4.3 ft upstream from the middle of the thrie-beam rail by a 2270P vehicle, as shown in Figure 56. The excessive deformation and hinging raised concerns for potential vehicle snag and instability. Other safety measures, including occupant risk values, barrier deflection, vehicle roll and pitch angles, and vehicle climb did not appear critical. Due to the excessive deformation and pocketing potential, single 12-gauge and single 10-gauge rail variations were not considered for further evaluation.



(a)



(b)

Figure 56. Simulations of Thrie Beam and Toe Plate Model (a) Single 12-Gauge Rail, and (b) Single 10-Gauge Rail

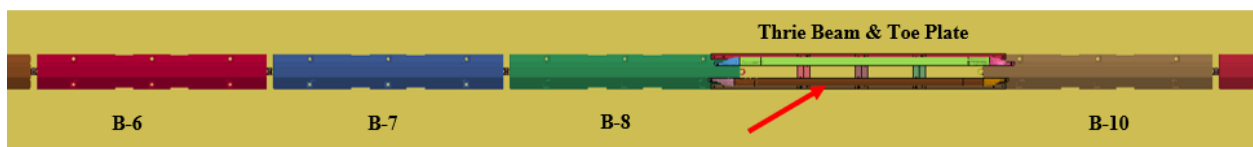
### 5.3.2 Nested Thrie-beam rail

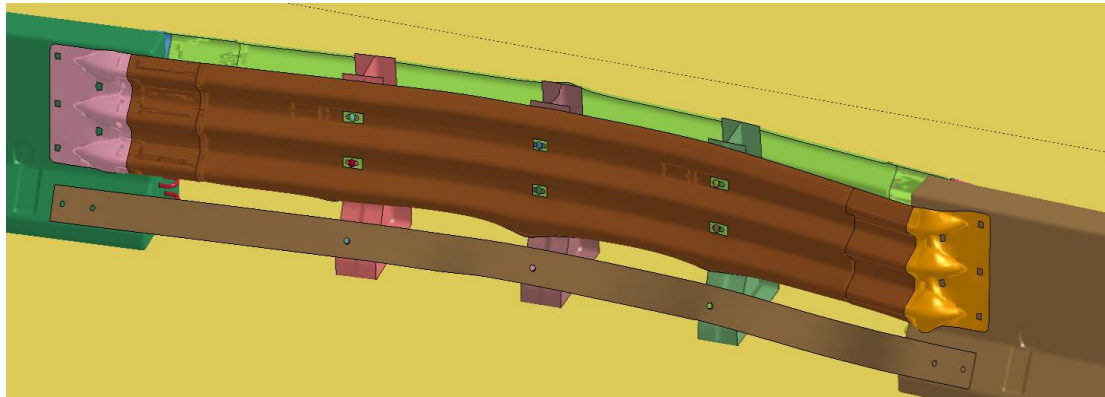
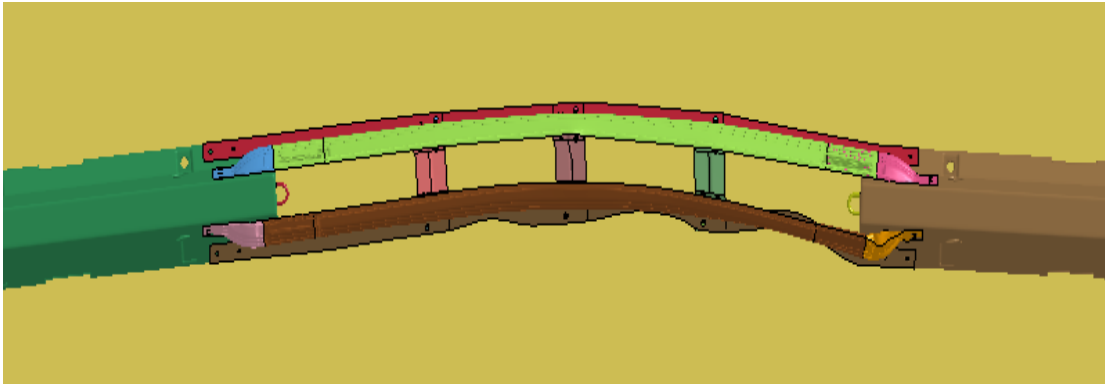
Further simulations were conducted with nested thrie-beam rail including nested 12-gauge rail, nested 10-gauge rail, and triple-nested 12-gauge rail. A summary of the simulation results of nested rail designs when impacted 4.3 ft upstream from the middle of the thrie-beam rail by a 2270P vehicle is shown in Table 9. All nested rail designs, including nested 12-gauge, nested 10-gauge, and nested with three layers of 12-gauge rail provided sufficient structural strength and reduced the localized crush and deflection of the rail, as shown in Figure 57. The roll, pitch, and yaw angles and ORA/OIV values for all nested rail configurations were within MASH limits, as shown in Table 9. Sequential images of the nested 12-gauge rail simulation when impacted 4.3 ft upstream from the middle of the thrie-beam rail by a 2270P vehicle are shown in Figure 58. While all three of these rail configurations were found to improve the gap-spanning hardware's performance, it was noted that 12-gauge thrie beam is a common rail element used in approach guardrail transitions and would be readily available in most state DOT inventories. As such, the nested 12-gauge thrie-beam rail configuration was recommended for further use in the design concept.

Table 9. Summary of Simulation Results: Thrie Beam and Toe Plate Design with Three ¼-in. Thick Stiffeners

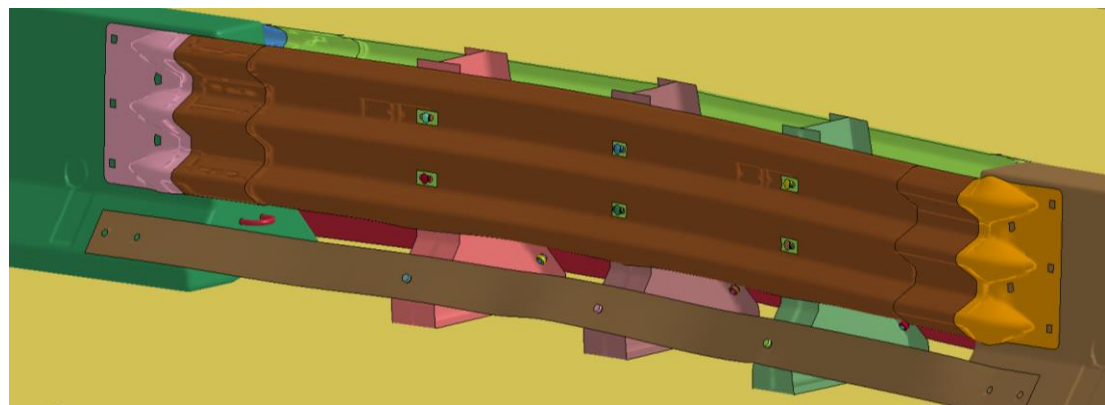
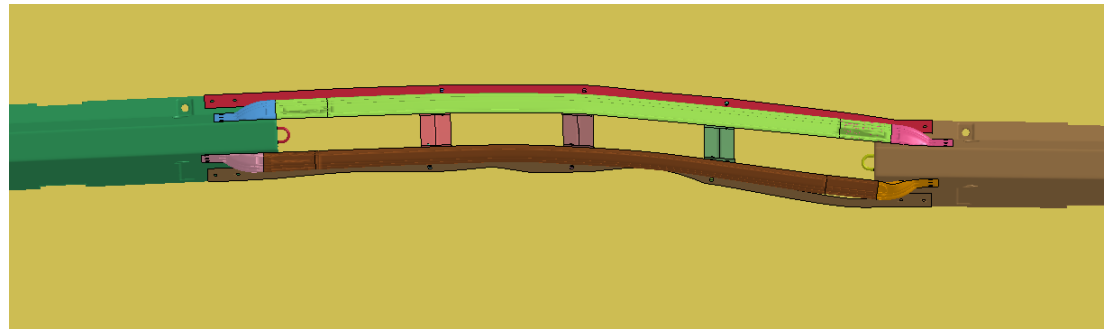
Simulated Thrie Beam Thickness	Impact Point	Lateral Dynamic Deflection (in.)	Lat. OIV (ft/s)	Long. OIV (ft/s)	Lat. ORA (g's)	Long. ORA (g's)	Roll (deg.)	Pitch (deg.)	Yaw (deg.)
Nested 12-Gauge Rail	4.3 ft Upstream from Middle of Thrie-Beam Rail	67.9	-19.0	-17.1	-11.6	-5.2	-13.2	6.7	-38.4
Nested 10-Gauge Rail	4.3 ft Upstream from Middle of Thrie-Beam Rail	57.5	-19.4	-18.0	-12.9	-4.7	-21.1	4.8	-37.4
3 Layers of Nested 12-Gauge Rail	4.3 ft Upstream from Middle of Thrie-Beam Rail	55.2	-19.7	-17.4	-11.2	-4.3	-21.8	4.8	-37.0
MASH Limits	N/A	N/A	≤ 40	≤ 40	≤ 20.49	≤ 20.49	< 75	< 75	N/A

N/A – Not Applicable





(a)



(b)

Figure 57. Simulations of Thrie Beam and Toe Plate Model (a) Nested 12-Gauge Rail and (b) Nested 10-Gauge Rail

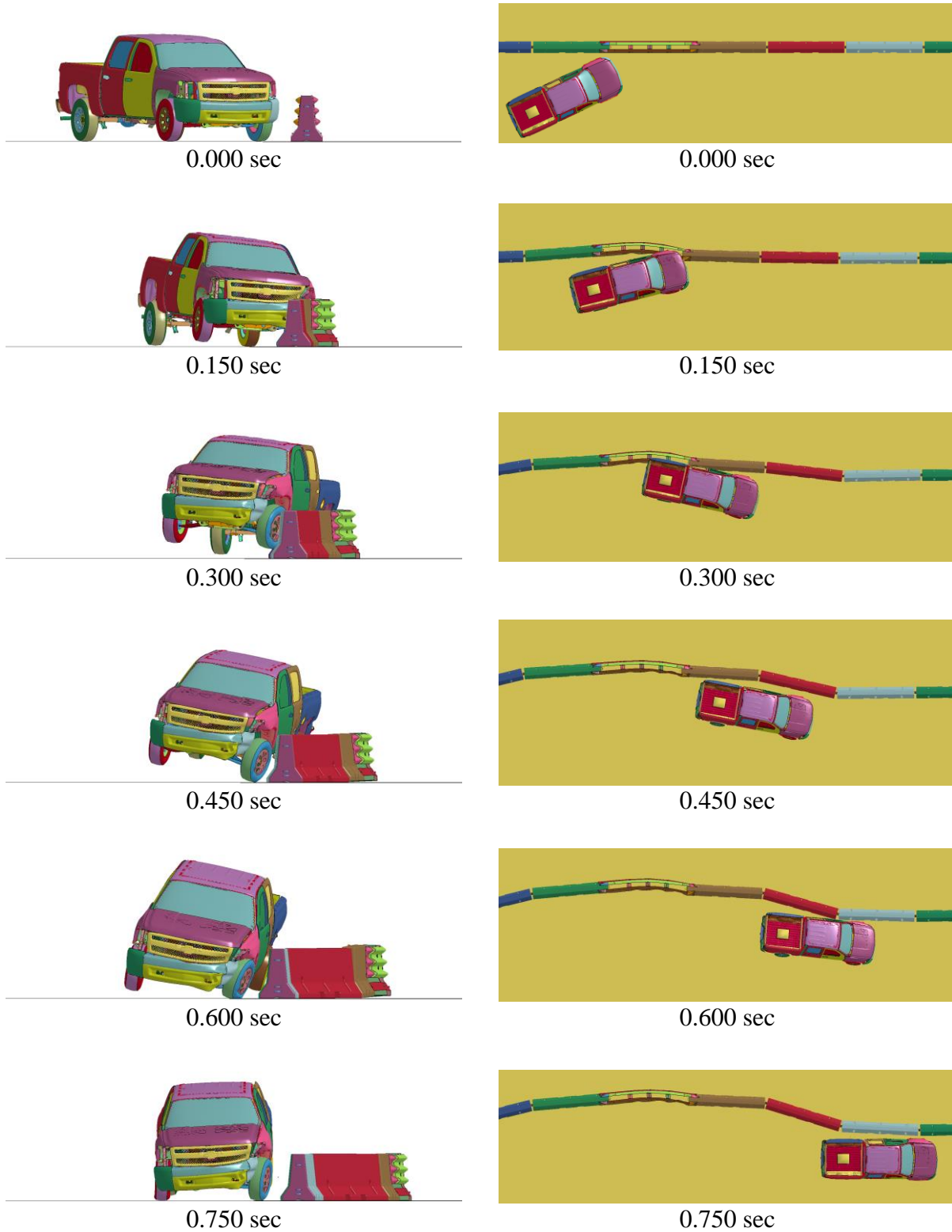


Figure 58. Sequential Images, Impact Point 4.3 ft Upstream from Middle of Nested 12-Gauge Thrie-beam rail

### 5.4 Multiple Impact Points Analysis – Test Designation No. 3-11

Additional simulations were conducted upstream from the gap and at additional points along the gap-spanning hardware to further evaluate the performance of the revised design with nested 12-gauge thrie beam, ¼-in. thick toe plates, and internal stiffeners. Impact points were selected 4.3 ft upstream from several barrier joints as well as 4.3 ft upstream from the midspan of the gap spanning hardware, as shown in Figure 59. These simulations were conducted to further investigate barrier loading, pocketing, and load transfer across the joint.

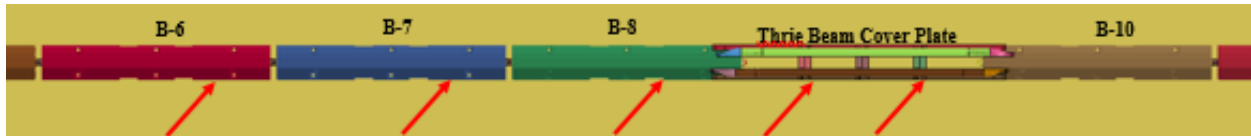
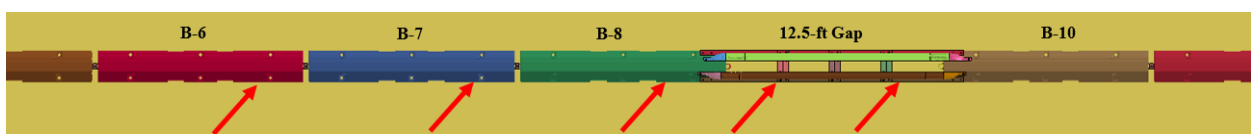


Figure 59. Simulated Impact Points

The simulation results suggested that the nested 12-gauge thrie-beam and toe-plate system with three stiffeners showed no structural issues for the selected impact points, as shown in Table 10. None of the ORA and OIV occupant risk values exceeded the MASH limits. The system deflection was 15 percent lower than that observed for a free-standing PCB system with no gap. The deflection of the barrier system with the gap hardware installed showed a tendency to form a knee or kink in the deflecting PCB segments that may induce vehicle instabilities. This issue was further investigated and is discussed in a subsequent section. The roll and pitch angle and ORA and OIV values for all impact locations yielded results that were well below the MASH limits, as shown in Table 10.

Table 10. Summary of Simulation Results: Nested 12-Gauge with ¼-in. Thick Stiffeners and Toe Plate

Impact Point	Lat. OIV (ft/s)	Long. OIV (ft/s)	Lat. ORA (g's)	Long ORA (g's)	Roll (deg.)	Pitch (deg.)	Yaw (deg.)	Lateral Dynamic Deflection (in.)	Increase in Bumper Height (in.)
4.3 ft US from B-10	-17.0	-15.1	-9.8	-4.0	-33.6	6.7	-49.6	70.0	3.3
4.3 ft US from Middle of Rail	-19.0	-17.1	-11.6	-5.2	-13.2	6.7	-38.4	67.9	8.0
4.3 ft from DS End of B-8	-16.7	-17.0	-10.3	-6.6	-19.0	8.5	-36.6	66.2	10.0
4.3 ft US from Joint of B-7 & B-8	-18.7	-16.0	-19.1	-9.8	-8.6	15.2	-34.3	70.0	12.4
4.3 ft US from Joint of B-6 & B-7	-16.0	-14.4	-19.7	-7.2	-27.4	9.3	-49.5	70.2	5.8



## 5.5 Nested 12-Gauge Rail and 37.5-in. Gap

Additional simulations were conducted to investigate the performance of the three-beam and toe-plate concept at reduced gap lengths to determine if the behavior of the system was adversely affected by shorter gaps. The model with a 12.5-ft gap was modified to simulate a 37.5-in. gap adjacent to the PCB segments, as shown in Figure 60. Note that no internal stiffeners were used for the shorter gap simulations. Several simulations were conducted on nested 12-gauge rail impacted at various points, as shown in Figure 61. A summary of the simulation results is shown in Table 11.

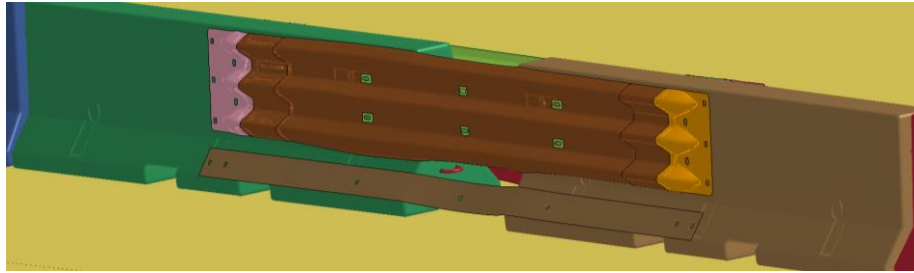


Figure 60. 37.5-in. Gap Simulation with Nested 12-Gauge Rail

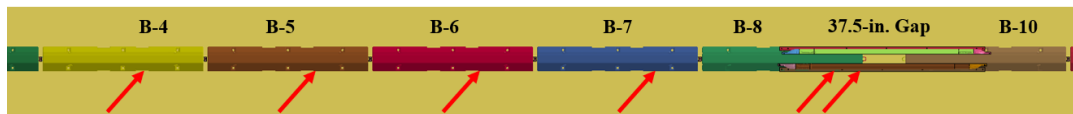


Figure 61. Impact Points for Simulated Cases with 37.5-in. Gap

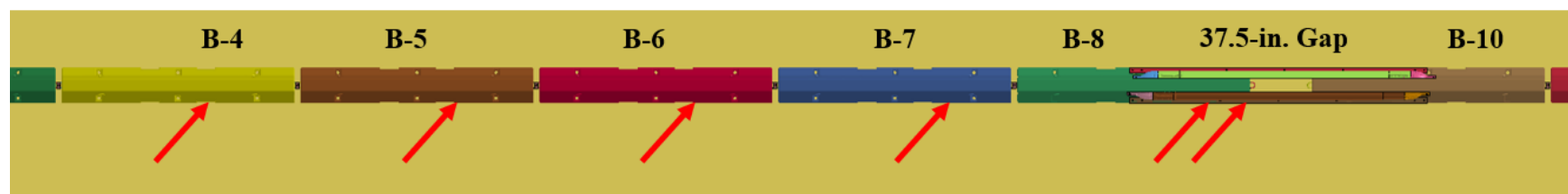
As shown in Table 11, the simulation results suggested that the lateral barrier deflection for all the impacts decreased as compared to the deflection of a free-standing PCB system with no barrier gaps. This reduction in deflection was likely due to the gap-spanning hardware forming a large continuous barrier segment across barrier nos. B-8 and B-10. The inertia of the combined barriers in that region likely reduced barrier deflection as compared to the standard continuous barrier system. The structural performance of the gap spanning hardware was good for the shorter barrier gap as the unsupported span was reduced and most of the hardware was supported directly by the body of the adjacent PCB segments. No concerns with vehicle capture and redirection or occupant risk values were noted.

The simulation results did indicate that certain impacts formed a knee or kink at joint locations between barrier segments, which extended forward laterally from the original barrier line and impacted the vehicle's door. This knee contact did not appear to be detrimental to the vehicle or the barrier performance in the simulations. An impact of this type into the vehicle's door has been shown to increase vehicle instability in previous research regarding minimum system lengths for free-standing PCB [41]. However, full-scale crash testing conducted during that research effort indicated that the knee did not cause sufficient instability to induce roll of the vehicle without the significant increase in the lateral deflection of the barrier system caused by reduced barrier system length. For the PCB gap spanning hardware developed in this research, lateral barrier deflection actually decreased as compared to the free-standing F-shape PCB system. Thus, based on previous investigation, the formation of the knee in the barrier segments was not deemed a concern moving forward.

Table 11. Summary of Simulation Results: Nested 12-Gauge Rail

Impact Location	Lateral OIV (ft/s)	Long. OIV (ft/s)	Lateral ORA (g's)	Long. ORA (g's)	Roll (deg.)	Pitch (deg.)	Yaw (deg.)	Lateral Barrier Deflection (in.)	Ext. from Barrier Line (in.)	Increase in Bumper Height (in.)
DS End of B-8	-18.7	-17.0	-11.8	-5.7	-16.2	5.7	-40.8	56.7	3.5	4.9
4.3 ft US from Middle of Rail	-19.2	-18.3	-12.9	-4.8	-18.2	13.0	-33.7	47.9	2.0	6.6
4.3 ft US from Joint of B-7 & B-8	-19.0	-15.4	-14.8	-10.4	-9.3	15.8	-37.6	70.9	7.2	4.8
4.3 ft US from Joint of B-6 & B-7	-16.0	-15.4	-18.6	-8.0	-24.8	12.9	-46.5	67.5	2.7	5.7
4.3 ft US from Joint of B-5 & B-6	-16.0	-11.8	-17.7	-9.3	-26.8	11.0	-45.4	67.8	4.6	5.6
4.3 ft US from Joint of B-4 & B-5	-16.7	-10.5	-13.2	-6.9	-20.7	28.9	-48.7	78.4	6.3	6.2

74



## 5.6 Summary and Conclusions

To evaluate the three beam and toe plate concept design (concept no. 4), several simulations were conducted with four different variations of three-beam rails, including single and nested 12-gauge and 10-gauge rail. All the configurations were simulated with three internal stiffeners made from 1/4-in. thick plate at 3-ft spacing and two 1/4-in. thick x 6-in. wide x 192-in. long toe-plates. Single 12-gauge and 10-gauge rails were not suitable for the design due to excessive deformation and plastic hinge formation. The nested 12-gauge rail section was selected to investigate further as it exhibited reduced deformation and is a commonly available section in state DOT inventories.

Multiple impact point simulations were conducted with nested 12-gauge rail. The results suggested that the selected three-beam rail design demonstrated no major issues for the multiple impact points and none of the occupant risk values exceeded MASH limits. The results also demonstrated reduced deflection in the region of the gap-spanning hardware as compared to free-standing PCBs with no gap. The simulation did indicate potential for a knee to form in the barrier segments as they deflected that extended laterally in front of the original barrier line. This knee had a tendency to contact the side and/or doors of the impacting pickup which, in previous research, had been shown to increase vehicle instability when coupled with increased lateral barrier deflection [41]. However, in the case of the system developed herein, it was not believed to be a critical behavior as the lateral deflection of the barrier decreased due to the presence of the PCB gap spanning hardware.

## 6 SELECTION OF PREFERRED DESIGN CONCEPT

The design details and simulation results for the two-piece cover plate (concept no. 7) and the thrie beam and toe plate (concept no. 4) gap-spanning concepts were discussed with the Midwest Pooled Fund Program member states. The two gap-spanning hardware concepts were compared based on overall safety performance in the preliminary models, design complexity, and ease of fabrication and construction. Both proposed design concepts demonstrated the potential to meet MASH TL-3 safety requirements. A comparison of the specialized parts, weight, and potential performance concerns is shown in Table 12. The thrie beam and toe plate design was lighter as compared to the two-piece cover plate and would include fewer fabricated parts. The two-piece cover plate design was more complex for fabrication when considering construction tolerances. The two-piece cover plate concept also required lifting equipment to move and transport due to the high weight of the individual cover plates. As such, it was determined that thrie beam and toe plate design would be easier to assemble, move, and transport.

The comparisons were presented to the Midwest Pooled Fund Program member states, and a unanimous decision was reached to move forward with the nested thrie beam and toe plate configuration. This decision was made based on the simulation results that indicated that all vehicle trajectory, occupant risk values, and other safety criteria were below the MASH recommended limits for various impact locations. Additionally, the nested thrie beam and toe plate concept was preferred due to the ease of fabrication and construction as it would not require any new components other than standard hardware, toe plates, and stiffeners supporting the rails.

Table 12. Comparison of Candidate Design Concepts for PCB Gap-Spanning Hardware

<b>Evaluation Variables</b>	<b>Two-Piece Cover Plate</b>	<b>Thrie Beam and Toe Plate</b>
Weight	1,405 lb	1,114 lb
Special Fabricated Parts	Two Cover Plates Six Stiffeners	Two Lower Plates Three Stiffeners
Performance Concerns	Vehicle snag on cover plate Construction tolerances Required lifting equipment	Knee formation

## 7 SELECTED CONCEPT DESIGN SIMULATION AND CRITICAL IMPACT POINT ANALYSIS

Additional simulations were performed to fully develop the thrie beam and toe plate design with nested 12-gauge thrie-beam rail, internal stiffeners, and toe plates. These simulations were used to identify potential modifications which could minimize the risk of test failure in terms of increased occupant risk values, deflection, and potential for snagging and pocketing. Additionally, these simulations were used to determine critical impact points (CIPs) for full-scale crash testing and evaluation of the system. Design modifications were implemented into the simulation model as concerns were identified during the analysis. The simulations were conducted on gap sizes of 12.5 ft with the 2270P vehicle model. Subsequent simulations were conducted on a gap size of 3 ft. The impact points were located (1) along the thrie beam and toe plate to evaluate the occupant risk, vehicle trajectory, the potential for vehicle snag and pocketing as well as the structural performance of the gap-spanning hardware; (2) on barrier nos. B-5, B-6, and B-7 at 4.3 ft upstream from the barrier joints to evaluate potential issues on the approach to the gap-spanning hardware; and (3) downstream from the gap-spanning hardware on barrier no. B-10 to evaluate any potential performance issues created when impacting downstream from the hardware. The impact points on the system with a 12.5-ft gap, ranging from 11 in. to 513.1 in. upstream from barrier no. B-10, are shown in Figure 62.

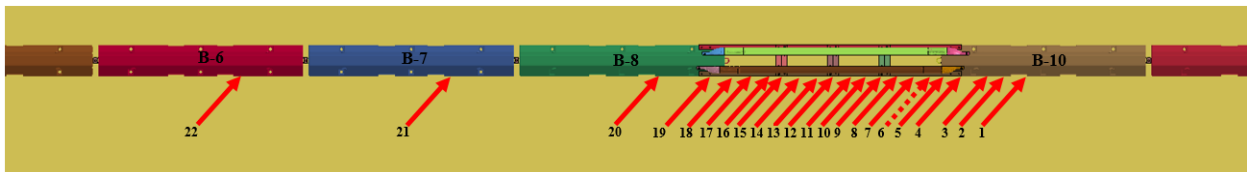


Figure 62. Simulated Impact Points, 12.5-ft Long Gap

The initial gap-spanning hardware design that was simulated consisted of two nested 12-gauge thrie-beam rail sections, three internal 1/4-in. thick stiffeners, and two 1/4-in. x 6-in. x 192-in. steel toe plates. A summary of the simulation results is shown in Table 13. All the simulated impact points met the ORA and OIV MASH criteria. Two impact points located 359.1 in. and 513.1 in. upstream from barrier no. B-10 indicated relatively high lateral ORA values (19.7 g's). However, LS-DYNA simulation tends to overpredict lateral ORA and it is believed that the high simulated occupant risk values can be partially attributed to an overly stiff rear suspension in the Silverado pickup truck model. Therefore, the slightly higher ORAs were not deemed a concern and were not considered when selecting the preferred design alternative.

The impacts at 11 in., 22.4 in., and 35.9 in. upstream from barrier no. B-10 (i.e., simulation nos. 6, 7, and 8) resulted in a relatively high roll angle. Note that the vehicles in all three of these simulations were continuing to roll at the time the simulations were terminated. However, had the simulations continued, all three would have resulted in vehicle rollovers. Therefore, this configuration did not meet the TL-3 MASH criteria in terms of vehicle stability (roll <75 degrees) and required further investigation.

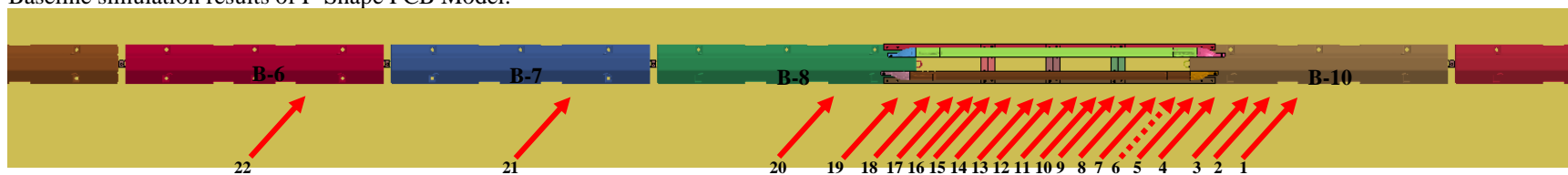
Table 13. Summary of Simulation Results: Critical Impact Point Investigation, Nested 12-Gauge Rail

Sim. No.	Impact Point US or DS from Barrier No. B-10	Toe Plate		Lat. OIV (ft/s)	Long. OIV (ft/s)	Lat. ORA (g's)	Long. ORA (g's)	Roll (deg.)	Pitch (deg.)	Lat. Barrier Deflection (in.)	Pass/Fail
		Thickness (in.)	Height (in.)								
5	0 in.	¼	6	-19.3	-13.1	-12.6	-4.1	-37.3	12.0	76.6	Pass
6	11.0 in. Upstream	¼	6	-19.3	-14.1	-13.6	-4.8	-61.4	5.6	79.5	Fail <sup>1</sup>
7	22.4 in. Upstream	¼	6	-19.0	-15.4	-16.0	-8.0	-83.5	8.1	75.0	Fail
8	35.9 in. Upstream	¼	6	-19.3	-15.4	-14.2	-6.0	-52.6	33.1	74.3	Fail <sup>1</sup>
9	48 in. Upstream	¼	6	-17.7	-15.7	-13.4	-5.9	-31.3	6.1	79.6	Pass
10	59.3 in. Upstream	¼	6	-17.0	-15.1	-9.8	-4.0	-33.6	6.7	70.0	Pass
11	74.9 in. Upstream	¼	6	-15.7	-15.1	-12.3	-4.5	-23.0	11.0	74.1	Pass
12	79.0 in. Upstream	¼	6	-16.1	-16.1	-12.0	-4.4	-23.6	9.8	72.1	Pass
13	92.4 in. Upstream	¼	6	-19.7	-18.0	-13.7	-5.0	-31.0	30.9	63.5	Pass
14	108.0 in. Upstream	¼	6	-18.4	-16.1	-13.9	-4.9	-5.6	3.1	38.2	Pass <sup>1</sup>
15	118.7 in. Upstream	¼	6	-18.7	-16.4	-11.2	-3.9	-10.9	5.7	52.0	Pass
16	130.4 in. Upstream	¼	6	-18.4	-16.1	-14.1	-5.8	-8.5	8.1	53.3	Pass
17	143.0 in. Upstream	¼	6	-19.0	-17.1	-11.6	-5.2	-13.2	6.7	67.9	Pass
18	156.6 in. Upstream	¼	6	-17.7	-16.0	-12.6	-4.4	-7.7	5.4	74.8	Pass
20	205.1 in. Upstream	¼	6	-16.7	-17.0	-10.3	-6.6	-19.0	8.5	66.2	Pass
21	359.1 in. Upstream	¼	6	-18.7	-16.0	-19.1	-9.8	-8.6	15.2	70.0	Pass
22	513.1 in. Upstream	¼	6	-16.0	-14.4	-19.7	-7.2	-27.4	9.3	70.2	Pass
-	51 in. Downstream B9	N/A	N/A	-17.7	-17.0	-7.6	-12.7	-15.9	20.2	81.1	Pass <sup>2</sup>
MASH Limits		N/A	N/A	≤ 40	≤ 40	≤ 20.49	≤ 20.49	< 75	< 75	N/A	-

N/A – Not Applicable

<sup>1</sup> Maximum roll value was not reached prior to conclusion of simulation.

<sup>2</sup> Baseline simulation results of F-Shape PCB Model.



## **7.1 Investigation of Roll Angle Concern – 12.5-ft Long Gap**

An investigation was conducted to identify the causes of the vehicle rollover and excessive roll angle at impact locations of 11 in., 22.4 in., and 35.9 in. upstream from barrier no. B-10 (i.e., simulation nos. 6, 7, and 8), as shown in Table 13. The simulations of free-standing PCB and the PCB with gap-spanning hardware were compared in terms of barrier deflection, rotation, and toe plate deformation. A sequential comparison of the simulated barrier deflection was conducted between the PCB with gap-spanning hardware for a 12.5-ft long gap and the freestanding PCB, as shown in Figures 63 and 64. An initial visual inspection of the performance of the two models noted that there was a reduction in vehicle climb and minor differences in the deflected barrier shape for the model with the gap-spanning hardware. However, no conclusive reason for the increased vehicle roll could be identified.

Further investigation revealed that there was excessive deformation and bending of the toe plate in the region just upstream from barrier no. B-10 which caused wheel snag on the upstream end of barrier no. B-10 for the previously noted impact locations, as shown in Figure 65. Thus, it was noted that modifications to the toe plate to reduce its deformation would improve vehicle stability and potentially resolve the excessive roll angle concern.

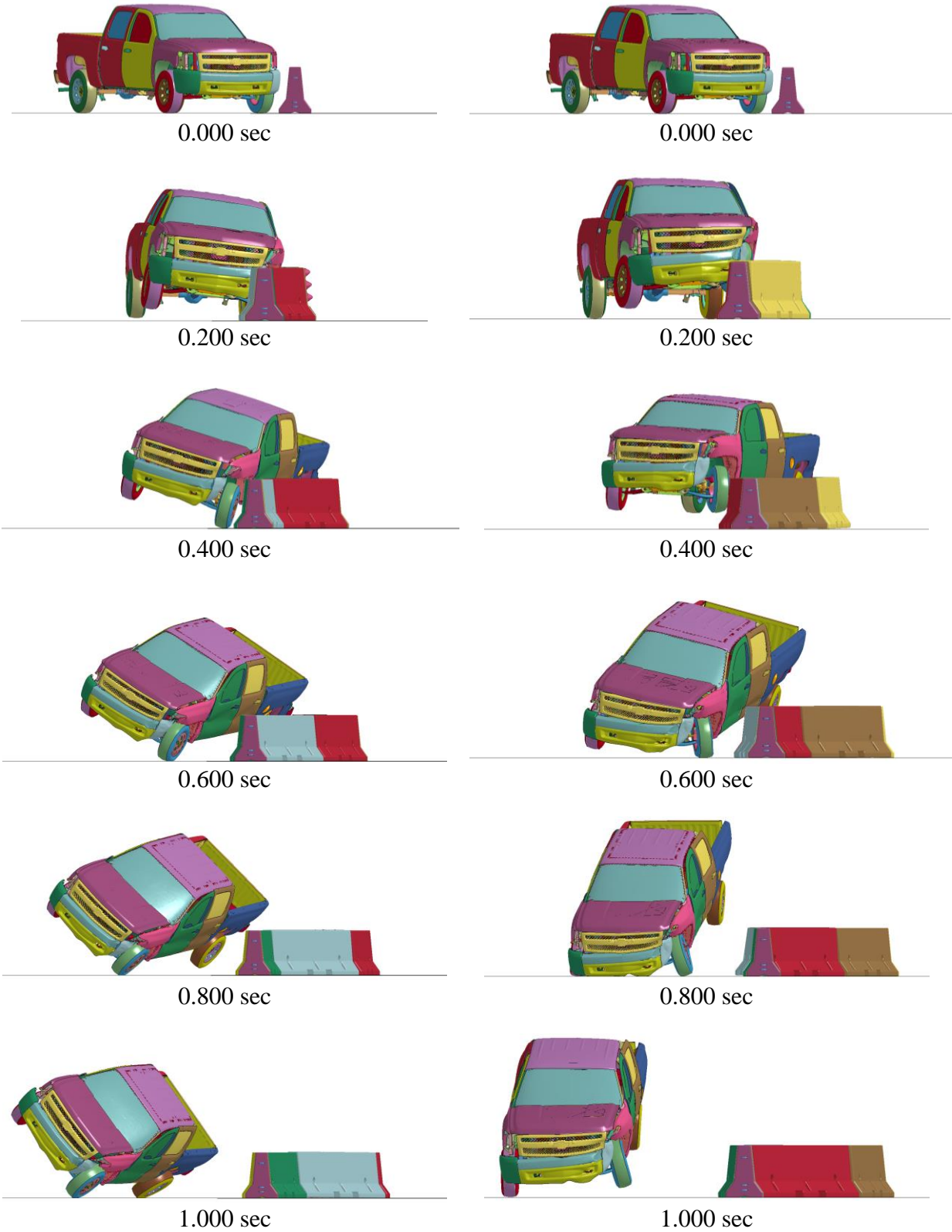


Figure 63. Sequential Images, Downstream View: PCB with Gap-Spanning Hardware, Thrie Beam and Toe Plate (Left), and Free-Standing, F-Shape, PCB Model (Right)

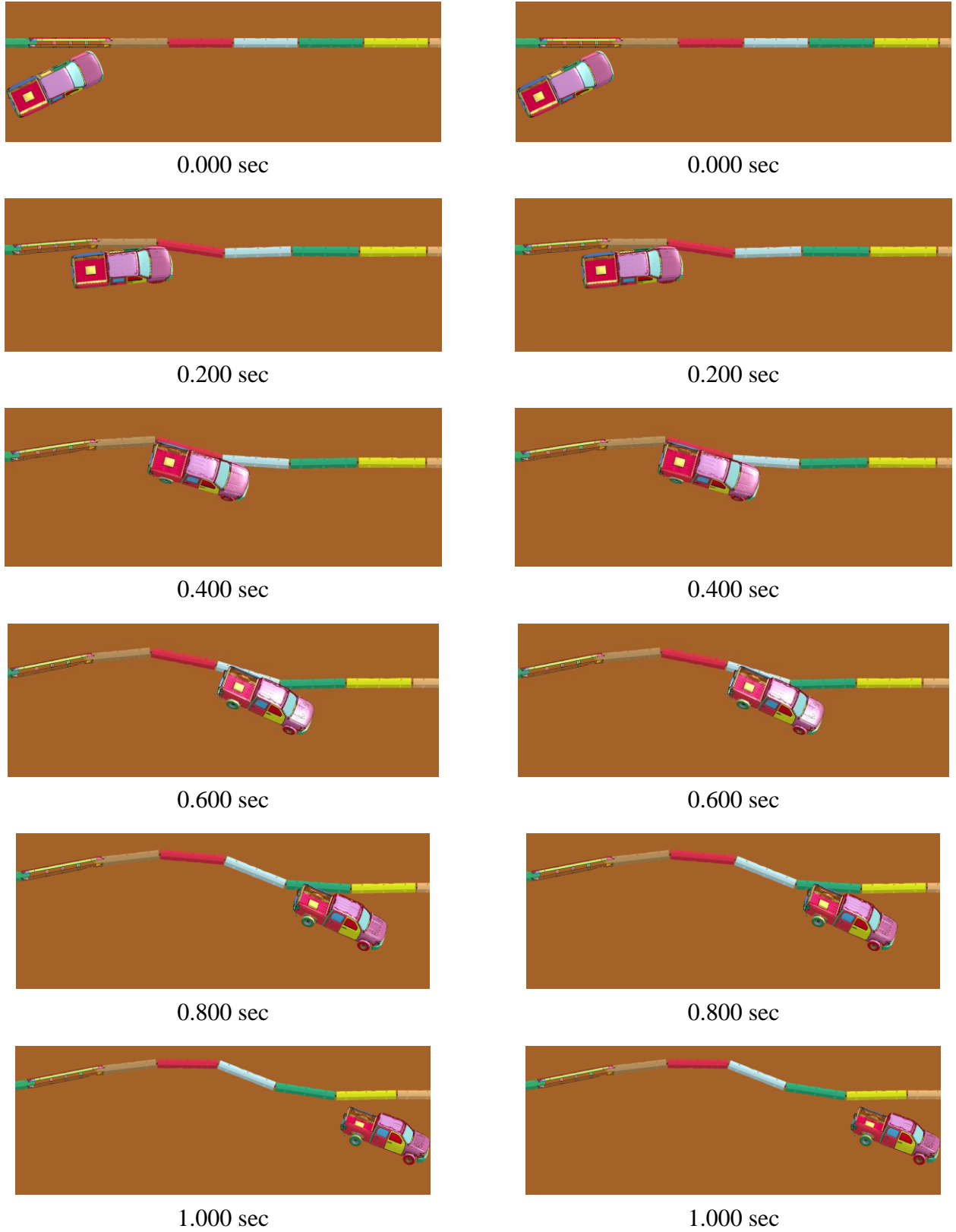


Figure 64. Sequential Images, Overhead View: PCB with Gap-Spanning Hardware, Thrie Beam and Toe Plate (Left), and Free-Standing F-Shape PCB Simulation (Right)

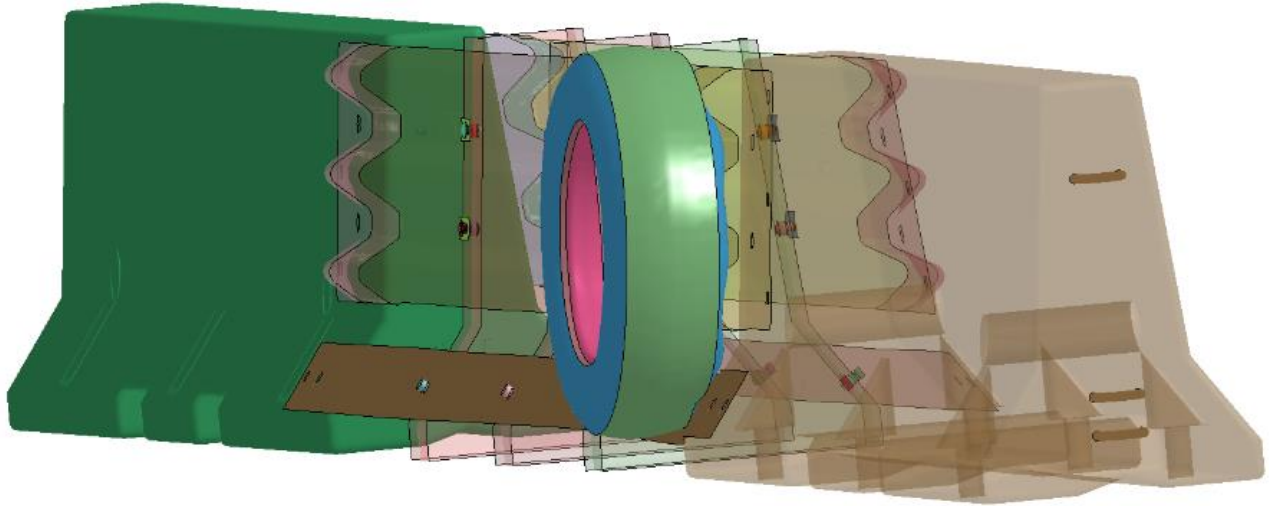


Figure 65. Toe Plate Deformation and Wheel Snag

### 7.1.1 Toe Plate Design Modifications – 12.5-ft Long Gap

Further simulations were conducted to identify potential modifications to the toe plate design for reducing localized deformations to the toe plate and mitigating the rollover concern. Initially, the toe plate thickness was increased from  $\frac{1}{4}$  in. to 1 in., and simulations with the 1-in. thick toe plate were conducted at impact locations of 11 in., 22.4 in., and 36 in. upstream from barrier no. B-10. The simulations resulted in reduced roll angles well below the MASH limits, as shown in Figure 66. These results indicated that increasing the strength of the toe plate could reduce the amount of vehicle roll. Toe plate deformation at the downstream end of the gap was still observed, but the deformations were reduced, resulting in reduced roll angle.

A parametric study was then conducted to identify the optimum thickness and height of the toe plate. In addition to the original  $\frac{1}{4}$ -in. x 6-in. toe plate, simulations with toe plates measuring 1-in. x 6-in.,  $\frac{1}{4}$ -in. x 8 $\frac{1}{2}$ -in.,  $\frac{1}{2}$ -in. x 8 $\frac{1}{2}$ -in., and  $\frac{5}{8}$ -in. x 8 $\frac{1}{2}$ -in. were evaluated. Results from these simulations are shown in Table 14. Both  $\frac{1}{4}$ -in. thick toe plate designs resulted in vehicle rollover due to excessive plate deformation and wheel snag on the PCB. Thus, these thin plates were withdrawn from further consideration. The  $\frac{1}{2}$ -in. x 8 $\frac{1}{2}$ -in. plate reduced wheel snag and vehicle roll as compared to the thinner plates, but still exhibited excessive roll when the vehicle impacted 22-in. upstream from the end of barrier no. B-10 (simulation no. 7c). Both the  $\frac{5}{8}$ -in. x 8 $\frac{1}{2}$ -in. toe plate and the 1-in. x 6-in. toe plate significantly reduced the localized deformations in the toe plate, as shown in Figure 67, and both were effective in reducing wheel snag and brought the simulated vehicle roll values to within MASH requirements (roll <75 degrees). While both of the thicker toe plates demonstrated the ability to mitigate rollover, the  $\frac{5}{8}$ -in. thick x 8 $\frac{1}{2}$ -in. high toe plate was preferred to limit materials and associated costs.

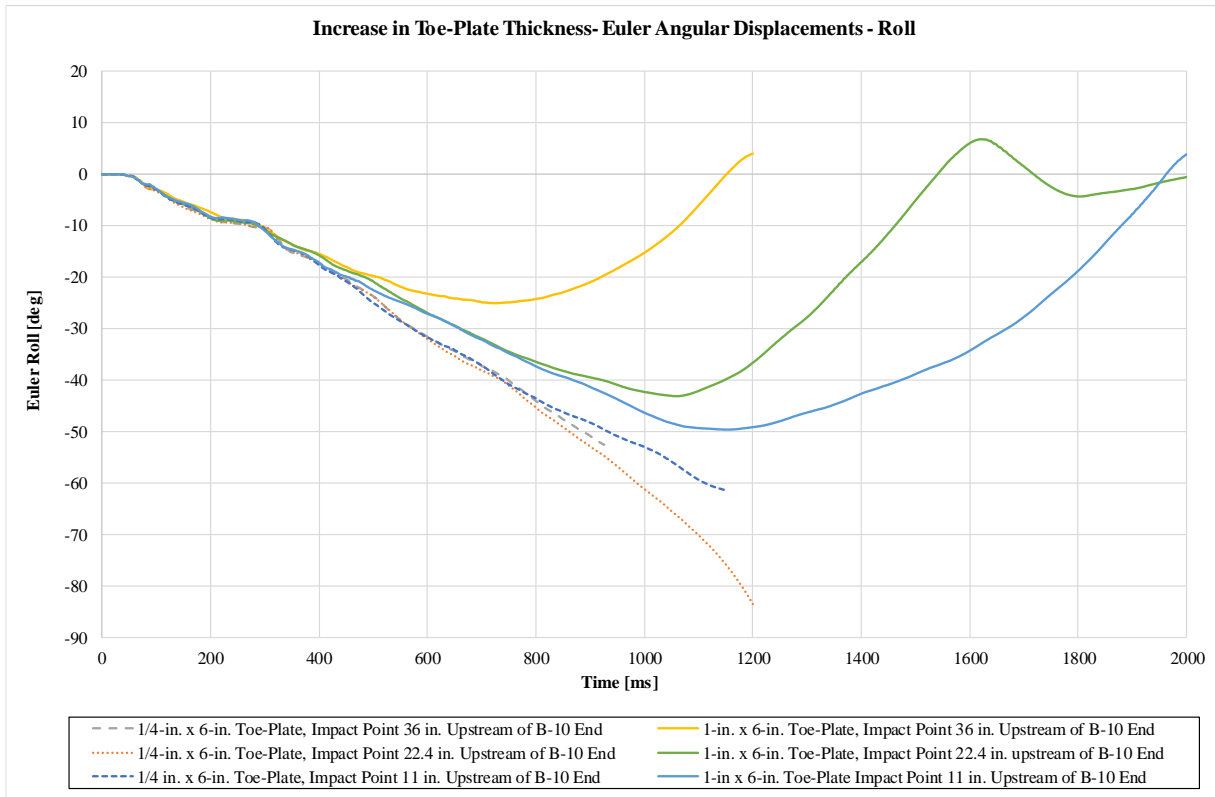


Figure 66. Comparison of Roll Angles with Increase in Toe Plate Thickness, 12.5-ft Gap

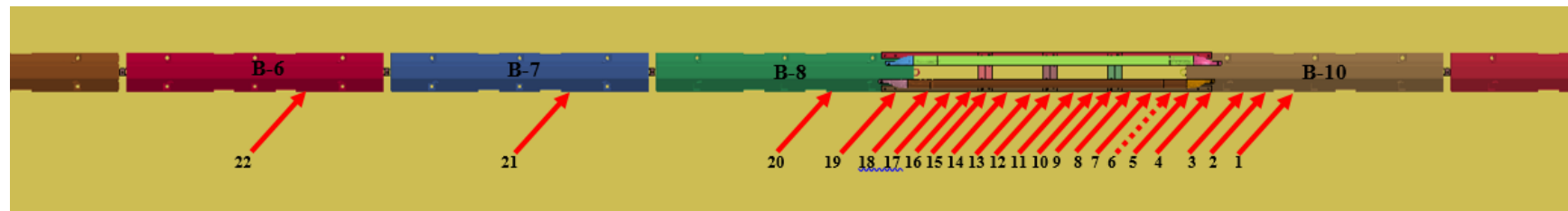
Table 14. Summary of Simulation Results: 12.5-ft Long Gap, Toe Plate Variations

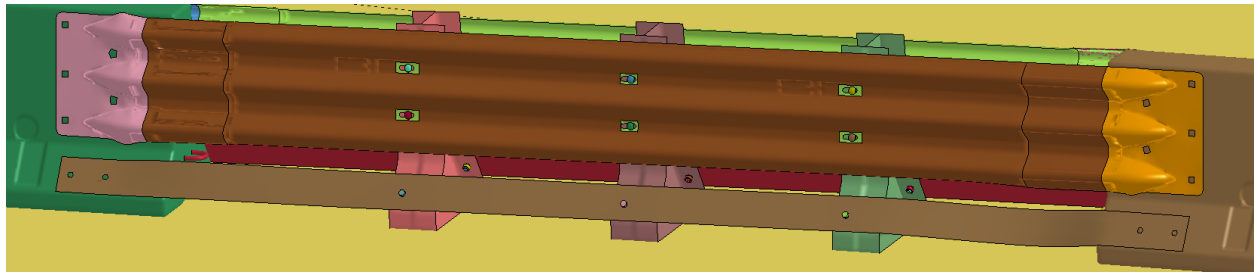
Sim. No.	Impact Point Upstream from B-10 (in.)	Toe Plate Design		Lateral OIV (ft/s)	Long. OIV (ft/s)	Lateral ORA (g's)	Long. ORA (g's)	Roll (deg.)	Pitch (deg.)	Lateral Deflection (in.)	Pass/Fail
		Thickness (in.)	Height (in.)								
5	0.0	¼	6	-19.3	-13.1	-12.6	-4.1	-37.3	12.0	76.6	Pass
6	11.0	¼	6	-19.3	-14.1	-13.6	-4.8	-61.4	5.6	79.5	Fail <sup>1</sup>
6a	11.0	1	6	-19.3	-13.4	-11.9	-4.3	-48.6	5.8	72.7	Pass
6b	11.0	¼	8½	-19.0	-14.1	-13.6	-7.7	-189.6	-13.7	77.9	Fail
6c	11.0	½	8½	-19.0	-14.1	-13.6	-7.7	-54.1	6.7	73.5	Pass
6d	11.0	⅝	8½	-19.7	-13.8	-12.5	-7.4	-49.2	6.9	71.6	Pass
7	22.4	¼	6	-19.0	-15.4	-16.0	-8.0	-83.5	8.1	75.0	Fail
7a	22.4	1	6	-19.0	-13.8	-10.5	-3.1	-43.1	5.5	71.2	Pass
7b	22.4	¼	8½	-18.7	-14.1	-13.9	-7.6	-112.4	9.0	78.5	Fail
7c	22.4	½	8½	-18.7	-14.4	-11.2	-5.1	-82.9	8.6	74.2	Fail
7d	22.4	⅝	8½	-19.0	-14.4	-12.7	-4.3	-38.9	6.6	71.0	Pass
8	35.9	¼	6	-19.3	-15.4	-14.2	-6.0	-52.6	33.1	74.3	Fail <sup>1</sup>
8a	35.9	1	6	-19.3	-14.8	-8.3	5.2	-25.0	6.8	71.5	Pass
8c	35.9	½	8½	-19.3	-15.1	-10.5	5.0	-47.4	7.3	74.3	Pass
8d	35.9	⅝	8½	-19.3	-15.4	-8.2	-4.9	-34.2	8.2	70.6	Pass
MASH Limits		N/A	N/A	≤ 40	≤ 40	≤ 20.49	≤ 20.49	< 75	< 75	N/A	-

N/A – Not Applicable

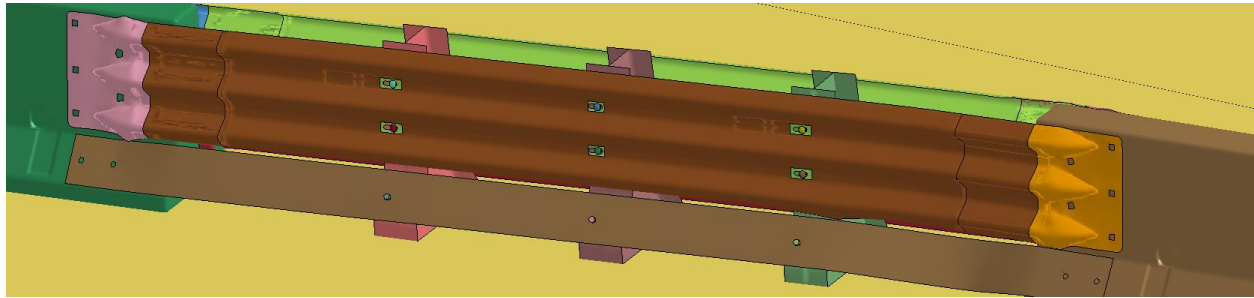
<sup>1</sup> Maximum roll value was not reached prior to conclusion of simulation.

84





(a)



(b)

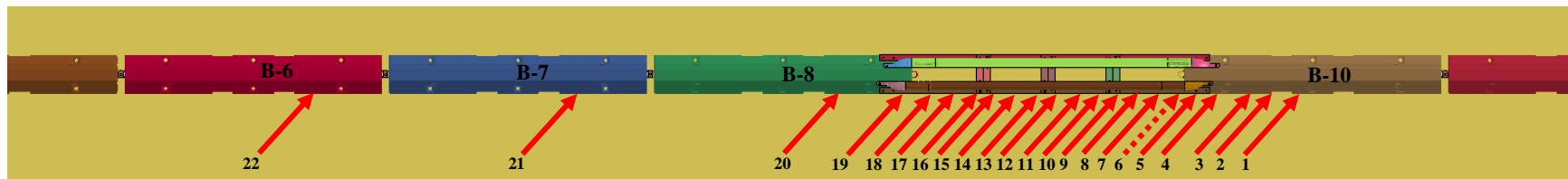
Figure 67. Post-Impact Deformations for (a) 1-in. x 6-in. Toe Plate and  $\frac{5}{8}$ -in. x 8½-in. Toe Plate

A complete set of simulations were conducted with the  $\frac{5}{8}$ -in. x 8½-in. toe plate with impact points spread over the entire PCB gap system, as shown in Table 15. The increased height and thickness of the toe plate resulted in a more stable vehicle redirection. The vehicle roll angles for all the impact locations were well below the MASH limits, as shown in Table 15. The maximum vehicle roll of 49.2 degrees was observed at impact location of 11 in. upstream from barrier no. B-10.

Table 15. Summary of Simulation Results: 5/8-in. Thick, 8½-in. High Toe Plate

Location No.	Impact Point US or DS from Barrier No. B-10	Toe-Plate Design		Lateral OIV (ft/s)	Long. OIV (ft/s)	Lateral ORA (g's)	Long. ORA (g's)	Roll (deg.)	Pitch (deg.)	Lateral Barrier Deflection (in.)
		Thickness (in.)	Height (in.)							
1	60.0 in. Downstream	5/8	8½	-17.7	-11.8	-15.2	-4.0	-24.6	17.4	79.8
2	48.2 in. Downstream	5/8	8½	-18.4	-12.5	-15.2	4.2	-32.0	10.5	78.7
3	35.0 in. Downstream	5/8	8½	-18.7	-13.1	-19.0	4.9	-30.1	10.5	77.3
6	11.0 in. Upstream	5/8	8½	-19.7	-13.8	-12.5	-7.4	-49.2	6.9	71.3
7	22.4 in. Upstream	5/8	8½	-19.0	-14.4	-12.7	-4.3	-38.9	6.6	70.6
8	36.0 in. Upstream	5/8	8½	-19.3	-15.4	-8.2	-4.9	-34.2	8.2	70.7
9	48 in. Upstream	5/8	8½	-18.0	-15.1	-8.4	-3.2	-29.9	7.8	68.0
10	59.3 in. Upstream	5/8	8½	-16.4	-15.4	-9.0	-4.7	-28.3	8.8	67.3
11	72.0 in. Upstream	5/8	8½	-16.7	-14.8	-9.9	4.7	-28.3	7.1	63.7
12	83.0 in. Upstream	5/8	8½	-17.7	-16.0	-11.8	-5.7	-22.8	5.4	63.9
13	96.3 in. Upstream	5/8	8½	-17.4	-15.7	-13.9	-5.4	-19.1	5.2	61.5
14	108.0 in. Upstream	5/8	8½	-18.7	-16.4	-13.9	-5.4	-14.1	4.7	53.3
15	119.0 in. Upstream	5/8	8½	-18.7	-16.4	-11.2	-3.9	-10.9	5.7	52.0
16	130 in. Upstream	5/8	8½	-18.4	-16.0	-14.1	-5.8	-8.5	8.1	53.3
17	143.0 in. Upstream	5/8	8½	-18.4	-16.0	-12.5	6.5	-13.7	8.3	53.3
18	155.6 in. Upstream	5/8	8½	-18.4	-16.1	-12.0	-3.0	-16.0	6.5	55.1
19	172.2 in. Upstream	5/8	8½	-18.0	-18.4	-10.2	-4.1	-13.6	8.5	59.8
N/A	MASH Limits	N/A	N/A	≤ 40	≤ 40	≤ 20.49	≤ 20.49	< 75	< 75	N/A

N/A – Not Applicable



## 7.2 Investigation of Maximum Load in the Gap-Spanning Hardware

Further analysis was conducted on the PCB with a 12.5-ft long gap with nested 12-gauge thrie beam and  $\frac{5}{8}$ -in. thick x 8½-in. high toe plates along with three internal stiffeners to evaluate the structural loading at impacts all along the system. These simulated impact points are listed in Tables 16 and 17. Forces transferred through the thrie beam and toe plate were measured at two cross-sections through the gap-spanning hardware, one near the downstream end of the gap and the other near the upstream end of the gap. The tensile, shear, and resultant forces along the nested thrie-beam rails and toe plate were recorded for each simulated impact point. The force time histories were filtered using the Butterworth (BW) method with a frequency of 100 Hz which corresponded to a SAE J2111 CFC Class 60 filter. Results measured at the downstream and upstream cross sections were tabulated in Tables 16 and 17, respectively.

In the simulations, the cross-sectional forces of the rail and toe plate were closely examined to determine the most critical impact point. The impact point located 72.0 in. upstream from barrier no. B-10 had the highest tensile and resultant forces. This case had maximum tensile forces of 113.9 kips and 92.9 kips at the impact side toe plate and impact side of the rail, respectively. This suggested that this impact point would be critical for evaluation of the structural capacity of the gap-spanning hardware and its connection.

The tensile loads in the toe plate were also examined to determine the number of anchors that would be required to anchor the plate to each adjacent PCB. Typical mechanical screw anchors were anticipated to be used in the design. These anchors would be loaded in shear, and the ultimate shear capacity for these anchors had been identified to be at least 25 kips in a previous study [42]. Based on the predicted tensile load of 92.9 kips, it was recommended that a minimum of four anchors be used to attach the toe plate to the PCBs on each side of the barrier gap.

Table 16. Downstream Cross-Sectional Forces for Various Impact Points on 12.5-ft Gap

Sim. No.	Impact Point US from Barrier No. B-10 (in.)	Impact Side Toe Plate			Back Side Toe Plate			Impact Side Rail			Back Side Rail		
		Tensile Force (kips)	Shear Force (kips)	Resultant Force (kips)	Tensile Force (kips)	Shear Force (kips)	Resultant Force (kips)	Tensile Force (kips)	Shear Force (kips)	Resultant Force (kips)	Tensile Force (kips)	Shear Force (kips)	Resultant Force (kips)
6	11.0	56.1	8.6	56.3	83.2	16.0	83.6	68.5	16.4	68.9	71.5	15.3	72.6
7	22.4	55.6	8.3	55.7	89.9	13.1	90.1	73.1	10.5	73.2	80.1	12.2	80.9
8	35.9	60.7	8.4	60.7	84.8	12.8	84.8	75.5	12.8	75.7	77.7	10.7	78.32
9	48.0	89.8	12.2	90.3	94.3	16.9	95.0	72.0	12.1	72.4	79.1	10.6	79.7
10	59.3	46.5	16.6	46.9	107.9	22.3	107.9	86.9	15.9	87.0	79.4	11.6	79.5
11	72.0	42.0	17.4	42.2	113.9	24.2	114.0	92.9	14.9	93.1	79.4	14.0	80.1
12	83.0	42.2	17.4	45.5	109.0	25.9	109.1	93.7	11.4	93.8	73.7	14.0	74.7
13	96.3	42.6	19.4	45.6	107.0	26.3	107.2	91.4	10.4	91.5	83.1	14.4	84.3
14	108.0	42.6	17.4	44.5	106.9	26.3	107.1	85.6	9.8	85.7	84.4	15.4	85.4
15	119.0	55.9	14.7	56.7	100.3	25.9	102.3	78.5	9.4	78.6	84.8	14.0	85.8
16	130.3	53.7	10.8	54.2	89.0	25.6	92.1	80.0	8.1	80.2	77.6	15.8	78.4
17	143.0	49.6	10.4	49.9	106.9	25.6	107.6	77.0	9.3	77.3	77.8	13.1	78.1
18	155.6	55.5	10.4	55.7	95.9	22.6	96.9	75.1	10.7	75.4	79.0	12.4	79.5

88

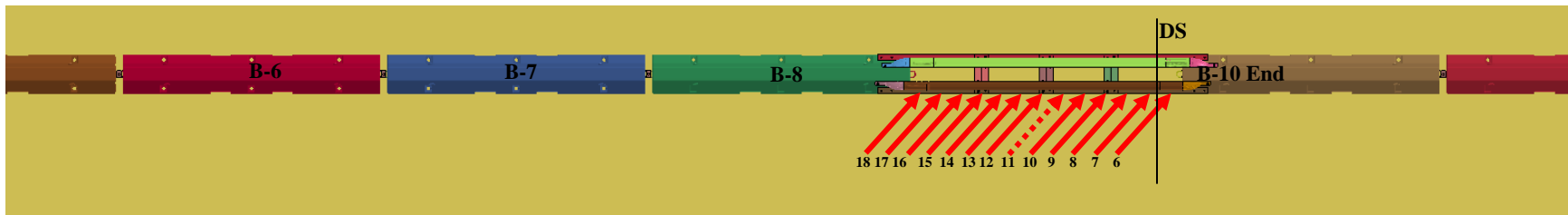
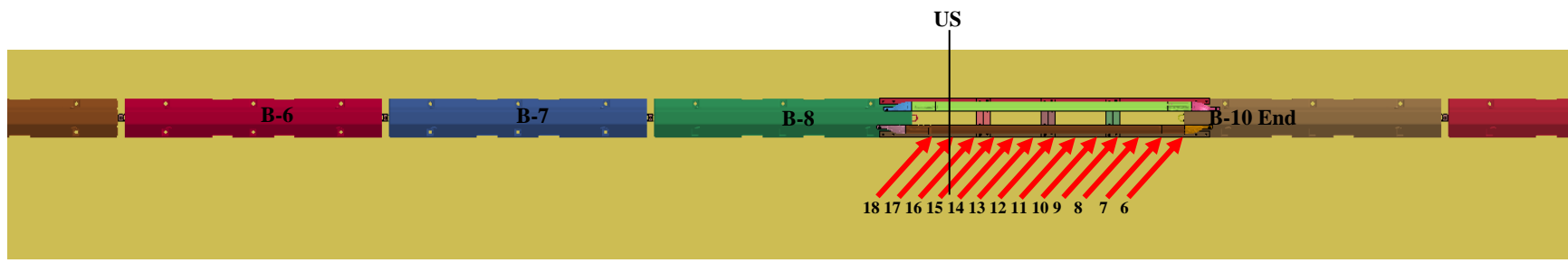


Table 17. Upstream Cross-Sectional Forces for Various Impact Points on 12.5-ft Gap

Sim. No.	Impact Point US from Barrier No. B-10 (in.)	Impact Side Toe Plate			Back Side Toe Plate			Impact Side Rail			Back Side Rail		
		Tensile Force (kips)	Shear Force (kips)	Resultant Force (kips)	Tensile Force (kips)	Shear Force (kips)	Resultant Force (kips)	Tensile Force (kips)	Shear Force (kips)	Resultant Force (kips)	Tensile Force (kips)	Shear Force (kips)	Resultant Force (kips)
6	11.0	51.4	8.6	51.5	76.2	10.3	76.3	56.8	6.4	56.9	64.6	8.6	64.8
7	22.4	53.3	8.7	53.5	85.4	11.4	85.5	68.1	6.8	68.4	73.5	6.0	73.7
8	35.9	57.6	8.8	57.8	81.2	12.7	81.4	66.6	6.8	66.7	71.4	6.4	71.5
9	48.0	84.5	8.2	84.8	93.1	13.9	93.5	63.3	7.2	63.6	75.5	7.1	75.7
10	60.2	39.9	9.3	40.4	103.5	13.7	103.8	77.5	6.4	77.8	72.8	6.9	72.9
11	72.0	34.3	10.0	35.6	112.1	13.3	112.5	80.7	7.3	80.9	73.8	8.5	73.9
12	83.0	38.9	11.2	40.3	108.5	12.7	108.8	79.4	7.8	79.5	69.2	10.0	69.4
13	96.3	37.0	12.7	38.8	104.4	14.8	104.8	81.0	5.9	81.1	78.1	8.8	78.5
14	108.0	38.9	14.1	41.1	106.8	16.2	107.0	78.8	6.2	78.9	82.2	12.0	82.7
15	118.6	53.3	15.3	55.4	104.0	17.3	104.4	75.2	9.2	75.4	82.9	13.8	83.6
16	130.3	51.6	16.0	53.9	94.4	17.0	94.5	75.5	13.1	75.7	76.4	12.5	77.1
17	143.0	47.3	13.7	49.1	109.9	13.7	110.0	75.4	15.8	75.5	78.0	14.0	79.0
18	155.6	53.7	14.1	54.2	98.0	14.0	98.1	75.3	18.9	75.4	82.6	12.8	83.4

89



### 7.3 Simulation of Revised Design – 3-ft Gap

Further analysis was conducted to investigate the performance of the revised design with a reduced gap length of 3 ft. A single internal stiffener was added to the midspan of the gap-spanning hardware for this analysis with the reduced gap, as shown in Figure 68. The inclusion of the internal stiffener was expected to reduce the system deformation, vehicle snag, and vehicle pocketing concerns. However, the simulation results demonstrated an increased vehicle roll angle of 74.1 degrees for an impact point 36 in. downstream from the barrier gap.

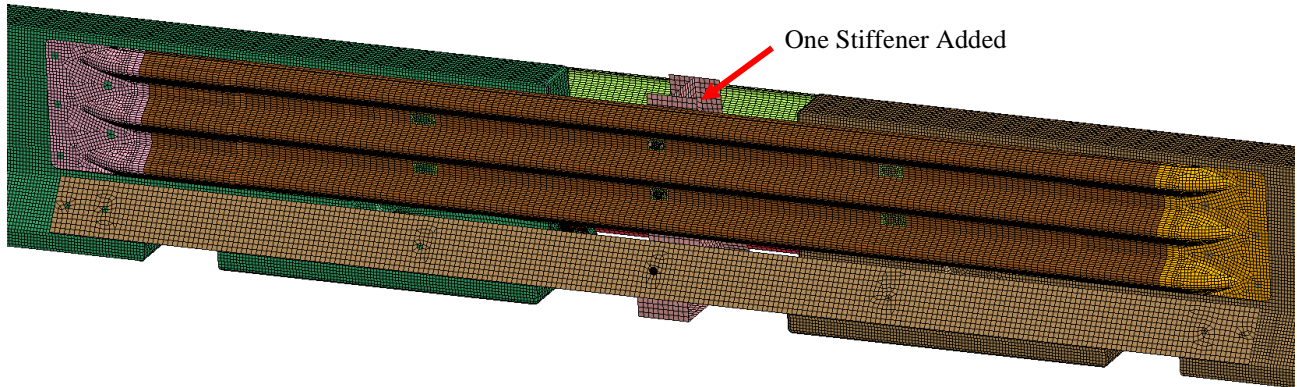


Figure 68. 3-ft Long Gap-Spanning Configuration with One Stiffener Added

Review of the simulation results found that impacts downstream from the barrier gap where the thrie beam was extended on the face of the PCB were causing the front wheel of the 2270P vehicle to be held down by the thrie-beam rail element, as shown in Figure 69. This behavior was believed to be holding the front corner of the vehicle down during redirection and causing increased vehicle roll. The climb, or vertical displacement, of the front wheel of the 2270P vehicle was measured for three impact points on the thrie beam downstream from the barrier gap and one impact point downstream from the PCB gap hardware that only interacted with the face of the PCB, as shown in Figure 70. In these simulations, similar wheel entrapment and accompanying increased vehicle roll magnitude was observed for impact points on the downstream end of the nested thrie beams. However, the wheel climb for the impact point on the face of the PCB showed that the wheel climb of the barrier face was increased and vehicle roll was reduced.

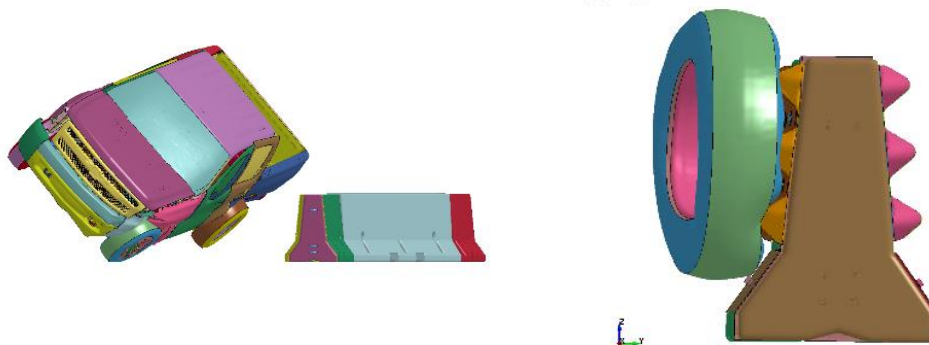


Figure 69. Wheel Entrapment and Vehicle Roll for Impact Downstream from Barrier with 3-ft Long Barrier Gap

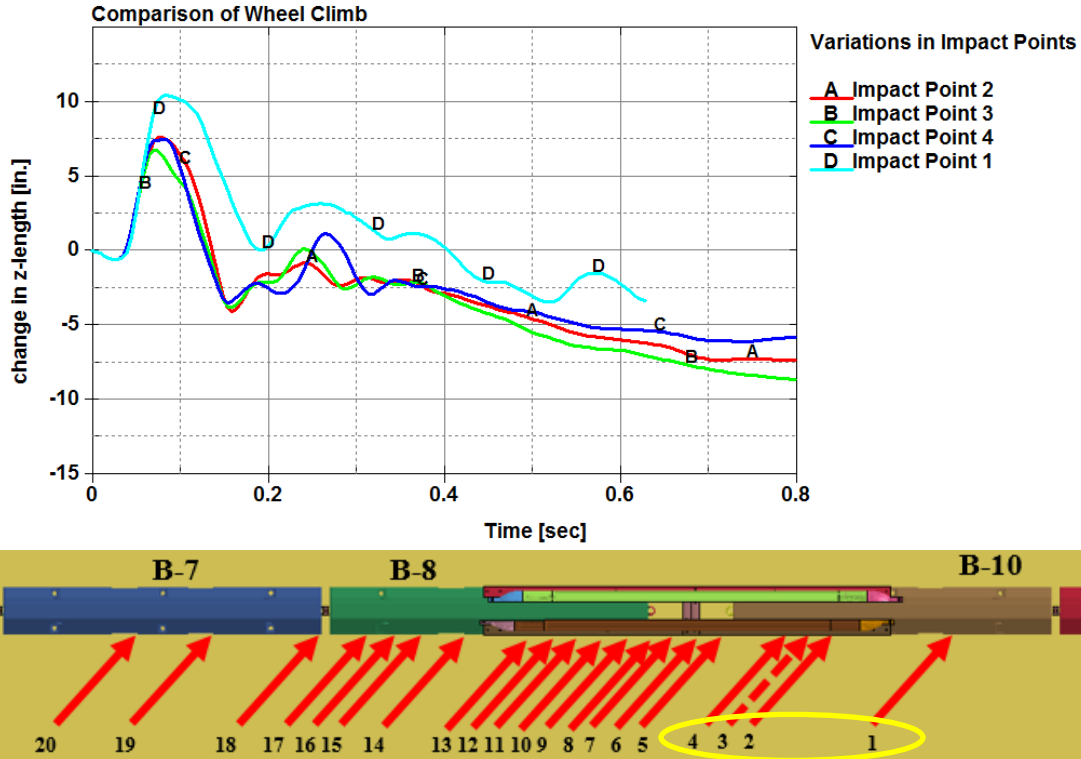


Figure 70. Wheel Climb for Impact Points Downstream from a 3-ft Long Barrier Gap

Similarly, simulations of impacts 36 in. downstream from the barrier gap were compared for both the 12.5-ft long and 3-ft long barrier gaps in terms of wheel climb and barrier roll. The wheel climb (i.e., vertical z-displacement) and vehicle roll angle for two cases with gap lengths of 3 ft and 12.5 ft and an impact point 36 in. downstream from the gap are shown in Figures 71 and 72. The impact downstream from the 12.5-ft long gap demonstrated increased wheel climb and reduced vehicle roll. This indicated that the presence of the thrie beam on the face of the PCB for reduced barrier gap lengths could create increased vehicle roll and instability.

After confirming the cause of the increased vehicle roll behavior, the researchers reviewed crash testing of a similar PCB configuration as a comparison point. Previously, MwRSF developed and full-scale crash tested a MASH TL-3 transition from free-standing PCB to a permanent concrete median barrier [43]. The transition design included nested thrie beam sections that overlapped the last F-shape PCB segment adjacent to the connection of the transition to the permanent concrete median barrier. This configuration was very similar to the thrie-beam rail overlap on the PCB in the proposed gap-spanning hardware design. During the testing and evaluation of the transition design, full-scale crash test no. TBCT-1 was conducted on an impact point 56 $\frac{3}{8}$ -in. upstream from the end of the permanent concrete median barrier and on the nested thrie beam overlapping the PCB, as shown in Figure 73. In test no. TCBT-1, the impacting 2270P vehicle was safely captured and redirected with moderate vehicle roll. This suggested that the LS-DYNA simulation of the gap-spanning hardware may be over-predicting the propensity for vehicle instability for impacts downstream from the barrier gap. However, the possibility of increased vehicle instability could not be ruled out. As such, it was noted that this impact location should be considered as a critical impact point for the analysis of the gap-spanning hardware design.

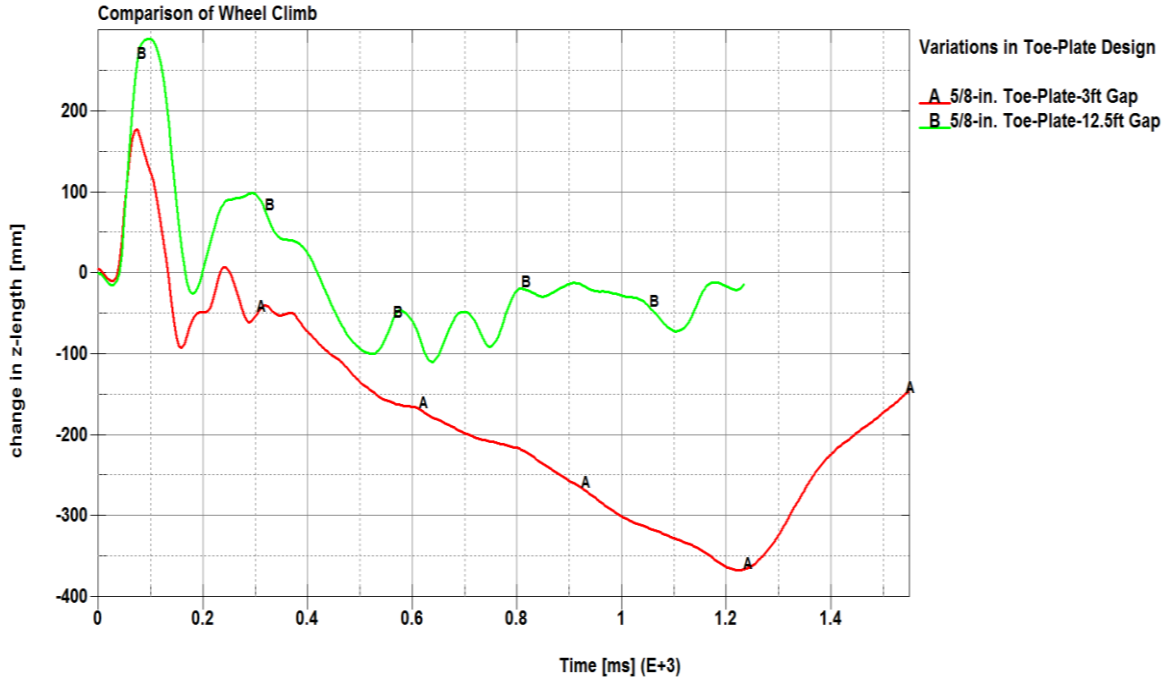


Figure 71. Comparison of Wheel Climb for 3-ft and 12.5-ft Long Gap

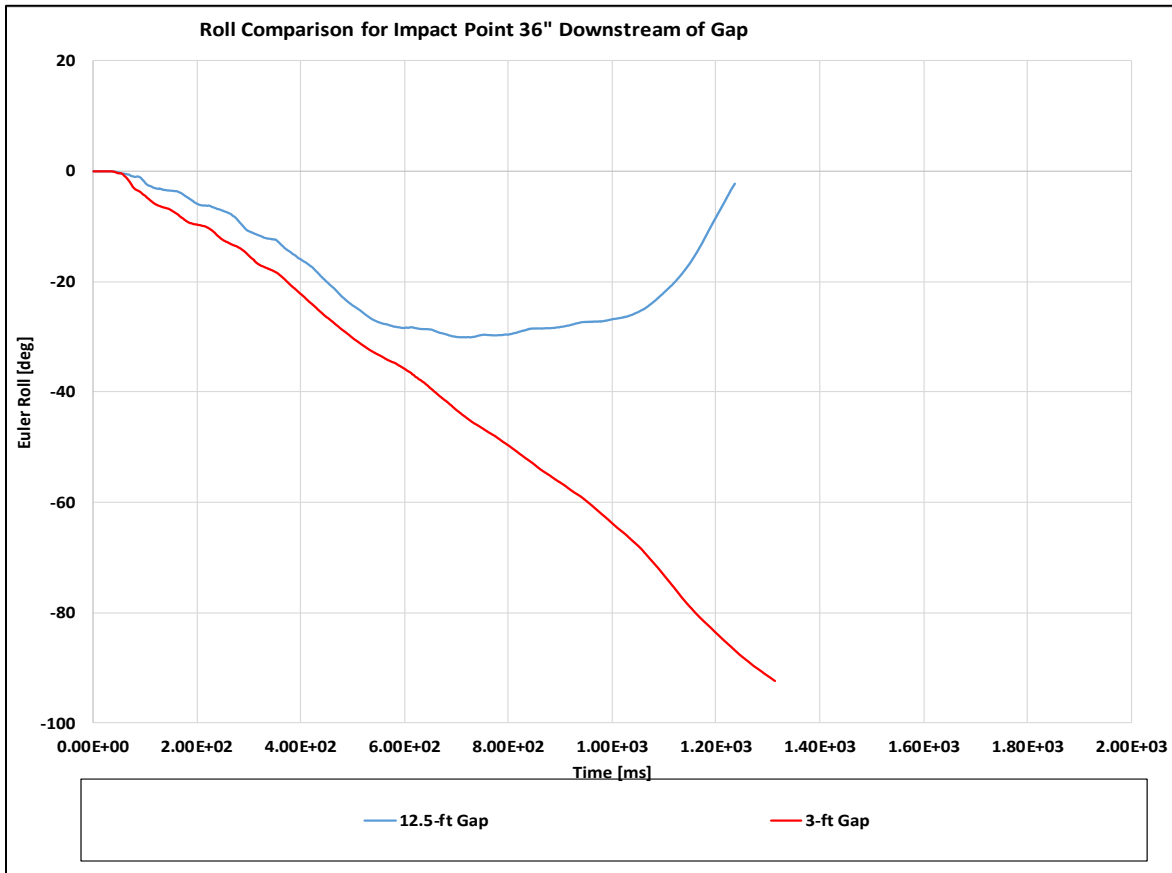


Figure 72. Comparison of Vehicle Roll Angle for 3-ft and 12.5-ft Long Gap



Figure 73. Free-Standing PCB Transition to Permanent Concrete Median Barrier, Test No. TCBT-1

## 7.4 Recommend Full-Scale Crash Testing and Critical Impact Point Selection

### 7.4.1 Recommended Full-Scale Crash Tests

Roadside hardware systems, such as the PCB gap spanning hardware developed herein, must satisfy impact safety standards to be declared eligible for federal reimbursement by the Federal Highway Administration (FHWA) for use on the National Highway System (NHS). For new hardware, these safety standards consist of the guidelines and procedures published in MASH 2016 [1]. The PCB gap spanning hardware evaluated in this report functions primarily as a longitudinal barrier. According to TL-3 of MASH 2016, longitudinal barrier systems must be subjected to two full-scale vehicle crash tests, as summarized in Table 18.

Table 18. MASH 2016 TL-3 Crash Test Conditions for Longitudinal Barriers

Test Article	Barrier Section	Test Designation No.	Test Vehicle	Vehicle Weight, lb	Impact Conditions		Evaluation Criteria <sup>1</sup>
					Speed, mph	Angle, degrees	
Longitudinal Barrier	Length-of-Need	3-10	1100C	2,420	62	25	A,D,F,H,I
		3-11	2270P	5,000	62	25	A,D,F,H,I

<sup>1</sup> Evaluation criteria are explained in MASH.

It should be noted that the MASH 2016 test matrix detailed herein represents the recommended crash tests that should be performed. However, some of the crash tests for longitudinal barriers were deemed non-critical and unnecessary. For the PCB gap spanning hardware system, the 1100C vehicle test, test designation no. 3-10, was deemed non-critical for evaluation of the barrier system. Previous testing of PCBs and safety shape barriers has indicated that small cars interact in a safe manner with this type of roadside hardware. In test no. 2214NJ-1, a MASH test designation no. 3-10 full-scale crash test was successfully conducted on a permanent New Jersey shape concrete parapet under NCHRP Project 22-14(2) [44]. In TTI test report no. 607911-1&2, a MASH test designation no. 3-10 full-scale crash test was successfully conducted on a free-standing F-shape PCB similar to the barrier used in this study [45]. These two tests indicate that safety shape barriers are capable of successfully capturing and redirecting an 1100C vehicle in both free-standing PCB and permanent concrete parapet applications. Additionally, the increased toe height of New Jersey shape barriers tends to produce increased vehicle climb and instability as compared to the F-shape geometry. Thus, one would expect that the PCB gap-spanning hardware with similar geometry evaluated in this study would perform similarly to these previous MASH 1100C vehicle tests in terms of capture and redirection, and the 1100C vehicle would not be critical for structural loading of the hardware and lateral deflection of the barrier system. As such, it was believed that test designation no. 3-10 with the 1100C vehicle would be non-critical for evaluation of the PCB gap-spanning hardware for use with F-shape PCBs.

MASH 2016 test designation no. 3-11 was the more critical evaluation test due to concerns for increased barrier loading during 2270P impacts and to determine dynamic deflection and working width. Thus, only test designation no. 3-11 was conducted on the PCB gap-spanning hardware evaluated herein. It should be noted that any tests deemed non-critical and unnecessary

may eventually need to be performed if additional knowledge gained over time or revisions to the MASH 2016 criteria demonstrates a concern or need.

It should also be noted that the PCB gap-spanning hardware possessed a minor transition in barrier shape between the gap-spanning hardware and the F-shape PCB. However, the gap-spanning hardware was designed to minimize snag on the shape transition by making the basic shape of the hardware the same as the F-shape PCB and utilizing hardware that limited the exposure of vertical edges that could cause snag at the attachment points. It was believed that these factors would provide for smooth vehicle traversal across the hardware transition. Additionally, the PCB gap-spanning hardware reduced the deflection of the PCB system to some degree, which would indicate the presence of a stiffness transition in the barrier system that could potentially require evaluation. Impacts simulated upstream from the PCB gap spanning hardware did not indicate any issues with the PCB gap spanning hardware in terms of the reduced deflection, vehicle snag, occupant risk, barrier pocketing, or vehicle stability. As such, evaluation of the PCB gap spanning hardware system transition was deemed non-critical.

#### **7.4.2 Critical Impact Points**

The simulation analysis of the final configuration of the PCB gap-spanning hardware system was reviewed to select CIPs for full-scale crash testing and evaluation of the system to MASH TL-3. The final configuration for the proposed gap-spanning hardware utilized two nested 12-gauge thrie-beam rail sections and a  $\frac{5}{8}$ -in. thick x  $8\frac{1}{2}$ -in. high toe plate at the toe of two adjacent barrier segments with internal stiffeners spaced at  $37\frac{1}{2}$  in. Full system details are presented in Chapter 8.

Review of the simulation data noted that simulations were conducted on a wide variety of impact points on the PCB gap-spanning hardware including impact points upstream from the gap in the PCB segments, points along the PCB gap-spanning hardware, and points downstream from the gap in the PCB segments. Additionally, these impact points were simulated on the maximum gap length of 12.5 ft and a shorter gap of 3 ft. These impact points were reviewed for a variety on potential concerns, including the structural capacity of the gap spanning hardware, pocketing and snag, vehicle stability, and occupant risk.

As noted previously, impacts upstream from the PCB gap near the transition to the gap-spanning hardware did not pose a safety concern relative to the performance of the barrier system. Simulations in this region showed no issues with the stiffness transition or barrier pocketing. Additionally, the analysis demonstrated that vehicle snag was not a critical behavior due the use of the thrie-beam rail and toe plate elements that connect the system to the PCB segments. A limited concern was noted for impacts upstream from the barrier gap regarding the formation of knees that extended forward laterally during the deflection of the barrier and impacted the side of the vehicle. However, it was noted that previous F-shape PCB research found that this knee formation only posed a safety concern for vehicle stability if the barrier deflections were significantly larger than typical free-standing PCB deflections observed. However, the PCB gap-spanning hardware detailed herein tended to reduce barrier deflections and the simulation analysis indicated no vehicle stability issues. Thus, impacts upstream from the PCB gap-spanning hardware were deemed not critical.

More pertinent CIPs were noted for impacts on the PCB gap-spanning hardware itself and impacts downstream from the barrier gap. Because no similar system for spanning longitudinal gaps in PCBs has been previously tested, an evaluation of the maximum loading of the system was required to ensure the structural capacity of the system was adequate to redirect MASH TL-3 vehicles at 62 mph and an angle of 25 degrees. Analysis of the simulation results for the maximum 12.5-ft long gap identified that an impact point 72.0 in. upstream from the end of the barrier gap yielded the highest tensile and resultant forces. Thus, this point was selected as the CIP for a full-scale crash test with the pickup truck according to MASH test designation no. 3-11.

The simulation effort identified a second potential CIP when simulating impact points downstream from the barrier gap for the 3-ft long gap. Simulations in this region indicated a potential for the thrie-beam rail overlapping the PCB to trap the front wheel of the impacting pickup truck and prevent the wheel from climbing the barrier face. This restraint of the tire motion in the simulation model induced vehicle roll motion toward the barrier that was near the MASH limit in several cases and exceeded it leading to rollover in other simulations. Comparison of this behavior with similar full-scale crash testing of an F-shape PCB with a similar, overlapped thrie-beam rail configuration suggested that the simulation may be overly conservative in terms of vehicle roll, but the potential for vehicle instability could not be ruled out. As such, a second MASH test designation no. 3-11 is proposed with a CIP 12 in. downstream from the upstream end of the first PCB segment on the downstream end of the gap-spanning hardware.

Thus, two full-scale crash tests were proposed under MASH test designation no. 3-11 impact conditions. The first test would evaluate the maximum structural loading of the PCB gap-spanning hardware, and the second test would evaluate potential vehicle instability. The proposed CIPs for these two tests were as follows.

1. An impact point on the PCB gap-spanning hardware with the largest possible barrier gap of 12.5 ft located 72 in. upstream from the first PCB segment on the downstream end of the gap-spanning hardware.
2. An impact point on the PCB gap-spanning hardware system with an approximately 3-ft long barrier gap located 12 in. downstream from the upstream end of the first PCB segment on the downstream end of the gap-spanning hardware.

## 8 PCB GAP-SPANNING HARDWARE – FINAL DESIGN

### 8.1 Design Details

The final design details for the PCB gap-spanning hardware designed herein were developed for the first full-scale crash test of the system, test no. GSH-1. The full-scale crash testing was to be conducted in a following research phase. Test no. GSH-1 was to be conducted according to MASH test designation no. 3-11 with the largest longitudinal barrier gap and an impact point located 72 in. upstream from the first PCB segment on the downstream end of the gap-spanning hardware. The gap-spanning hardware system consisted of a stiffened thrie-beam section which spanned across a 12.5-ft long gap in a series of fifteen PCBs, as shown in Figures 74 through 88.

The PCB gap-spanning hardware was designed for use with the Midwest F-shape PCB system that has previously been evaluated to MASH TL-3. The system was to be composed of fifteen F-shape PCBs, each measuring 12 ft – 6 in. long with a 5,000-psi minimum concrete compressive strength. The barrier segments were connected by 1¼-in. diameter ASTM A36 steel pins inserted into the ¾-in. diameter, overlapping, reinforcing loop bars extending from the ends of the PCB sections. Details of the PCB connections are shown in Figure 76. A 12.5-ft long gap was placed between barrier nos. 8 and 9, which was covered by the stiffened thrie-beam guardrail gap-spanning hardware.

The PCB gap-spanning hardware design comprised thrie-beam guardrail sections attached to the front and back sides of the PCBs adjacent to the longitudinal gap with thrie-beam terminal connectors using wedge bolt anchors. Three steel lateral spacers were inserted between the parallel guardrail sections reduce the unsupported span length of thrie beam panels. The number of stiffeners installed between the thrie-beam guardrails could be adjusted depending on the length of the longitudinal gap. To minimize wheel snag during impacts with the system, steel toe plates were configured to span across the longitudinal gap and were anchored to the lower concrete sloped surface of the PCBs.

The stiffened thrie-beam guardrail section of the test installation consisted of two nested 12.5-ft long segments of 12-gauge thrie-beam rail with 10-gauge thrie-beam terminal connectors spliced together end-to-end with ⅝-in. diameter x 2-in. long ASTM A307 Grade A guardrail bolts. The guardrail sections with terminal connectors were anchored to both the traffic and non-traffic sides of the PCBs adjacent to the gap using five ¾-in. diameter x 6-in. long Powers Fasteners galvanized wedge bolts at each end. The thrie-beam section on the traffic side of the installation was offset 5 in. upstream relative to the thrie-beam section on the opposite side of the barrier, as shown in Figure 76. The five thrie-beam terminal anchors could not be placed in the standard thrie beam terminal anchor locations for each end of the thrie beam panels due to interference with reinforcing steel in the PCB segments. As such, anchors were installed in alternative positions at some end terminal locations as denoted in Figures 77 and 78.

Three welded steel spacer assemblies, constructed of ¼-in. thick ASTM A36 steel plates, were installed between the two thrie-beam rail sections which further increased the stiffness and strength of the barrier and gap-spanning hardware, as shown in Figure 75. Additionally, a ⅝-in. thick x 8½-in. tall ASTM A572 Grade 50 steel toe plate was bolted to the base of barrier nos. 8 and 9 on each side of the system. The toe-plates were configured with beveled edges on the ends

to mitigate wheel snag. Each steel toe plate spanned the 12.5-ft long gap and was anchored to the PCB with four  $\frac{3}{4}$ -in. diameter x 6-in. long Powers Fasteners galvanized wedge bolts at each toe plate end.

Note that the details shown here are only for the largest longitudinal barrier gap. As noted previously, longitudinal gaps for the PCB gap spanning hardware may vary between 12.5 ft and 6 in. Installation of the gap-spanning hardware over variable gap lengths must follow basic guidance to allow for proper installation of the spacers and positioning of the hardware across the longitudinal gap. This guidance, along with other implementation guidance, will be provided following the full-scale crash testing and evaluation in Phase II of the research effort.

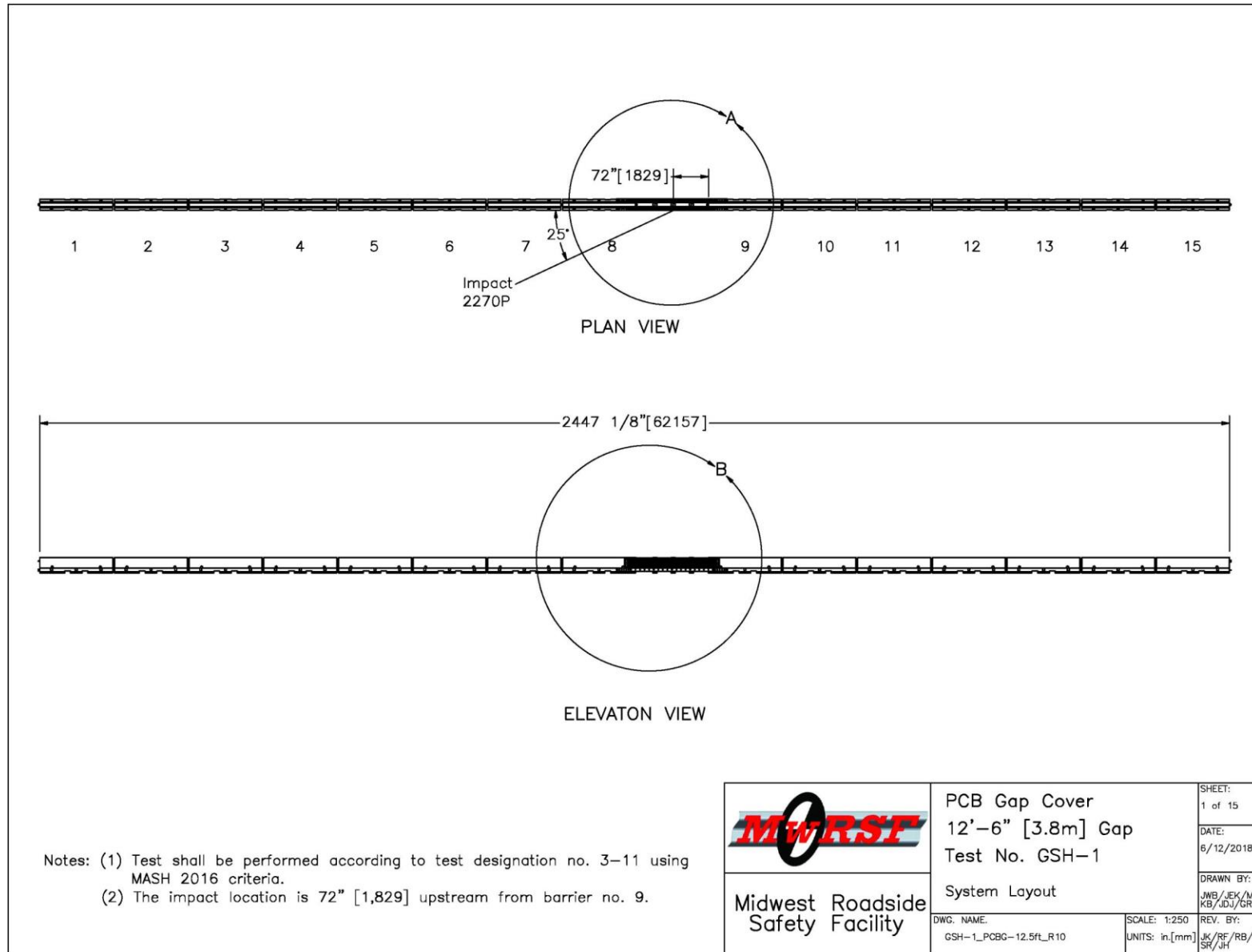


Figure 74. Test Installation Layout, Test No. GSH-1

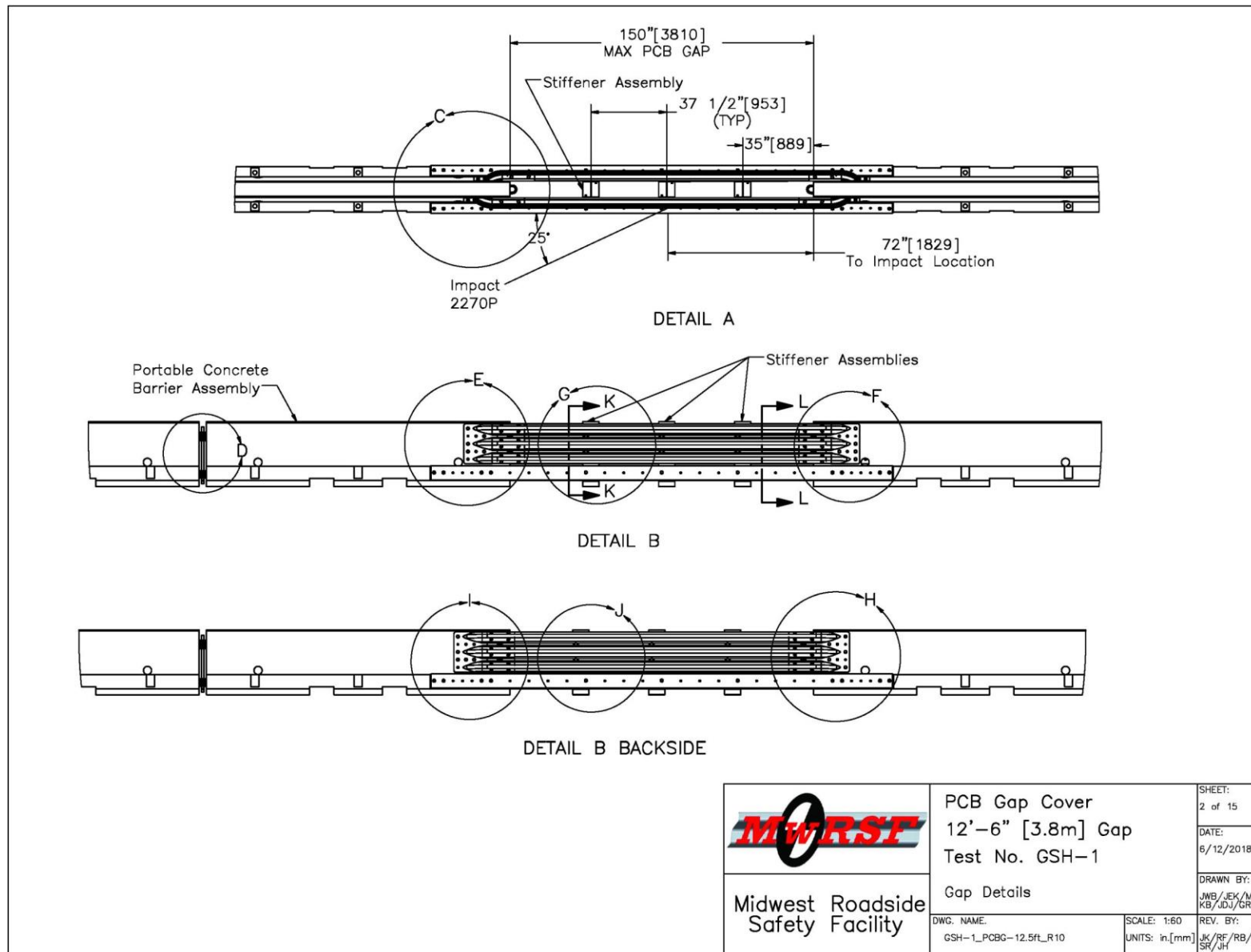


Figure 75. Gap Details, Test No. GSH-1

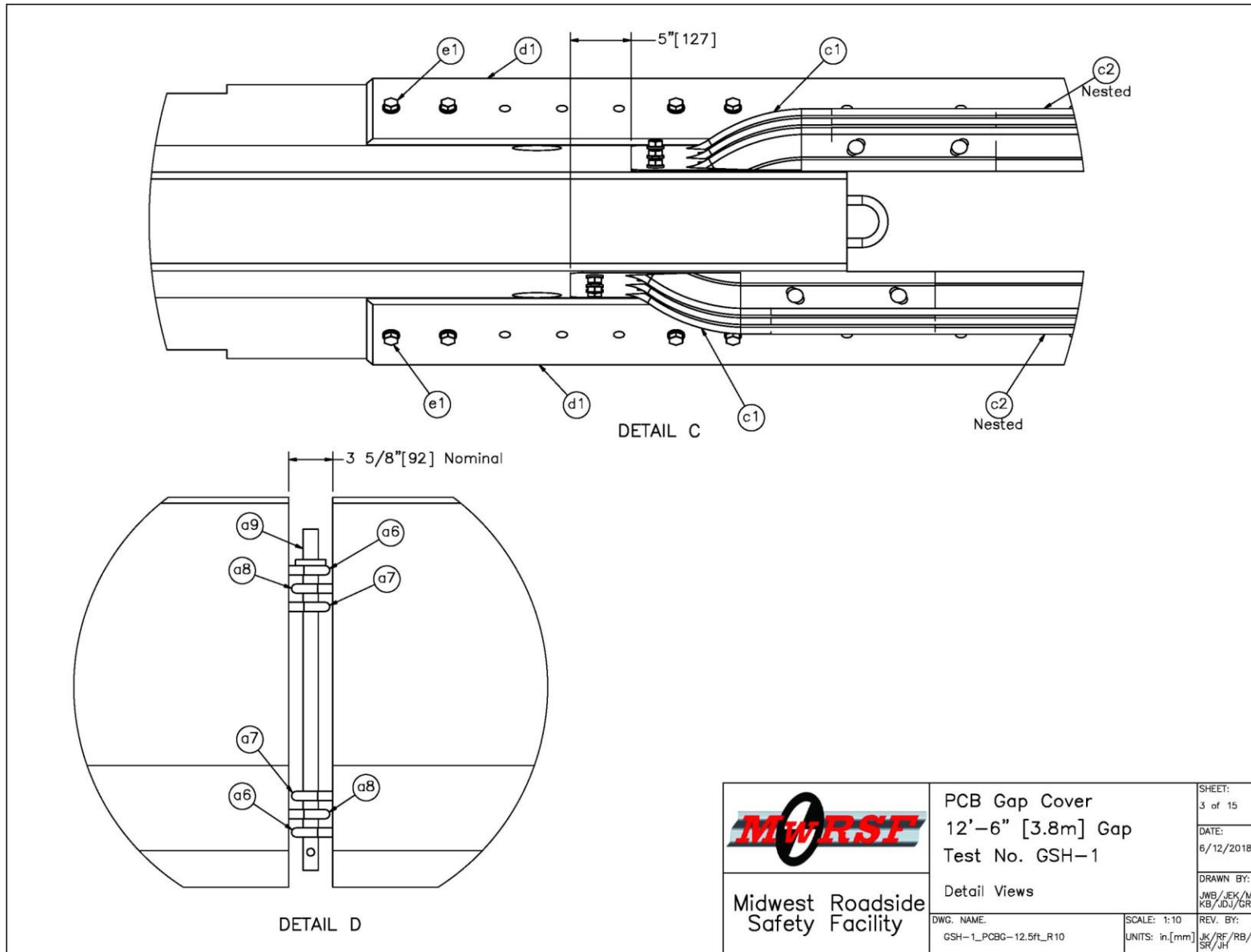


Figure 76. Detail C and Detail D Views, Test No. GSH-1

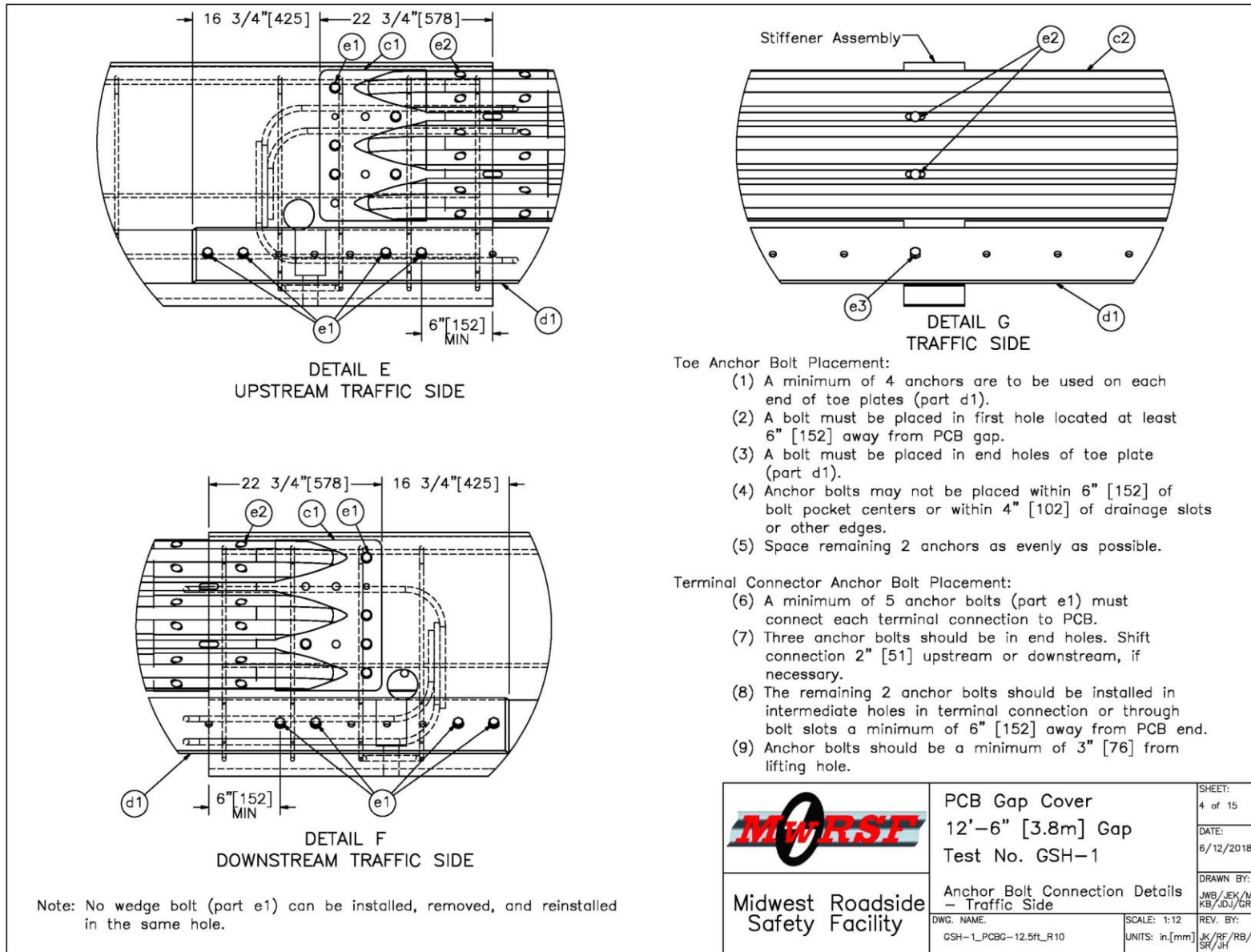


Figure 77. Anchor Bolt Connection Details – Traffic Side, Test No. GSH-1

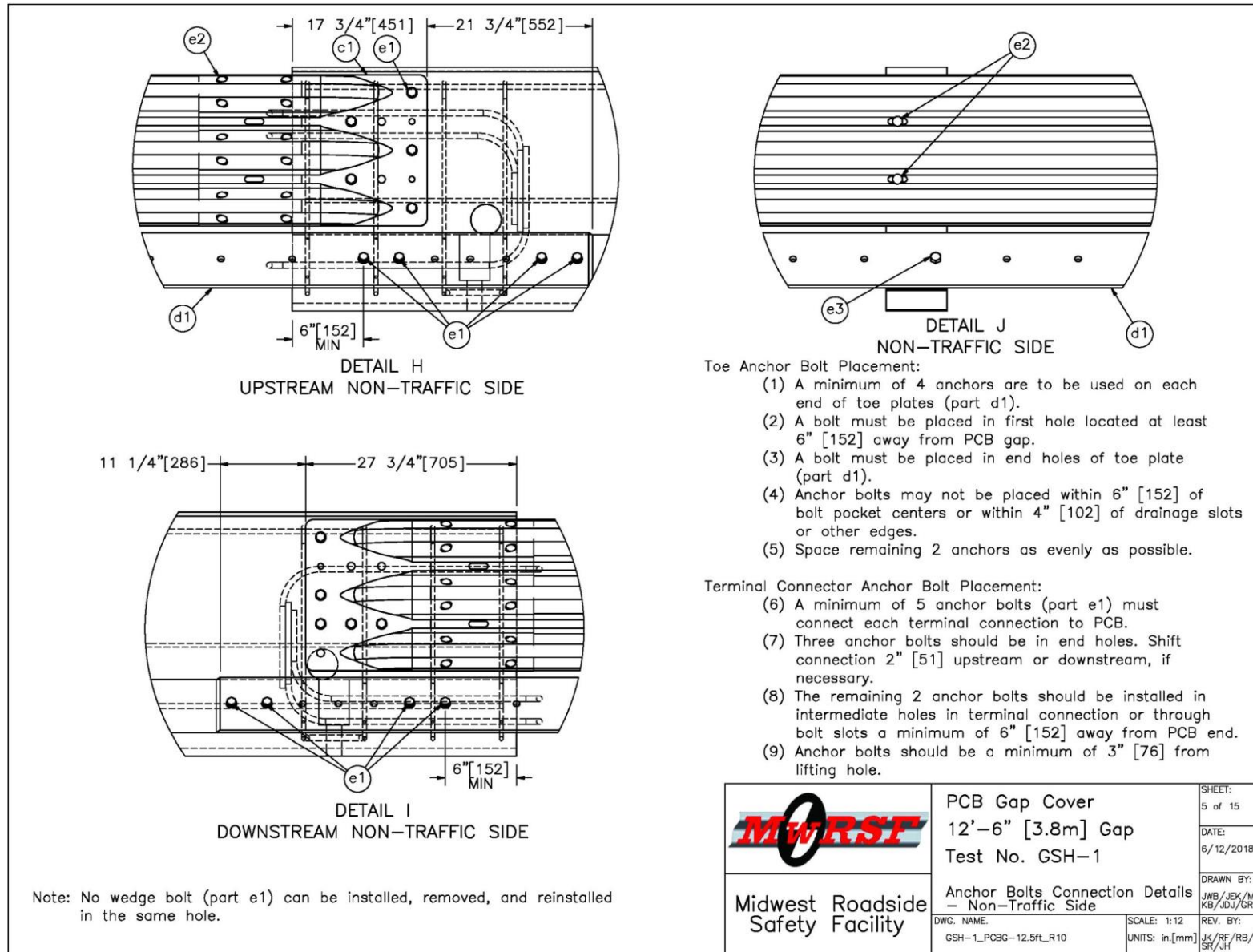


Figure 78. Anchor Bolts Connection Details – Non-Traffic Side, Test No. GSH-1

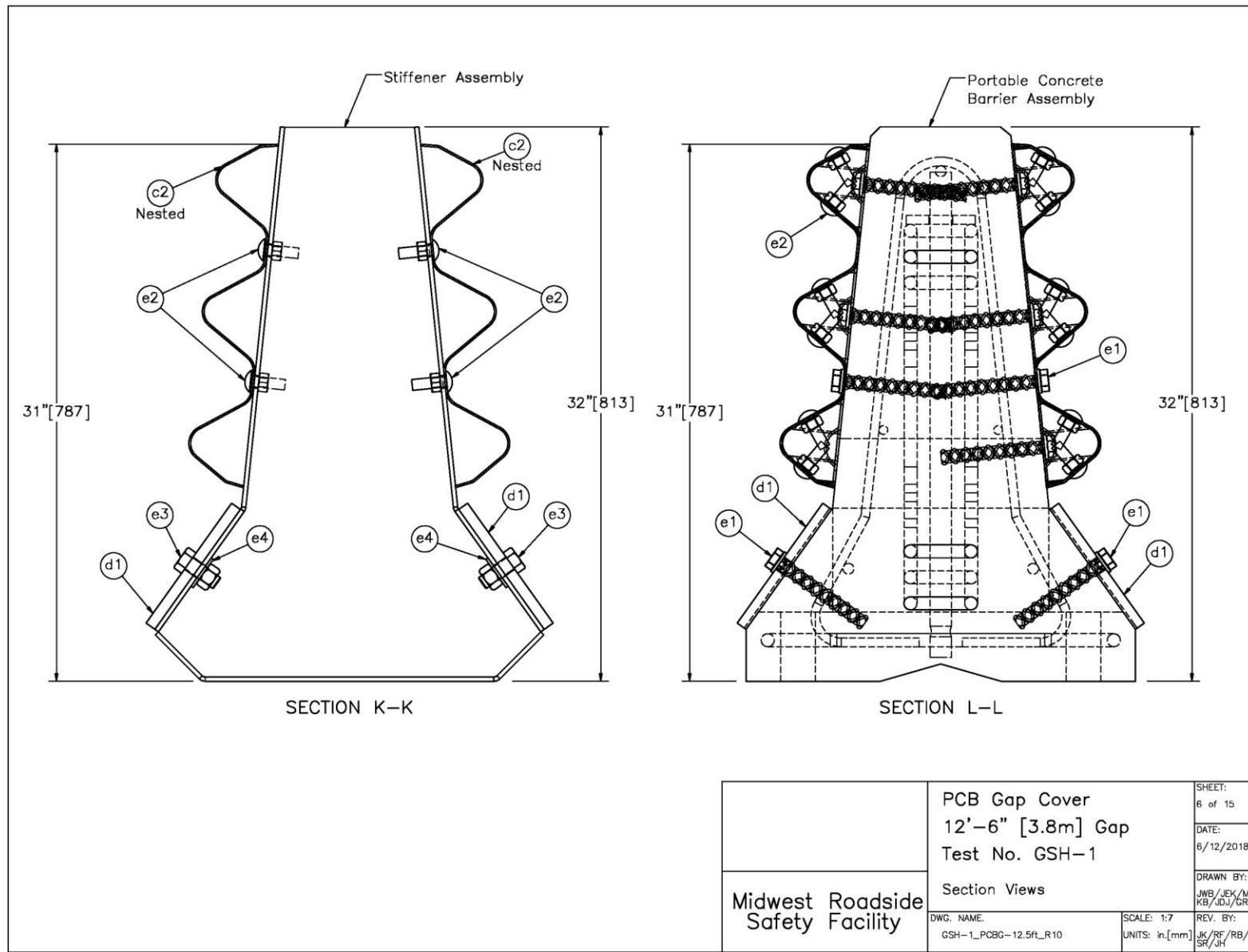


Figure 79. Section K-K and Section L-L Views, Test No. GSH-1

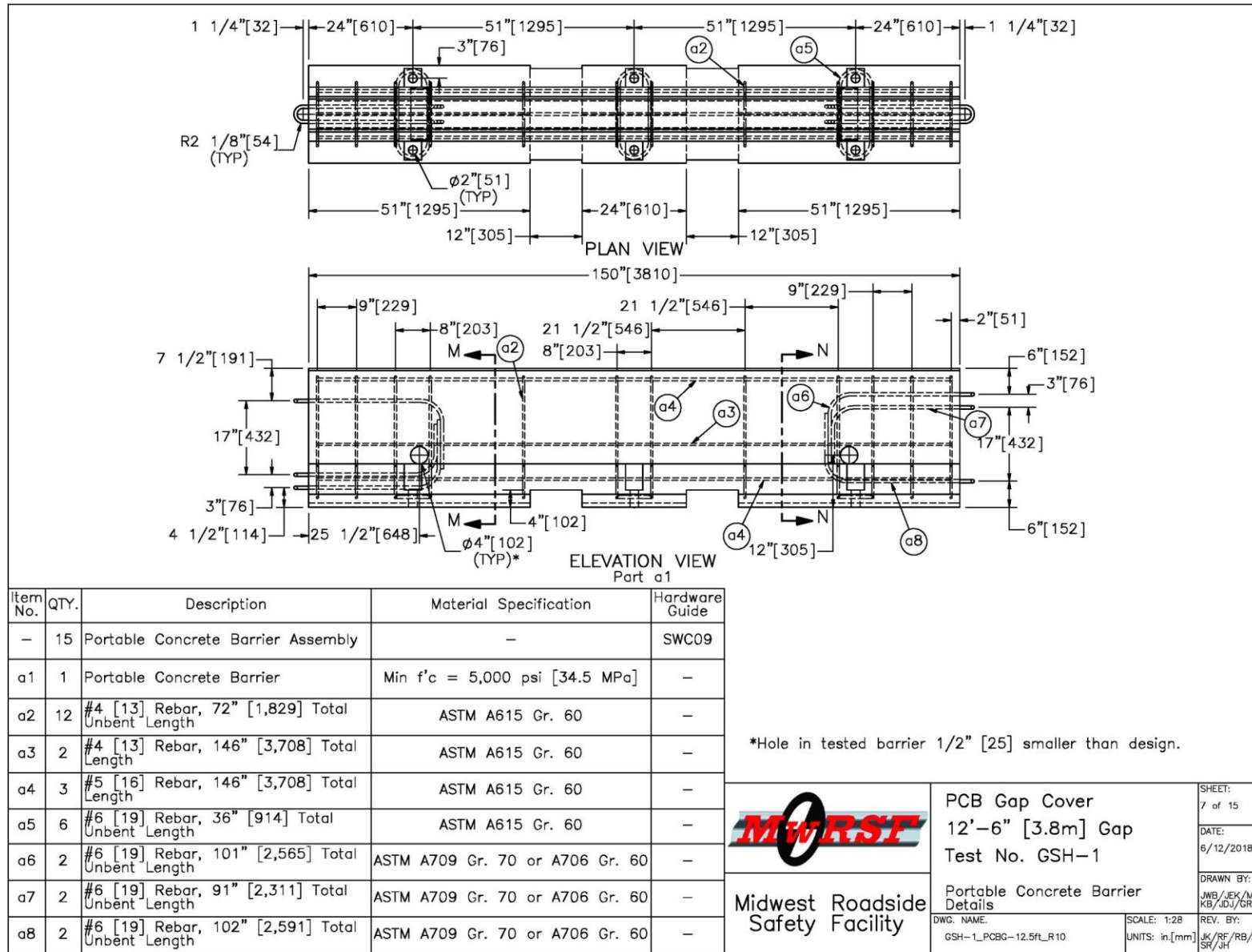


Figure 80. PCB Details, Test No. GSH-1

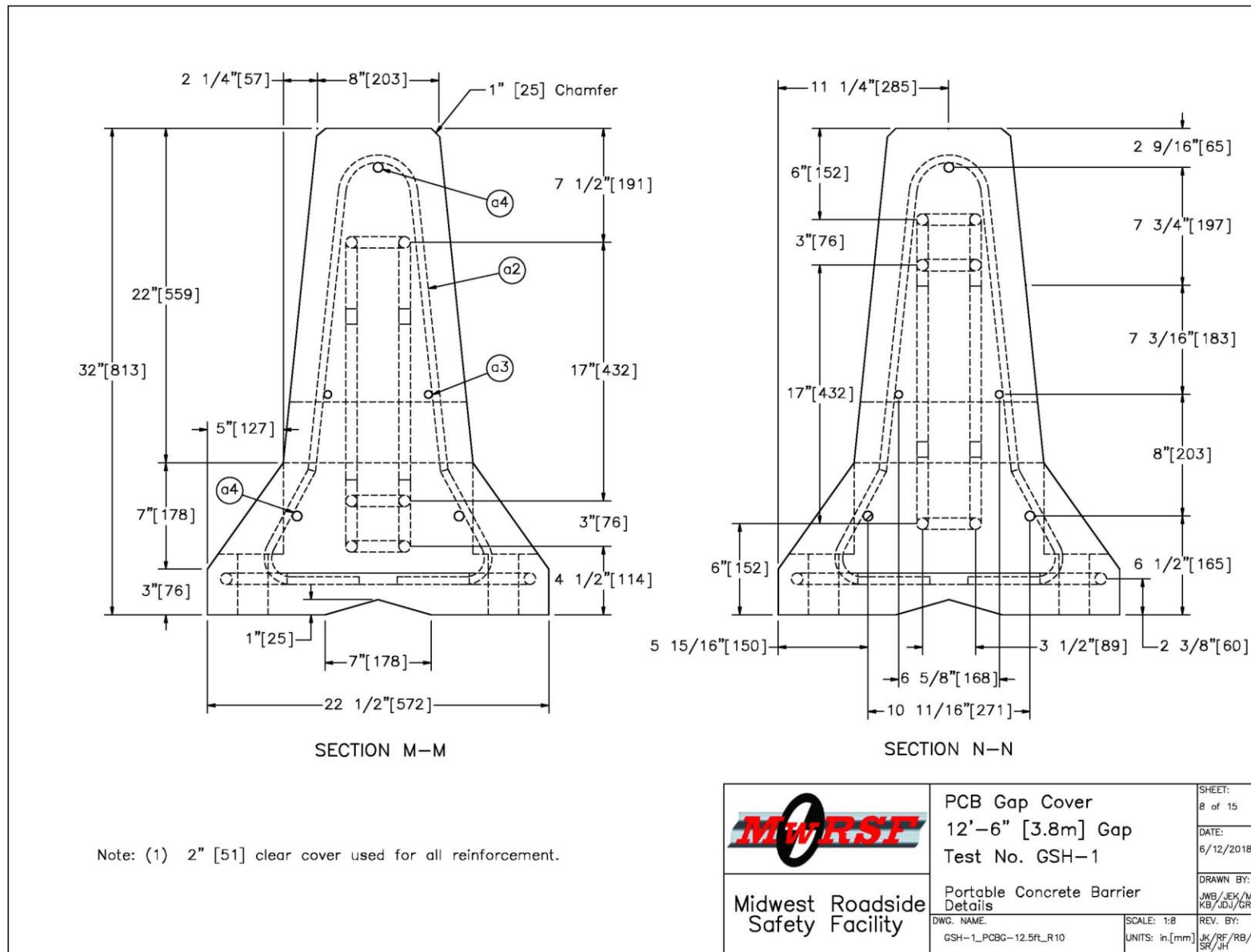


Figure 81. PCB Details, Section M-M and Section N-N, Test No. GSH-1

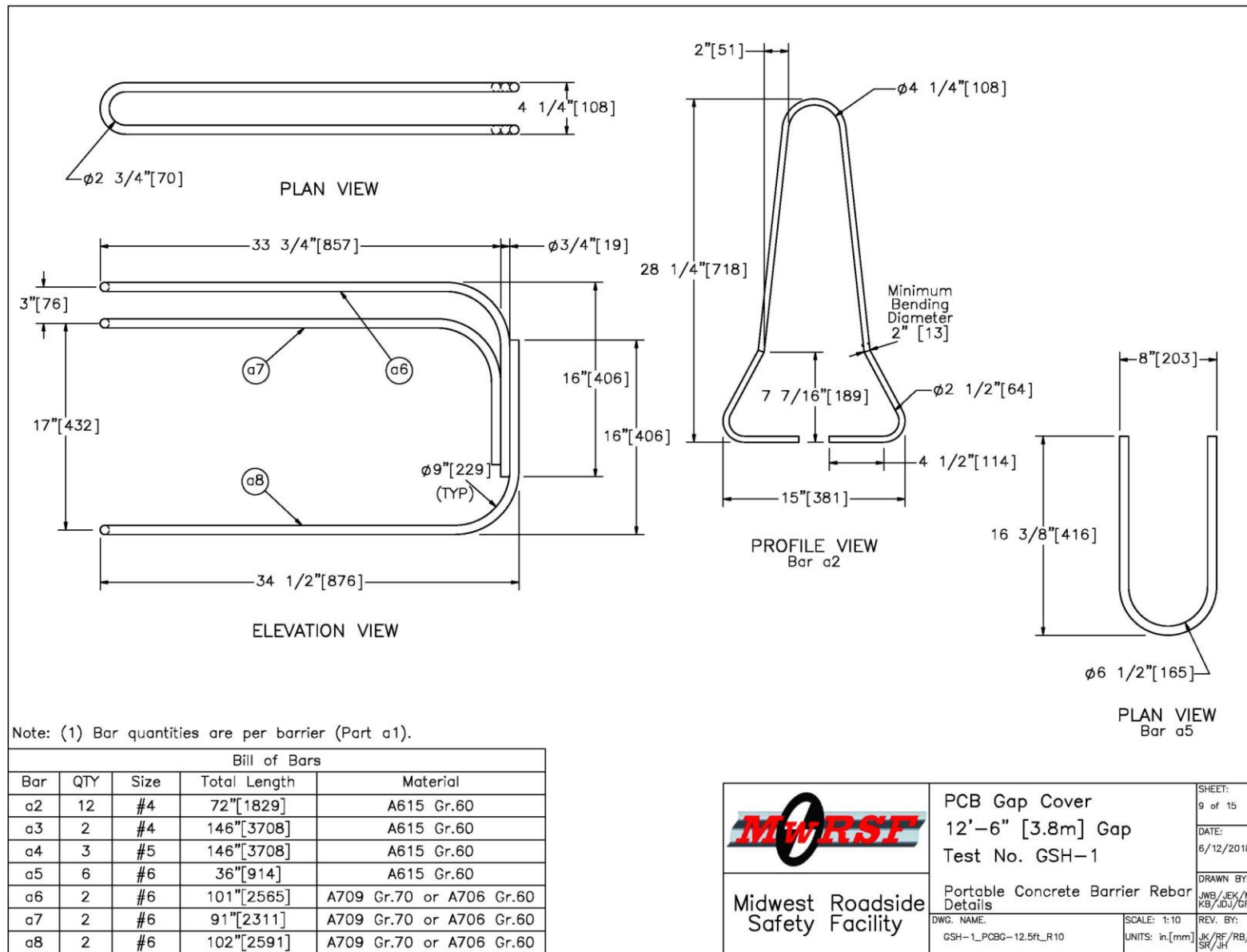


Figure 82. PCB Rebar Details, Test No. GSH-1

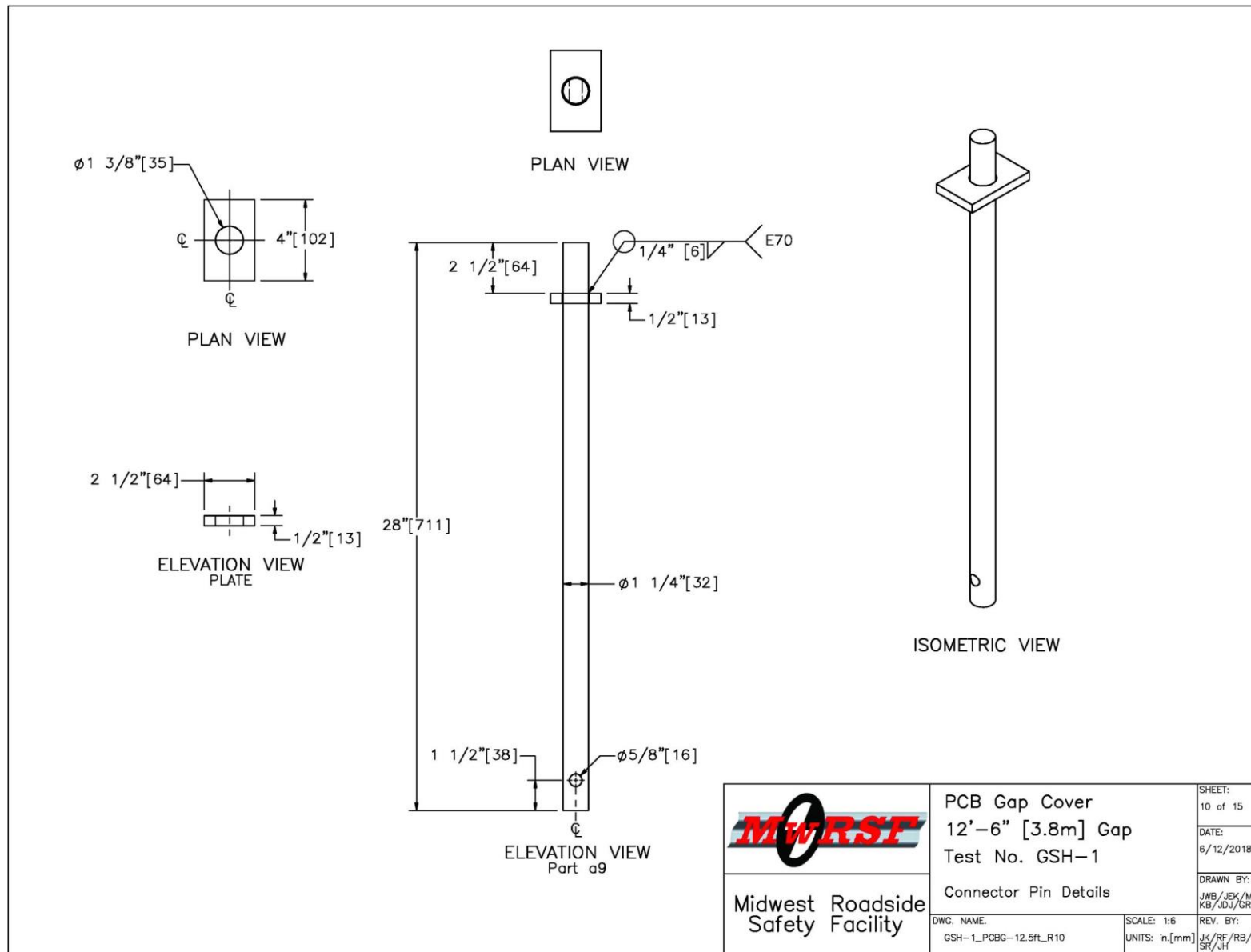


Figure 83. Connector Pin Details, Test No. GSH-1

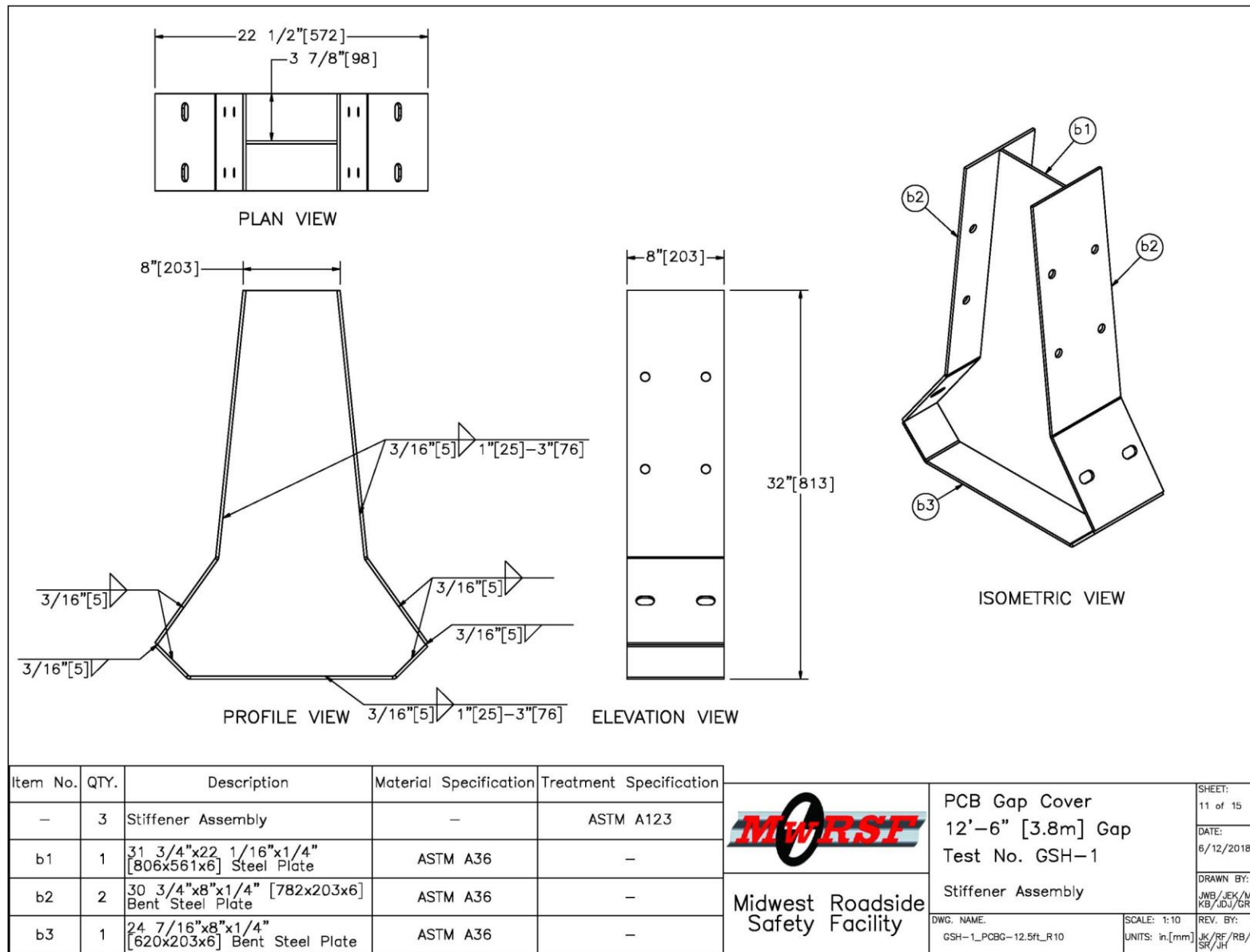
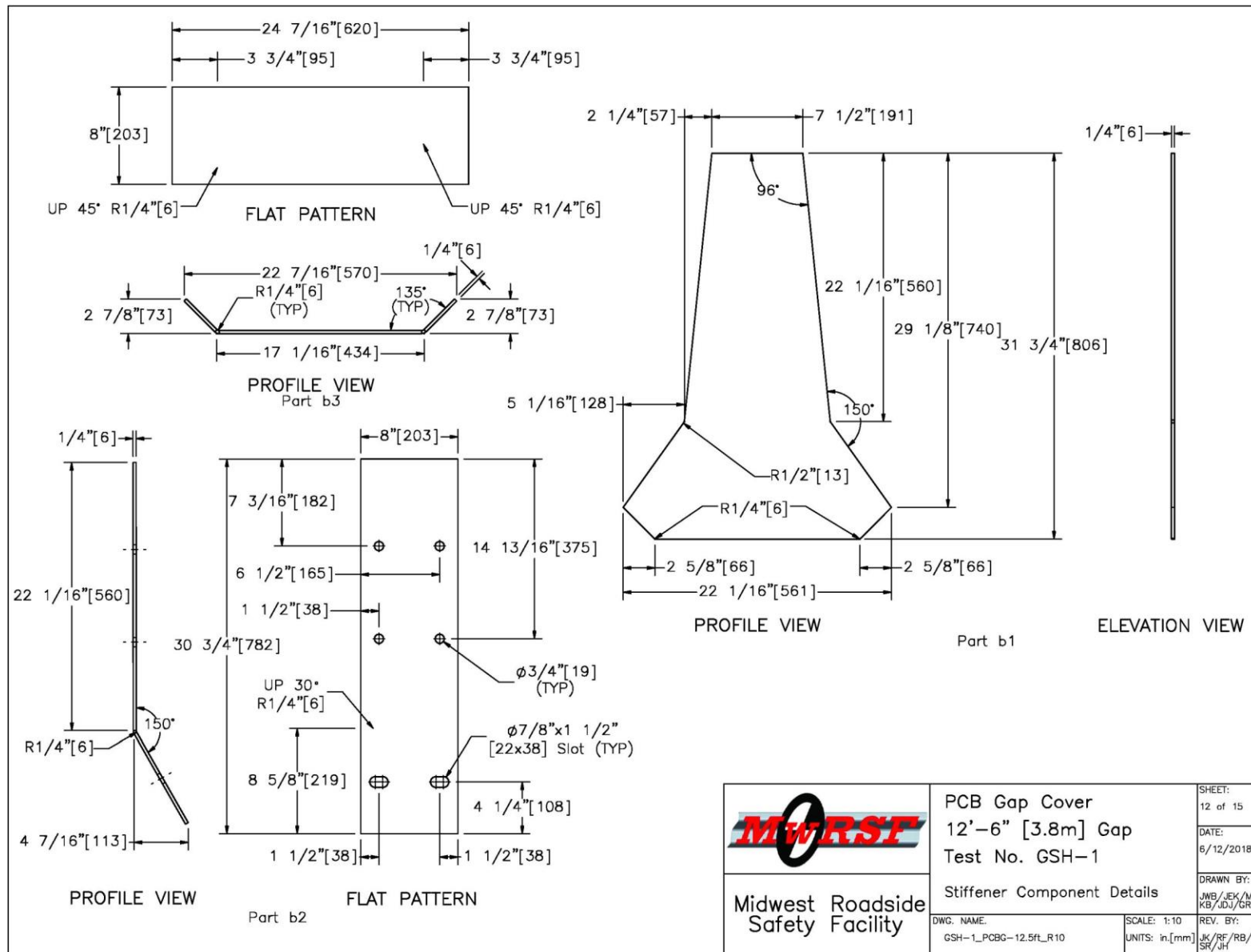


Figure 84. Stiffener Assembly, Test No. GSH-1



 <b>Midwest Roadside Safety Facility</b>	<b>PCB Gap Cover</b> 12'-6" [3.8m] Gap Test No. GSH-1	SHEET: 12 of 15 DATE: 6/12/2018
	Stiffener Component Details	DRAWN BY: JWB/JEK/M KB/JDJ/GRL
DWG. NAME: GSH-1_PCBG-12.5ft_R10	SCALE: 1:10 UNITS: in.[mm]	REV. BY: JK/RF/RB/ SR/JH

Figure 85. Stiffener Component Details, Test No. GSH-1

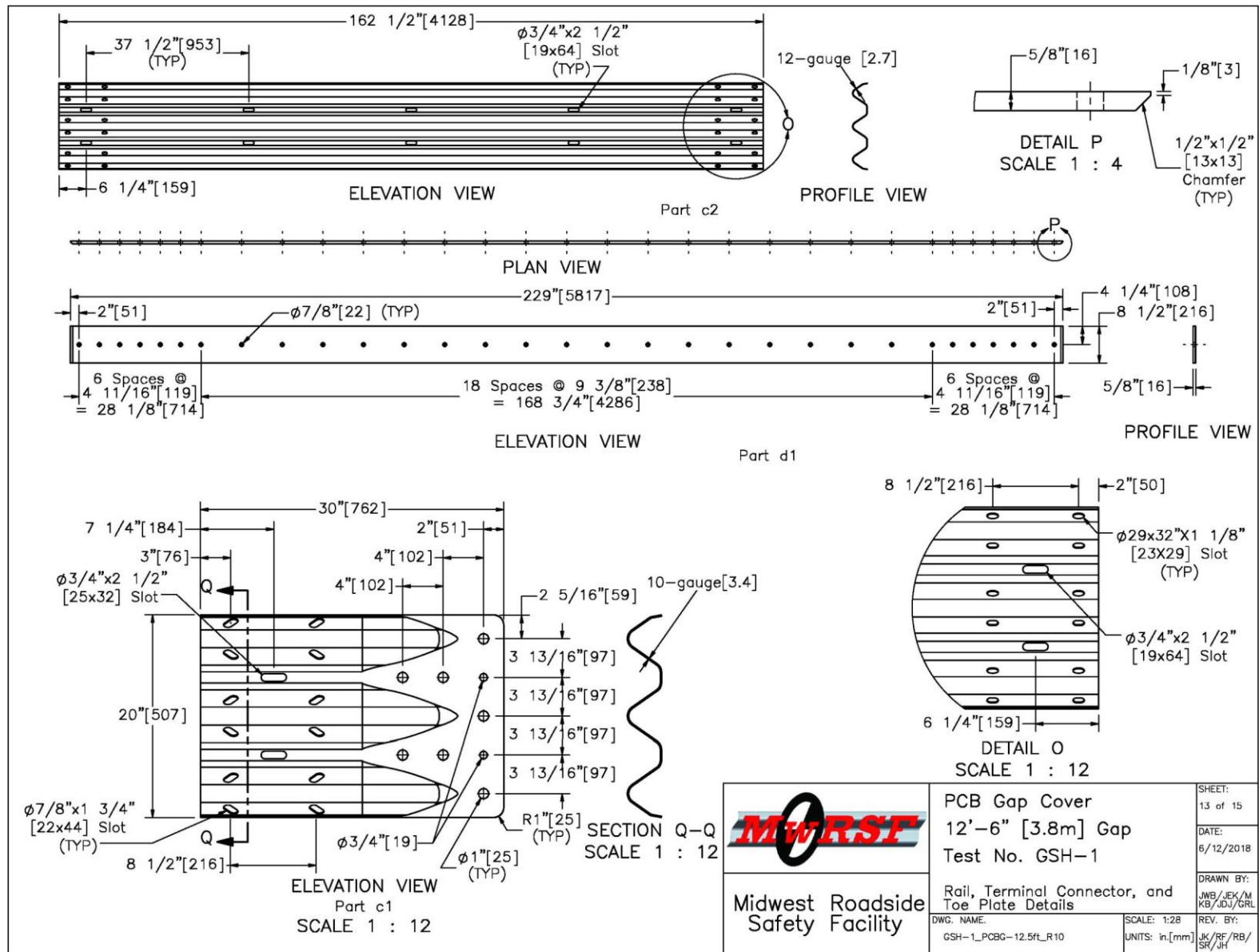


Figure 86. Rail, Terminal Connector, and Toe Plate Details, Test No. GSH-1

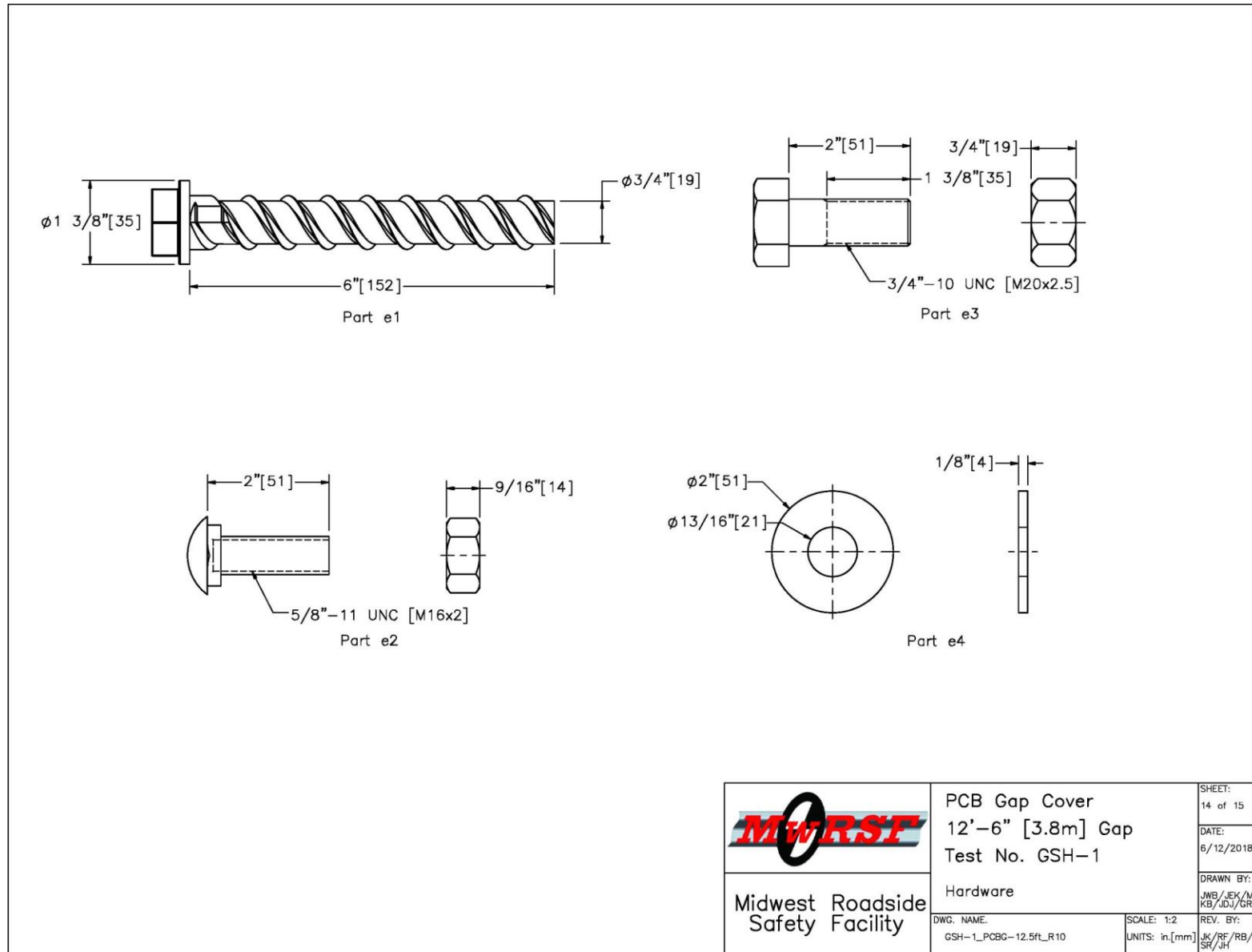


Figure 87. Hardware, Test No. GSH-1

Item No.	QTY.	Description	Material Specification	Treatment Specification	Hardware Guide								
a1	15	Portable Concrete Barrier	Min f'c = 5,000 psi [34.5 MPa]	—	—								
a2	180	#4 [13] Rebar, 72" [1,829] Total Unbent Length	ASTM A615 Gr. 60	—	—								
a3	30	#4 [13] Rebar, 146" [3,708] Total Length	ASTM A615 Gr. 60	—	—								
a4	45	#5 [16] Rebar, 146" [3,708] Total Length	ASTM A615 Gr. 60	—	—								
a5	90	#6 [19] Rebar, 36" [914] Total Unbent Length	ASTM A615 Gr. 60	—	—								
a6	30	#6 [19] Rebar, 101" [2,565] Total Unbent Length	ASTM A709 Gr. 70 or A706 Gr. 60	—	—								
a7	30	#6 [19] Rebar, 91" [2,311] Total Unbent Length	ASTM A709 Gr. 70 or A706 Gr. 60	—	—								
a8	30	#6 [19] Rebar, 102" [2,591] Total Unbent Length	ASTM A709 Gr. 70 or A706 Gr. 60	—	—								
a9	13	1 1/4" [32] Dia., 28" [711] Long Connector Pin	ASTM A36	—	FMW02								
b1	3	31 3/4"x22 1/16"x1/4" [806x561x6] Steel Plate	ASTM A36	—	—								
b2	6	30 3/4"x8"x1/4" [782x203x6] Bent Steel Plate	ASTM A36	—	—								
b3	3	24 7/16"x8"x1/4" [620x203x6] Bent Steel Plate	ASTM A36	—	—								
c1	4	10-gauge [3.4] Thrie Beam Terminal Connector	AASHTO M180 Min. Yield Strength = 50 ksi [345 MPa] Min. Ultimate Strength = 70 ksi [483 MPa]	ASTM A123 or A653	RTE01b								
c2	4	12'-6" [3,810] 12-gauge [2.7] Thrie Beam Section	AASHTO M180	ASTM A123 or A653	RTM04b								
d1	2	229"x8 1/2"x5/8" [5,817x216x16] Steel Plate	ASTM A572 Gr. 50	ASTM A123	—								
e1	36	3/4" [19] Dia., 6" [152] Long Powers Fasteners Wedge Bolt+	As Supplied	As Supplied	FBX02								
e2	60	5/8"-11 UNC [M16x2], 2" [51] Long Guardrail Bolt and Nut	Bolt - ASTM A307 Gr. A Nut - ASTM A563A	ASTM A153 or B695 Class 55 or F2329	FBB02								
e3	6	3/4"-10 UNC [M20x2.5], 2" [51] Long Heavy Hex Head Bolt and Nut	Bolt - ASTM F3125 Gr. A325 Type 1 or equivalent Nut - ASTM A563DH or equivalent	ASTM A153 or B695 Class 55 or F1136 Gr. 3 or F2329 or F2833 Gr. 1	FBX20b								
e4	6	3/4" [19] Dia. Plain Flat Washer	ASTM F844	ASTM A123 or A153 or F2329	FWC20a								
<table border="1" style="width: 100%; border-collapse: collapse;"> <tr> <td rowspan="2" style="text-align: center; vertical-align: middle;">   <b>Midwest Roadside Safety Facility</b> </td> <td style="text-align: center;"> <b>PCB Gap Cover</b>                      12'-6" [3.8m] Gap                      Test No. GSH-1                 </td> <td style="font-size: small;">                     SHEET: 15 of 15                       DATE: 6/12/2018                       DRAWN BY: JWB/JEK/MKB/JDJ/GRL                 </td> </tr> <tr> <td style="text-align: center;">                     Bill of Materials                 </td> <td style="font-size: small;">                     REV. BY: JK/RF/RB/SR/JH                 </td> </tr> <tr> <td style="font-size: x-small;">                     DWG. NAME: GSH-1_PCBG-12.5ft_R10                 </td> <td style="font-size: x-small;">                     SCALE: 1:2                      UNITS: in.[mm]                 </td> <td></td> </tr> </table>						 <b>Midwest Roadside Safety Facility</b>	<b>PCB Gap Cover</b> 12'-6" [3.8m] Gap Test No. GSH-1	SHEET: 15 of 15  DATE: 6/12/2018  DRAWN BY: JWB/JEK/MKB/JDJ/GRL	Bill of Materials	REV. BY: JK/RF/RB/SR/JH	DWG. NAME: GSH-1_PCBG-12.5ft_R10	SCALE: 1:2 UNITS: in.[mm]	
 <b>Midwest Roadside Safety Facility</b>	<b>PCB Gap Cover</b> 12'-6" [3.8m] Gap Test No. GSH-1	SHEET: 15 of 15  DATE: 6/12/2018  DRAWN BY: JWB/JEK/MKB/JDJ/GRL											
	Bill of Materials	REV. BY: JK/RF/RB/SR/JH											
DWG. NAME: GSH-1_PCBG-12.5ft_R10	SCALE: 1:2 UNITS: in.[mm]												

Figure 88. Bill of Materials, Test No. GSH-1

## 9 SUMMARY, CONCLUSIONS, AND RECOMMENDATIONS

Portable concrete barriers (PCBs) are commonly used to protect work-zone personnel and to shield motorists from hazards in construction areas. It is not uncommon to encounter longitudinal gaps within PCB installations due to the practice of constructing and connecting the barriers from different ends during setup or contractor operations. These gaps can range from 6 in. to a full barrier segment length of 12.5 ft and pose a serious safety concern for the errant motorist. Limited guidance is available for shielding this hazardous situation. Thus, a need existed to develop a crashworthy and efficient method for treating longitudinal gaps in adjacent runs of free-standing PCBs.

In the Phase I effort, detailed in this report, following a literature review of existing PCB gap treatments and the brainstorming of potential crashworthy systems capable of accommodating variable gap lengths, several design concepts were identified. The Midwest Pooled Fund Program member states selected two preferred design concepts, including concept no. 4 (three beam and toe-plate with internal stiffeners) and concept no. 7 (two-piece steel cover plate) for further evaluation. Concept no. 4 consisted of two nested, stiffened, three-beam guardrail sections attached to the front and back sides of the PCBs adjacent to the longitudinal gap. Concept no. 7 consisted of two cover plates with a standard pin and loop joint between the two pieces.

LS-DYNA computer simulation was utilized to model the two preferred concepts to evaluate their safety performance, evaluate structural loading, refine the designs, and determine critical impact points (CIPs) for full-scale crash testing.

With respect to concept no. 7 (two-piece cover plate), computer simulations were conducted with a vehicle impacting the PCB installation with cover plates spanning the gaps with variable gap lengths, cap thicknesses, quantity and spacing of stiffeners, and different impact points. Modifications including increased thickness of the cap, reinforcement of the base of the end plate, and the use of three ¼-in. thick internal stiffeners resolved excessive deformation concerns. The end plate sections were 5/8 in. thick with HSS3x3x5/8 box tube at the base to increase its structural rigidity. A pin and loop connection similar to that used on the F-shape PCB was used to connect the two-piece cover plates.

For concept no. 4 (three beam and toe-plate with internal stiffeners), simulations were conducted with four different variations of three-beam rail section, including single and nested 12-gauge and 10-gauge three-beam rails. Single 12-gauge and 10-gauge three-beam rails were found to be unsuitable due to excessive deformation and plastic hinge formation. The simulation results suggested that the nested 12-gauge three-beam rail with internal stiffeners and a steel toe plate could perform acceptably under MASH TL-3 impact conditions.

The design details and simulation results for gap-spanning concept nos. 7 (two-piece cover plate) and 4 (three beam and toe-plate with internal stiffeners) were discussed with the Midwest Pooled Fund Program member states. The two concepts were compared based on overall safety performance in the preliminary models, design complexity, and ease of fabrication and construction. A decision was reached to move forward with concept no. 4 based on the simulation results indicating the potential MASH TL-3 safety performance and the ease of fabrication and construction of the design.

Additional simulations were performed to fully develop the three beam and toe plate design concept. These simulations were used to identify potential modifications which could minimize the risk of test failure in terms of increased occupant risk values, deflection, and potential for snagging and pocketing. The simulations were conducted at various impact points including upstream from the barrier gap, on the gap-spanning hardware, and downstream from the barrier gap. These models led to modification and improvement of the toe plate design.

Finally, the computer simulations were applied to determine which MASH TL-3 full-scale crash tests were required to evaluate the system and what the CIPs should be for those tests. It was determined that two MASH test designation no. 3-11 full-scale crash tests should be conducted to evaluate the PCB gap-spanning hardware. Small car tests were deemed non-critical based on crash testing of previous barrier systems. The first test was to evaluate the maximum structural loading of the PCB gap-spanning hardware, and the second test was to evaluate potential vehicle instability. The proposed CIPs for these two tests were as follows.

1. An impact point on the PCB gap-spanning hardware with the largest possible barrier gap of 12.5 ft located 72 in. upstream from the first PCB segment on the downstream end of the gap-spanning hardware.
2. An impact point on the PCB gap-spanning hardware system with an approximately 3-ft long barrier gap located 12 in. downstream from the upstream end of the first PCB segment on the downstream end of the gap-spanning hardware.

Design details for the first full-scale crash test of the PCB gap-spanning hardware were provided. Further system details and implementation guidance were planned to be provided following full-scale crash testing in Phase II of the research.

## 10 REFERENCES

1. *Manual for Assessing Safety Hardware (MASH 2016), Second Edition*, American Association of State Highway and Transportation Officials (AASHTO), Washington, D.C., 2016.
2. Ross, H.E., Sicking, D.L., Zimmer, R.A., and Michie, J.D., *Recommended Procedures for the Safety Performance Evaluation of Highway Features*, National Cooperative Highway Research Program (NCHRP) Report 350, Transportation Research Board, Washington, D.C., 1993.
3. Polivka, K.A., Faller, R.K., Sicking, D.L., Rohde, J.R., Bielenberg, R.W., Reid, J.D., and Coon, B.A., *Performance Evaluation of the Free-Standing Temporary Barrier – Update to NCHRP 350 Test No. 3-11 with 28” C.G. Height (2214TB-2)*, National Cooperative Highway Research Program, Transportation Research Report TRP-03-174-06, Midwest Roadside Safety Facility, University of Nebraska-Lincoln, October 2006.
4. Safeguard Gate, Safety Barrier Product Manual, Retrieved from [https://www.csppacific.co.nz/uploads/literature/installation/ArmorGuard\\_Gate\\_Installation\\_Manual\\_2x16\\_AUS.pdf](https://www.csppacific.co.nz/uploads/literature/installation/ArmorGuard_Gate_Installation_Manual_2x16_AUS.pdf).
5. Frederick G. Wright, Jr. (2001). *FHWA Acceptance SafeGuard Gate System*. Letter to James Keaton, July 6, 2001, from the FHWA. Retrieved from [https://safety.fhwa.dot.gov/roadway\\_dept/countermeasures/reduce\\_crash\\_severity/barriers/pdf/b87.pdf](https://safety.fhwa.dot.gov/roadway_dept/countermeasures/reduce_crash_severity/barriers/pdf/b87.pdf).
6. Barrier Systems Inc. (2008). Product Specification ArmorGuard™ Gate System. Rio Vista, CA. Retrieved from [https://www.lindsay.com/uploads/files/sections/1173-tb\\_081031\\_rev\\_0\\_\\_\\_armorguard\\_gate\\_system.pdf](https://www.lindsay.com/uploads/files/sections/1173-tb_081031_rev_0___armorguard_gate_system.pdf).
7. Gerrit, A.D., Mazer, J.S. (2002). *U.S. Patent No. 6,485,224 B1*. Washington DC: U.S. Patent and Trademark Office.
8. Keaton, J.R., *ArmorGuard™ Barrier*. FHWA Acceptance Letter to Barrier Systems, Inc., 180 River Road, Rio Vista, California 94571, July 6, 2001. Retrieved from [https://www.lindsay.com/uploads/files/sections/1172-armorguard\\_gate\\_acceptance\\_letter.pdf](https://www.lindsay.com/uploads/files/sections/1172-armorguard_gate_acceptance_letter.pdf).
9. Denman, O.S., *ArmorGuard™ Barrier*. Letter to Barrier Systems, Inc., 180 River Road, Rio Vista, California 94571, March 25, 2008. Retrieved from [https://safety.fhwa.dot.gov/roadway\\_dept/countermeasures/reduce\\_crash\\_severity/barriers/pdf/b173.pdf](https://safety.fhwa.dot.gov/roadway_dept/countermeasures/reduce_crash_severity/barriers/pdf/b173.pdf).
10. Strybos, J.W., Morgan, J.R., and Ross, Jr., H.E., *Emergency Opening System for an Authorized Vehicle Lane*, Research Report TX-84/105-1F, Texas Transportation Institute, College Station, TX, March 1984.
11. Michie, J.D., *Recommended Procedures for the Safety Performance Evaluation of Highway Features*, NCHRP Report 230, Transportation Research Board, National Research Council, Washington, D.C., March 1981.

12. AASHTO, *Manual for Assessing Safety Hardware*, Washington, D.C., American Association of State Highway and Transportation Officials, 2009.
13. Bligh, R.P. and Menges, W.L., *Median Barrier Gate, Technical Memorandum #0-5210-9*, Texas Transportation Institute, College Station, TX, June 2010.
14. Bligh, R.P., Arrington, D.R., Sheikh, N.M., Silvestri, C., and Menges, W.L., *Development of a MASH TL-3 Median Barrier Gate*, Texas Department of Transportation, Research Report No. FHWA/TX-11/9-1002-2, Texas Transportation Institute, Texas A&M University, June 2011.
15. Owen S. Denman, *FHWA Acceptance of the BarrierGuard™ 800 System HSA-10/B-131*. Letter to Barrier Systems Inc. from the FHWA. November 30, 2004. Retrieved from [https://safety.fhwa.dot.gov/roadway\\_dept/countermeasures/reduce\\_crash\\_severity/barriers/pdf/b131.pdf](https://safety.fhwa.dot.gov/roadway_dept/countermeasures/reduce_crash_severity/barriers/pdf/b131.pdf).
16. George E. Rice, Jr. *FHWA Acceptance of the BarrierGuard™ 800 System*. Letter to Barrier Systems Inc. from the FHWA. May 8, 2007. Retrieved from [https://safety.fhwa.dot.gov/roadway\\_dept/countermeasures/reduce\\_crash\\_severity/barriers/pdf/b160.pdf](https://safety.fhwa.dot.gov/roadway_dept/countermeasures/reduce_crash_severity/barriers/pdf/b160.pdf)
17. Endersby, R.M., Talbot, J.E., *World Intellectual Property Organization No. WO 2007/148110 A1*. Geneva. World Intellectual Property Organization, 2007.
18. Hubert, J.P. and Mertens, M., *U.S. Patent No. US 2005/0249551 A1*, Patent and Trademark Office, Washington D.C., U.S. 2005.
19. Highway Care International, *BarrierGuard 800 Gate Product Manual Australia & New Zealand*, 2015. Retrieved from <https://webassets.valmont.com/valmontstaging/docs/librariesprovider35/manuals/bg-800-gate-manual-nchrp-350-rev-1b-11-15-australia-new-zealand.pdf?sfvrsn=2>.
20. Staron, L. A., *BarrierGate FHWA Acceptance Letter*, April 14, 1993. Retrieved August 9, 2016, from [https://safety.fhwa.dot.gov/roadway\\_dept/countermeasures/reduce\\_crash\\_severity/barriers/pdf/b-25.pdf](https://safety.fhwa.dot.gov/roadway_dept/countermeasures/reduce_crash_severity/barriers/pdf/b-25.pdf).
21. Quittner, J.P., *U.S. Patent No. 5,211,503*, Patent and Trademark Office, Washington D.C., U.S., 1993.
22. Energy Absorption Systems, Inc., *BarrierGate®*, 2005, Retrieved from <http://guides.roadsafellc.com/Documents/SGM20/Drawings/SGM20.pdf>
23. Rice, Jr., G.E., *FHWA Acceptance of the Vulcan Gate™ System*. Letter to Energy Absorption Systems Inc. from the FHWA. November 21, 2007. Retrieved from: [https://safety.fhwa.dot.gov/roadway\\_dept/countermeasures/reduce\\_crash\\_severity/barriers/pdf/b134c.pdf](https://safety.fhwa.dot.gov/roadway_dept/countermeasures/reduce_crash_severity/barriers/pdf/b134c.pdf).

24. Hotchkin, D.J., *U.S. Patent No. 8,393,822 B2*, Patent and Trademark Office, Washington D.C., U.S., 2013.
25. Vulcan Barrier, *Portable Steel*. Retrieved from <https://trinityhighway.com/wp-content/uploads/2019/04/Vulcan-Gate-4-19-19.pdf>.
26. Energy Absorption System, Inc. *Vulcan Barrier*. Retrieved from <https://trinityhighway.com/wp-content/uploads/2020/02/610435-Vulcan-Gate.pdf>.
27. Van Kirk, J.L., Stoughton, R.L., Stoker, J.R., and Nordlin, E.F., *Vehicular Impact Test on Steel Channel-Beams Spanning a Gap in a Continuous Concrete Median Barrier*, Report No. CA-TL-79-01, State of California Department of Transportation, February 1979.
28. Transportation Research Board, “*Recommended Procedures for Vehicle Crash Testing of Highway Appurtenances*,” Transportation Research Circular 191, February 1978.
29. State of California Department of Transportation Division of Engineering Services, *Concrete Barrier Type 60 Steel Channel Closure Details*, 2014.
30. State of New York Department of Transportation Office of Structures, *Modular Joint System Multicell Miscellaneous Details*, 2009.
31. Riddell, M., Wall, L.J., Wilkinson P.J., Addy, J.L., and Reynolds, M.G., *World Intellectual Property Organization No. 2008/062196 A1*, World Intellectual Property Organization, Geneva, 2008.
32. Griffith, M.S., *FHWA Acceptance of Zone guard Standard and Minimum Deflection Arrangements*, Letter to Mr. Gary Lallo from the FHWA, 2019. Retrieved from: [https://safety.fhwa.dot.gov/roadway\\_dept/countermeasures/reduce\\_crash\\_severity/barriers/pdf/b320.pdf](https://safety.fhwa.dot.gov/roadway_dept/countermeasures/reduce_crash_severity/barriers/pdf/b320.pdf).
33. Wilson, J.B.S, Serle, P.M., and Siroky, Z. *European Patent Office Patent No. 0 438 267 A1*, European Patent Office, Paris, 1991.
34. Cobb, L.C. and Wardell, R.A., *World Intellectual Property Organization Patent No. WO 86/03239*, World Intellectual Property Organization, Geneva, 1986.
35. Wahlund, L., Langassve, P., *World Intellectual Property Organization Patent No. WO 2005/003465 A1*, World Intellectual Property Organization, Geneva, 2005.
36. Ritter, R., *FHWA Acceptance of the Metal Transition for Branching Concrete Barrier*, Letter to Mr. Ben Powell, Powell Contracting Limited, 2017. Retrieved from: [https://safety.fhwa.dot.gov/roadway\\_dept/countermeasures/reduce\\_crash\\_severity/barriers/pdf/b281.pdf](https://safety.fhwa.dot.gov/roadway_dept/countermeasures/reduce_crash_severity/barriers/pdf/b281.pdf).
37. Hallquist, J.O., *LS-DYNA Keyword User’s Manual*, Livermore Software Technology Corporation, Livermore, California, 2007.

38. Bielenberg, R.W., Faller, R.K., Rohde, J.R., Reid, J.D., Sicking, D.L., and Holloway, J.C., *Development of Tie-Down and Transition Systems for Temporary Concrete Barrier on Asphalt Road Surfaces*, Research Report No. TRP-03-180-06, Midwest Roadside Safety Facility, University of Nebraska-Lincoln, Lincoln, Nebraska, February 23, 2007.
39. Bielenberg, R.W., Quinn, T.E., Faller, R.K., Sicking, D.L., and Reid, J.D., *Development of a Retrofit, Low-Deflection, Temporary Concrete Barrier System*, Research Report No. TRP 03-295-14, Midwest Roadside Safety Facility, University of Nebraska-Lincoln, Lincoln, Nebraska, March 31, 2014.
40. Mongiardini, M., Ray, M.H., Plaxico, C.A., Anghileri, M., *Procedures for Verification and Validation of Computer Simulations Used for Roadside Safety Applications*, National Cooperative Highway Research Program, NCHRP Report No. W179, Project No. 22-24, Worcester Polytechnic Institute, March 2010.
41. Bielenberg, R.W., Meyer, D.T., Faller, R.K., and Reid, J.D., *Length of Need and Minimum System Length for F-Shape Portable Concrete Barrier*, Research Report No. TRP-03-337-17, Midwest Roadside Safety Facility, University of Nebraska-Lincoln, Lincoln, Nebraska, May 3, 2017.
42. Bielenberg, R.W., *Dynamic Component Testing of Potential Alternative Anchors for the F-Shape Concrete Barrier Steel Strap Tie-Down System*, Final Report (Letter Report) to the Midwest States Pooled Fund Program, Report No. TRP-03-182-07, Midwest Roadside Safety Facility, University of Nebraska-Lincoln, Lincoln, Nebraska, April 9, 2007.
43. Wiebelhaus, M.J., Terpsma, R.J., Lechtenberg, K.A., Reid, J.D., Faller, R.K., Bielenberg, R.W., Rohde, J.R., and Sicking, D.L., *Development of a Temporary Concrete Barrier to Permanent Concrete Median Barrier Approach Transition*, Final Report to the Midwest State's Pooled Fund Program, Report No. TRP-03-208-10, Midwest Roadside Safety Facility, University of Nebraska-Lincoln, Lincoln, Nebraska, July 15, 2010.
44. Polivka, K.A., Faller, R.K., Sicking, D.L., Rohde, J.R., Bielenberg, R.W., Reid, J.D., and Coon, B.A., *Performance Evaluation of the Permanent New Jersey Safety Shape Barrier - Update to NCHRP 350 Test No. 3-10 (2214NJ-1)*, Report No. TRP-03-177-06, Midwest Roadside Safety Facility, University of Nebraska-Lincoln, Lincoln, Nebraska, October 13, 2006.
45. Sheikh, N.M., Menges, W.L., Kuhn, D.L., *MASH TL-3 Testing and Evaluation of Free-Standing Portable Concrete Barrier*, Test Report No. 607911-1&2, Texas A&M Transportation Institute, Texas A&M University, College Station, Texas, May 2017.

**END OF DOCUMENT**